Cooperative control of eco-driving trajectories for a fleet of electric connected and autonomous vehicles

Vinith Kumar Lakshmanan

université PARIS-SACLAY

Cooperative control of eco-driving trajectories for a fleet of electric connected and autonomous vehicles

Contrôle coopératif des trajectoires d'éco-conduite pour une flotte de véhicules électriques connectés et autonomes

Thèse de doctorat de l'université Paris-Saclay

École doctorale n° 580, Sciences et Technologies de l'Information et de la Communication (STIC)
Spécialité de doctorat: Automatique
GS Engineering and Systems Sciences (SIS), Référent : CentraleSupélec

Thèse préparée dans la unité de recherche IFP Energies Nouvelles (IFPEN), sous la direction de Dr. Antonio SCIARRETTA, la co-direction de Dr. Ouafae EL-GANAOUI MOURLAN.

Thèse soutenue à Paris-Saclay, le 23 Mai 2023, par

Vinith Kumar LAKSHMANAN

Composition du jury

Paola GOATIN Directeur de recherche, INRIA	Présidente du jury
Giorgio RIZZONI Ford Motor Company Chair in Mechanical & Aerospace Engr.,The Ohio State University	Rapporteur
Guillaume COLIN Professeur, Université d'Orléans	Rapporteur
Olivier ORFILA Directeur scientifique, VEDECOM	Examinateur
Meng WANG Head of Chair of Traffic Process Automation, Institute of Traffic Telematics Dr., IFP School	Examinateur

THESE DE DOCTORAT

NNT : 2023UPAST068

université PARIS-SACLAY

ÉCOLE DOCTORALE
Sciences et technologies de l'information et de la communication (STIC)

Titre: Contrôle coopératif des trajectoires d'éco-conduite pour l'efficacité énergétique d'une flotte de véhicules électriques connectés et autonomes

Mots clés: éco-conduite, contrôle coopératif, contrôle optimal

Résumé: Les véhicules électriques connectés et autonomes (CAV) qui maximisent l'efficacité énergétique peuvent être considérés comme une approche intégrée pour répondre aux différentes tendances, notamment la transition verte et numérique, dans l'industrie automobile. Les stratégies d'économie d'énergie pour les CAV peuvent être classées en écoroutage (ER) et écoconduite (ED). Avec l'augmentation de la pénétration des CAV, ces véhicules peuvent coopérer plutôt que de se disputer le droit de passage, ce qui donne naissance aux véhicules coopératifs connectés et automatisés (CCAV). En fonction du niveau d'information partagé et de la motivation pour l'efficacité énergétique, les stratégies d'ED des CCAV peuvent être catégorisées comme Non Coopératives (NC), Coopératives (C) et Coopératives Centralisées (CC). Les objectifs principaux de cette thèse sont d'évaluer expérimentalement une stratégie de base connue de NC-ED pour un seul CCAV, d'obtenir des solutions analytiques d'ED pour une flotte de CCAV électriques avec différents niveaux de coopération pour des scénarios de peloton et d'intersection sans signalisation, et d'évaluer l'influence des différents niveaux de coopération sur la consommation d'énergie de la flotte.

La thèse présente en premier lieu une stratégie NC-ED connue pour un seul CAV qui constitue la base de cette recherche. L'ED est formulé comme un Problème de Commande Optimale (OCP), pour un scénario de suivi de voiture et sans contraintes, et résolu par le Principe du Minimum de Pontryagin (PMP). La stratégie de suivi de voiture NC-ED de base prédit le mouvement du véhicule d'avant en cas d'accélération constante (CA) afin de permettre des solutions analytiques. Dans cette thèse, des modèles de prédiction plus sophistiqués du véhicule d'avant, à savoir le CA-AB et le EDM-LOSP, sont développés en l'absence de communication V2V. Les résultats indiquent que le véhicule ego utilisant l'EDM-LOSP est plus performant que le CA-AB avec un gain d'énergie de 4 %, tandis que le CA-AB est plus performant de 4.5 % que le CA de base sur des trajets urbains.

Le scénario de base NC-ED de suivi de voiture est étendu à un scénario ED en peloton. Un OCP est formulé pour les trois niveaux de coopération et des solutions analytiques sont obtenues à l'aide du PMP. Les pelotons utilisant les trois stratégies de coopération sont évalués par rapport à un scénario de référence utilisant un régulateur de vitesse adaptatif dans un environnement de simulation. Les résultats indiquent une économie d'énergie plus importante avec des niveaux de coopération plus élevés. Le peloton CC-ED présente une économie d'énergie meilleure de 2,5 %, sur un cycle WLTC High, par rapport au peloton NC-ED. Cette thèse présente en outre un OCP formulé pour un ensemble de CCAVs traversant en toute sécurité une intersection sans signalisation en minimisant la consommation d'énergie. L'OCP est formulé pour deux niveaux de coopération : NC-ED et C-ED. L'OCP est résolu à l'aide de PMP, des solutions sont présentés. Les deux stratégies sont évaluées par rapport à l'IDM comme référence pour différents débits. Les résultats indiquent que la stratégie C-ED est la plus performante, avec un gain énergétique de 23,7 %.

Enfin, cette thèse présente une approche expérimentale de mise en œuvre de la stratégie de référence NC-ED dans une voiture électrique Renault Zoé. Les solutions ED sont mises en œuvre via une tablette, qui affiche la vitesse optimale calculée pour que le conducteur puisse la suivre dans les secondes suivantes. La mise en œuvre de l'algorithme se compose de deux parties : un profil de vitesse prévu au début du voyage et un profil de vitesse ED calculé en temps réel afin de conseiller le conducteur. Dans ce travail, les profils de conduite sont analysés a posteriori pour étudier l'impact des hypothèses faites au début d'un voyage. Les résultats indiquent l'importance d'avoir des informations précises sur le trafic et les feux de circulation.

Title: Cooperative control of eco-driving trajectories for a fleet of electric connected and autonomous vehicles

Keywords: eco-driving, cooperative control, optimal control

Abstract: Electric Connected and Autonomous Vehicles (CAVs) that maximize energy efficiency can be considered an integrated approach to meet the various trends, mainly green and digital transition, in the automotive industry. Energy-saving strategies for CAVs on the vehicle level can be categorized into Eco-Routing (ER) and Eco-Driving (ED). With increased penetration of CAVs, such vehicles can cooperate rather than compete for right of way, giving rise to Cooperative Connected and Automated Vehicles (CCAVs). Based on the level of information shared and the motivation for energy efficiency, the behavior of CCAVs can be categorized into Non-Cooperative (NC), Cooperative (C), and Centralized Cooperative (CC) ED strategies. Each CCAV optimizes for itself in NC-ED and shares only its instantaneous states with its neighbors, while in C-ED, it shares its future intentions. Each CCAV's control action optimizes for the entire group in the CC-ED. The main objectives of this thesis are to experimentally assess a known baseline NC-ED strategy for a single CAV; to obtain analytical eco-driving solutions for a fleet of electric CCAVs, with varying levels of cooperation, for platooning and un-signalized intersection scenarios; and to evaluate the influence of the varying levels of cooperation, namely, NC-ED, C-ED, and CC-ED, on fleet energy consumption.

The thesis first introduces a known NC-ED strategy for a single CAV that forms the basis for this thesis. ED is formulated as an optimal control problem for an unconstrained and car-following scenario and solved using Pontryagin's Minimum Principle (PMP). The baseline NC-ED car-following strategy predicts the lead vehicle's motion under Constant Acceleration (CA) to facilitate analytical closed-form solutions. In a chapter of this thesis, more sophisticated lead vehicle prediction models, namely Constant Acceleration-Average Braking (CA-AB) and EDM-LOS based Predictor (EDM-LOSP), are developed in the absence of V2V communication. The results distinguished the performance of the predictors in urban routes, where the ego vehicle using EDM-LOSP performed better than CA-AB with 4 $\%$ energy gain, while CA-AB had 4.5 $\%$ over the baseline CA.

The baseline NC-ED car-following scenario is extended to a platooning ED scenario. An OCP is formulated for the three levels of cooperation, and analytical solutions are obtained using PMP. Platoons with the three cooperative strategies are evaluated against a baseline using Adaptive Cruise Control in a simulation environment. The results indicate higher energy saving with increased levels of cooperation. The CC-ED platoon performed best with 2.5 $\%$ energy saving over the NC-ED platoon on a WLTC High cycle.

This thesis further presents an OCP formulated for a set of CCAVs safely crossing an un-signalized intersection while minimizing energy consumption. The OCP is formulated for two levels of cooperation: NC-ED and C-ED. The conflicts that arise in an intersection are analyzed and transformed into constraints. The OCP with the constraints is solved using PMP, and analytical solutions are presented. The two strategies are evaluated against Intelligent Driver Model (IDM) as a baseline for various flow rates. The results indicate that C-ED performs best, with 23.7 $\%$ energy gains over IDM.

Finally, this thesis presents an experimental implementation of the baseline NC-ED strategy in a Renault Zoe electric car. The ED solutions are implemented via a tablet, that displays the computed optimal speed for the driver to follow in the next second. The implementation of the algorithm consists of two parts: an ED speed profile predicted at the trip's start under certain assumptions and an ED speed profile computed in real-time advising the driver. In this work, the driven profiles are analyzed a posteriori to study the impact of the assumptions made at the start of a trip. The results indicate the importance of having accurate information on traffic and traffic light behavior.

Acknowledgment

I would like to acknowledge both my supervisors, Dr. Antonio Sciarretta and Dr. Ouafae El-Ganaoui Mourlan, for giving me this opportunity and for their guidance and support through the past three years.

I would like to acknowledge my colleagues at the open office at IFPEN for the student-like environment we created, despite not being at an academic setup. From the lunch breaks to after works it has been a great pleasure and fun.

I also gratefully acknowledge my friends Gabriele and Ioanna, and my partner Noelie for their support and for enabling me to have a work-life balance.

Finally, I am indebted to my parents for providing me everything from my childhood so that I could have an education that they didn't.

Contents

1 - Introduction

The automotive sector is at the crossroads of various trends changing in the industry. In particular, trends related to green transition (electromobility, hydrogen fuel cells, etc.) and digital transition (connectivity, autonomous driving, software, etc).

Climate change mitigation has led the green transition, forcing automakers to embrace both fully and partially electrification. The year 2020 saw an increase of registrations for such cars more than double to 1.4 million in the European Union [1]. All European carmakers are set to widely increase their portfolio of electricity-powered cars in the coming years, with almost all of them publicly committing to ambitious electrification goals until 2030 [1].

The digital transition, mainly led by the vehicle itself and the consumer experience with it, is shifting the automotive sector from hardware-oriented to software and digital services. Connectivity and autonomous driving were identified as topics under digitalization having a high degree of impact and uncertainty on the automotive industry [2]. Major auto manufacturers have started building toward a fully automated vehicle, with Advanced Driver Assistance Systems (ADAS) such as Adaptive Cruise Control (ACC), parking, and lane-keeping assist, already available. It is expected that level 4 automated vehicles will be available for sale in the next decade [3]. Autonomous functions heavily rely on onboard sensors such as radar, lidar, and camera systems. In parallel, innovation in the field of Information and Communications Technology (ICT) technology, such as Vehicle-to-Vehicle (V2V) and Vehicle-to-Infrastructure (V2I), has exemplified the possibilities of autonomous functions. V2V communication enables vehicles to communicate and access information about the current state (speed, position, and acceleration) of other surrounding V2V-enabled cars, and V2I communication provides information on traffic congestion, traffic light status, and local speed suggestions.

To align with climate change mitigation goals and digitalization trends, electric Connected and Autonomous Vehicles (CAVs) that maximize energy efficiency can be considered as an integrated approach to this end.

1.1 . Eco-X Strategies

While several efforts focus on safety, software, and sensing, energy has not been the core consideration in developing CAVs. Even with Electric Vehicles (EV)[1], overcoming barriers such as range anxiety and increased acceptance by the public requires new energy-efficiency measures. Energy-saving strategies, also referred to

[1]The acronym EV refers to battery electric vehicles in this thesis unless stated otherwise

as eco-strategies, can correspond to the control of traffic infrastructure or vehicles. The strategies on infrastructure include dynamic control of speed limits and traffic light duty cycles to influence macroscopic traffic parameters. Vehicle-level control strategies can be classified into two categories: Eco-Routing (ER) and Eco-Driving (ED). The former involves finding routes with the lowest energy cost or environmental impact. The latter, which forms the main focus of this thesis, corresponds to finding a speed trajectory on a given route that minimizes energy consumption. A brief overview of the planning and control layers of a CAV is shown in Fig. 1.1. Mission planning at the highest layer decides the route for a given origin and destination, and motion planning generates the speed trajectory.

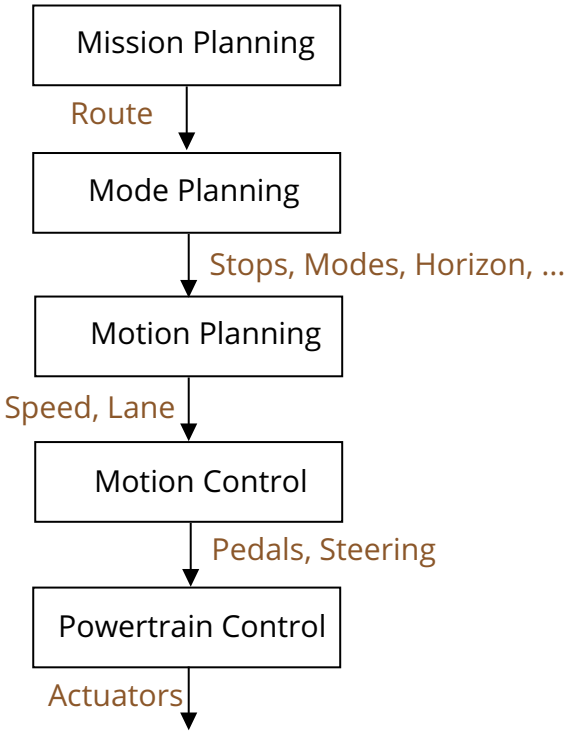

Figure 1.1: Logical Scheme of Planning and Control layers in a CAV

Some simple heuristic ED techniques acting directly on the vehicle speed or acceleration include maintaining a low and constant speed and smooth acceleration/deceleration. While these rules are intuitive and easy to implement, the true potential of ED can be achieved if it is regarded as a mathematical Optimal Control Problem (OCP). In such a framework, the OCP is formulated to minimize a cost while respecting all the motion constraints. In the context of ED, the energy (either electricity or fuel based on the powertrain) consumed is the minimized cost. The constraints a CAV is subject to can be twofold. The first is due to its physical actuators limitations, such as maximum torque or acceleration. The second depends on a CCAV's driving scenario, such as, avoiding a rear-end collision while

following a car or avoiding a lateral collision in an intersection. Formulation of such constraints requires guessing or predicting the surrounding vehicle behavior and traffic patterns.

1.2 . Cooperative Levels

With increased penetration of CAVs, opportunities increase to not only access current vehicle state information, but also deliberately exchange future intentions. Such behavior can ultimately reduce the need to predict the surrounding traffic patterns and vehicle behaviors or increase the certainty of such predictions, enabling better coordination and energy efficiency. Automated vehicles can also cooperate rather than compete for right of way giving rise to Cooperative Connected and Automated Vehicles (CCAVs). Such vehicles could be designed to exhibit altruistic behavior [4, 5] in coordinating their movements for a "common good", such as lowering traffic congestion or fleet energy consumption. Therefore, cooperation in this thesis refers to sharing of information and coordinating movements for a common good.

Based on the level of information shared and the motivation for energy efficiency, the behavior of CCAVs can be categorized into three types i.e., Non-Cooperative, Cooperative, and Centralized Cooperative ED strategies. In the Non-Cooperative ED (NC-ED), each CCAV optimizes for itself and shares only its instantaneous states with its neighbors (e.g., through measurements taken by other vehicles). In the Cooperative ED (C-ED) strategy, each CCAV still optimizes for itself but shares its future intentions with the neighboring vehicles. In the Centralized Cooperative ED (CC-ED), each CCAV's control action optimizes for the entire group. Figure 1.2 depicts the three levels of cooperation.

Several driving scenarios can be the object of ED. A few of them include accelerating to a cruise speed, cruising, green waving, eco-approach-and-departure, car-following/platooning, intersection crossing, and lane changing. This thesis will focus mainly on two ED scenarios, i.e.,platooning and intersection crossing.

1.3 . Car-Following/Platooning ED Scenario

A car-following ED scenario involves a vehicle closely following another while maintaining a safe inter-vehicle distance and minimizing energy consumption. Human drivers are often reactive when following other cars, as their view is usually blocked by the preceding vehicle. In fact, automated vehicles equipped with reactive control strategies such as ACC don't necessarily do better than convention baseline vehicles in terms of fuel economy [6]. Study [6], concluded that control algorithms relying upon the prediction of the preceding vehicle's future motion, consistently offered improvements in fuel economy. Accurately predicting the preceding vehicle's motion for the next few seconds is a challenging task. In fact, an

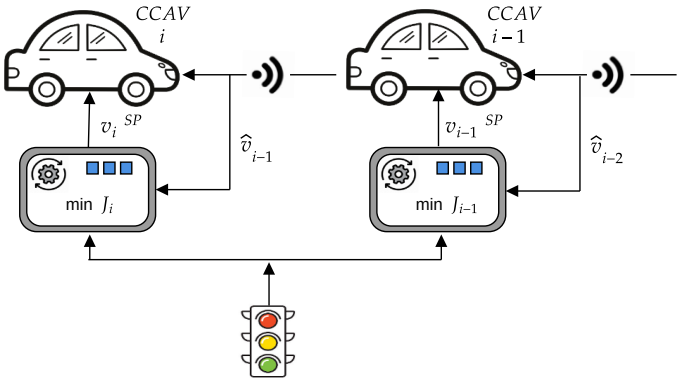

(a) NC-ED

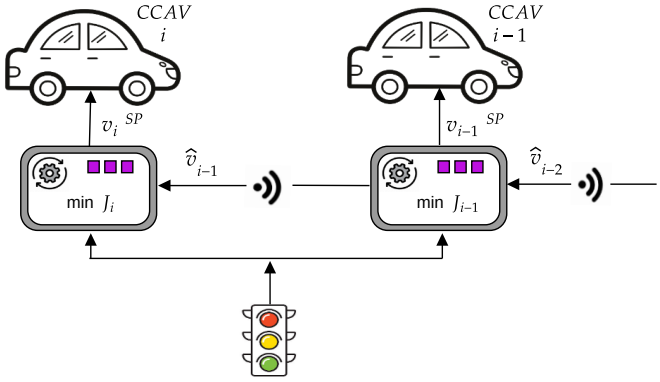

(b) C-ED

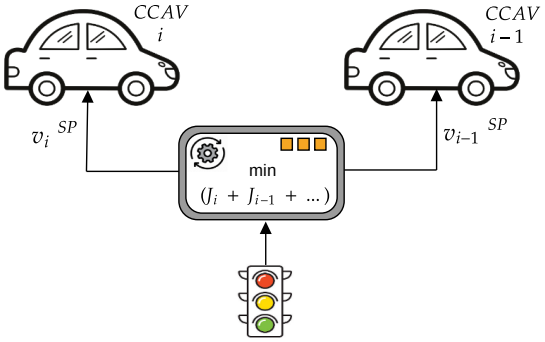

(c) CC-ED

Figure 1.2: Schematic showing the various cooperative schemes. Each CCAV is denoted by i, with v_i^{SP} and x_i representing the velocity set point and position of the i-th vehicle. $\hat{v}_{i-1}$ represents the velocity sensed (Non-Cooperative) or shared (Cooperative). The traffic lights communicate the SPaT information.

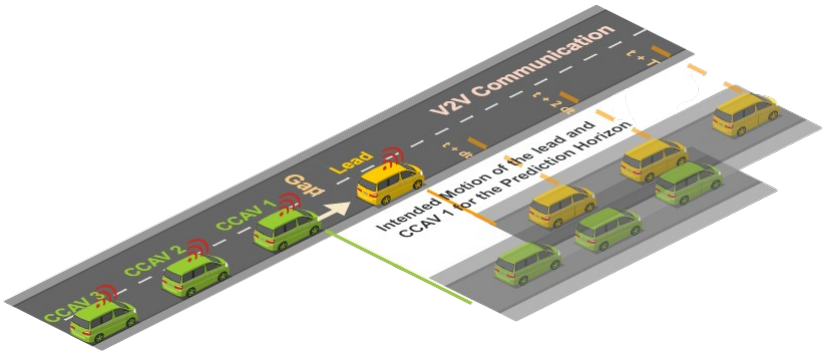

Figure 1.3: Schematic of eco-driving platooning scenario in a CCAV environment. Each CCAV communicates its intended motion to the following CCAV. This image was created on https://education.icograms.com/

inaccurate prediction could ultimately worsen energy consumption than a purely reactive control strategy [7, 8]. Aided with sensing capabilities CCAVs can sense the preceding vehicle's states and predict its motion using simple models such as constant velocity or constant acceleration to more complex non-linear and data-driven models. Prediction models for the preceding vehicle's motion form the basis of Chap. 3 of this thesis. In an environment of CCAVs, additional information via cooperative intention sharing from the preceding CCAV could improve prediction accuracy. Such a scenario is studied in Chap. 4. Note that each CCAV still optimizes for itself but only shares its intentions as stated in the Cooperative scheme.

A car-following scenario in which several vehicles coordinate in longitudinal formations is called platoons or strings. Tight platooning gained popularity for increased throughput. At short following distances, the aerodynamic drag coefficient is smaller especially in heavy-duty trucks, resulting in energy saving [9, 10]. In a platoon of CCAVs, each vehicle can share its intentions or coordinate its movements for a common goal, such as energy [11], string stability [12], or formation control [13], as in the Centralized Cooperative scheme. Information flow in platoons can vary from one implementation to another, such as, communication with predecessor only; with predecessor and leader only; or with predecessor, follower, and leader. A platooning scenario with intentions shared from the predecessor to the immediate follower is shown in Fig. 1.3. The study of different cooperative levels in a platooning ED scenario, formulated as an OCP, is the main focus of Chap. 4 of this thesis.

1.4 . Intersection ED Scenario

An intersection is a shared resource that only a limited number of vehicles can use simultaneously. In most intersections, priority is controlled by traffic lights with fixed timings scheduled offline or using stop signs. To reduce idling and improve

throughput, real-time traffic timing control using loop detectors measure traffic state to override the offline timetables. In a connected and automated environment,

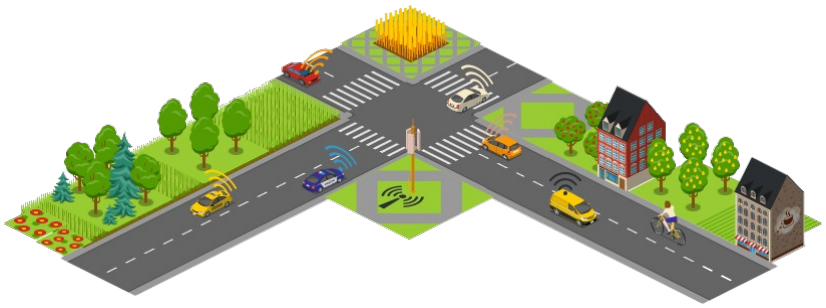

Figure 1.4: Schematic of eco-driving intersection scenario with a coordinator in a CCAV environment. This image was created on https://education.icograms.com/

intelligent traffic lights can communicate their Signal Phase and Timing (SPaT) to the upcoming CCAVs, allowing them to approach and depart the intersection to reduce travel time or energy consumption. The latter is often referred to as eco-approach-and-departure (eco-AND) in literature [14, 15]. However, with a 100 % penetration of CCAVs, vehicles can communicate and coordinate their arrival amongst each other or with a central coordinator, making physical traffic lights redundant. Such a scenario is depicted in Fig. 1.4. Some of the benefits of eliminating traffic lights in an all-automated environment are discussed in [16]. Chapter 5 of this thesis aims at finding ED speed profiles for CCAVs in an unsignalized intersection with varying levels of cooperation.

1.5 . Research Objective

Earlier works have studied the motion planning of CAVs in platooning and intersection crossing scenarios as a dynamic-constrained optimization problem. The studies predominantly consider their objective functions seeking to minimize either one or a combination of the following criteria: traffic congestion, energy consumption, or comfort. Scenario-specific objective functions, such as string stability in a platoon or criteria-based crossing order assignment in an intersection, are also considered in the formulation. Very few studies systematically evaluate the effects of cooperative behavior on energy consumption. Often solution methods to the motion planning optimization problem rely on numerical methods, and closed-form analytical solutions rarely exist. The various solutions methods to such problems can be categorized as variational, graph search, and incremental search sample [17]. Under this categorization, Pontryagin's Minimum Principle (PMP) is a variational approach that reduces the optimal control problem to a Two Point Boundary Value Problem (TPBVP), and the solution of such, if obtainable, leads to a closed-form

analytical solution. While numerical methods allow for complex non-linear formulations, their computation time limits them from a real-time implementation. In addition to being computationally fast, analytical solutions help us gain insight into system behavior, offering a clear view of how variables and interactions between them affect the result.

The main objectives of this thesis are as follows:

- To experimentally assess a known baseline Non-Cooperative ED strategy for a single CAV
- To obtain analytical eco-driving solutions for a fleet of electric CCAVs, with varying levels of cooperation, for platooning and un-signalized intersection scenarios
- To evaluate the influence of the varying levels of cooperation, namely, NC-ED, C-ED, and CC-ED, on fleet energy consumption.

1.6 . Thesis Outline

This thesis includes six chapters aiming to meet the stated research objective. Each chapter starts with a review of the relevant literature and the gaps in the topic addressed in it.

Chapter 2 This chapter reviews the works of a known baseline Non-Cooperative ED strategy for a single CAV [18, 19]. Its formulation, solution method, and implementation in unconstrained and car-following scenarios are discussed. The works presented in this chapter forms the basis for the rest of this thesis, especially chapters 4 to 6.

Chapter 3 The car-following scenario presented in Chap. 2 uses a simple Constant Acceleration (CA) model to predict the preceding/lead vehicle's motion to facilitate closed-form analytical solutions. However, more complex non-linear prediction models yield better prediction accuracy. Chap. 3 focuses on developing velocity predictors for a lead vehicle. Two predictors, namely, Constant Acceleration-Average Braking (CA-AB) and Enhanced Driver Model with Line-of-Sight Predictor (EDM-LOSP), are developed and applied to a mild-hybrid vehicle using Dynamic Programming (DP) based Eco-Driving Optimal Controller (EDOC). The performance of the proposed predictors is evaluated for energy efficiency and travel time.

Chapter 4 This chapter discusses the platooning ED scenario. Analytical solutions for an ED platoon of CCAVs are obtained for the three levels of cooperation. The performance of the algorithms is evaluated in terms of energy efficiency and string compactness against a standard ACC as the baseline. A theoretical analysis of the string stability of the three algorithms is also presented.

Chapter 5 The main objective of this chapter is to obtain analytical solutions to the ED problem of an electric CCAV crossing an un-signalized intersection subject to safety constraints. As in the platooning ED-Scenario, the aim is to explore the benefits of cooperation. However, only NC-ED and C-ED are presented and their results are evaluated in terms of energy consumption for varying traffic flows and compared against an Intelligent Driver Model (IDM) as a baseline

Chapter 6 This chapter accomplishes the first stated research objective. The baseline NC-ED strategy presented in Chapter 2 is implemented on an experimental setup involving a Renault Zoe electric car using a Visual Assistance System (VAS). The driver follows the advised speed on the VAS on a given route. The experiment results include a posteriori analysis of five trips on the impact of the assumptions made, namely traffic, traffic queue, and signal phase, on the predicted ED speed profiles.

Bibliography

[1] Caio Mazzi Alessandro Gasparotti Zinovia Panagiotidou Juna Dingemanse David Brown, Michael Flickenschild and Stefan Bratzel. The future of the eu automotive sector. Available at https://www.europarl.europa.eu/RegData/etudes/STUD/\2021/695457/IPOL$_$STU(2021)695457$_$EN.pdf (October 2021).

[2] Deloitte. The future of the automotive value chain - 2025 and beyond. Available at https://www2.deloitte.com/content/dam/Deloitte/us/Documents/\consumer-business/us-auto-the-future-of-the-automotive-value-chain.pdf (2017).

[3] Miranda Peterson Myriam Alexander-Kearns and Alison Cassady. The impact of vehicle automation on carbon emissions. Available at https://www.americanprogress.org/wp-content/uploads/2016/11/AutonomousVehicles-report.pdf (November 2016).

[4] Behrad Toghi, Rodolfo Valiente, Dorsa Sadigh, Ramtin Pedarsani, and Yaser P. Fallah. Social coordination and altruism in autonomous driving. IEEE Transactions on Intelligent Transportation Systems, 23(12):24791–24804, 2022.

[5] Erdem Biyik, Daniel A. Lazar, Ramtin Pedarsani, and Dorsa Sadigh. Altruistic autonomy: Beating congestion on shared roads. ArXiv, abs/1810.11978, 2018.

[6] Avi Chaim Mersky and Constantine Samaras. Fuel economy testing of autonomous vehicles. Transportation Research Part C: Emerging Technologies, 65:31–48, 2016.

[7] Eunjeong Hyeon. Speed Forecasting Strategies for the Energy-Optimal Car-Following of Connected and Automated Vehicles. PhD thesis, Michigan: Doctoral Thesis, 2022.

[8] Brackstone Mark and McDonald Mike. Car-following: a historical review. Transportation Research Part F: Traffic Psychology and Behaviour, vol. 2, no. 4:181–196, 1999.

[9] Assad Al Alam, Ather Gattami, and Karl Henrik Johansson. An experimental study on the fuel reduction potential of heavy duty vehicle platooning. In 13th International IEEE Conference on Intelligent Transportation Systems, pages 306–311, 2010.

[10] Sadayuki Tsugawa, Sabina Jeschke, and Steven E. Shladover. A review of truck platooning projects for energy savings. IEEE Transactions on Intelligent Vehicles, 1(1):68–77, 2016.

[11] Aaron Lelouvier, Jacopo Guanetti, and Francesco Borrelli. Eco-platooning of autonomous electrical vehicles using distributed model predictive control. 2017.

[12] William B. Dunbar and Derek S. Caveney. Distributed receding horizon control of vehicle platoons: Stability and string stability. IEEE Transactions on Automatic Control, 57(3):620–633, 2012.

[13] Mario di Bernardo, Alessandro Salvi, and Stefania Santini. Distributed consensus strategy for platooning of vehicles in the presence of time-varying heterogeneous communication delays. IEEE Transactions on Intelligent Transportation Systems, 16(1):102–112, 2015.

[14] Peng Hao, Guoyuan Wu, Kanok Boriboonsomsin, and Matthew J. Barth. Eco-approach and departure (ead) application for actuated signals in real-world traffic. IEEE Transactions on Intelligent Transportation Systems, 20:30–40, 2019.

[15] Haitao Xia, Guoyuan Wu, Kanok Boriboonsomsin, and Matthew J. Barth. Development and evaluation of an enhanced eco-approach traffic signal application for connected vehicles. 16th International IEEE Conference on Intelligent Transportation Systems (ITSC 2013), pages 296–301, 2013.

[16] A multiagent approach to autonomous intersection management. J Artif Intell Res, 31:591–656, 2008.

[17] Brian Paden, Michal Čáp, Sze Zheng Yong, Dmitry Yershov, and Emilio Frazzoli. A survey of motion planning and control techniques for self-driving urban vehicles. IEEE Transactions on Intelligent Vehicles, 1(1):33–55, 2016.

[18] Jihun Han, Ardalan Vahidi, and Antonio Sciarretta. Fundamentals of energy efficient driving for combustion engine and electric vehicles: An optimal control perspective. Automatica, 103:558–572, 2019.

[19] Antonio Sciarretta and Ardalan Vahidi. Energy-Efficient Driving of Road Vehicles. Springer, 2020.

2 - Eco-Driving Optimal Control for an Electric CCAV

This chapter introduces the known NC-ED baseline scenario.

2.1 . State-of-the-Art

Eco-driving aims to minimize energy consumption by adjusting the vehicle's speed directly or indirectly using ADAS advisory systems. With the advent of CCAVs, ED can be enforced more effortlessly and directly than with human drivers. As stated in the introduction, approaches to ED involve either using heuristics rules or more rigorous mathematical optimization formulation. While heuristic rules are generally intuitive, the full potential of ED can be achieved only if it is studied as OCP and implemented in a CCAV.

In the past decade, ED has been formulated as an OCP and solved using different methods [1] such as (i) Dynamic Programming (DP), (ii) Direct Methods and (iii) Indirect methods. DP was developed by Bellman [2], based on the principle of optimality to obtain globally optimal solutions. Reference [3] formulate an ED-OCP for an EV with a given route and the constraints defined by the route features and lead vehicle. Their solution obtained using DP shows a 19 $\%$ energy saving compared to constant acceleration/deceleration and cruising at constant speed. The authors in [4] obtained ED cycles for a Hybrid Electric Vehicle (HEV) using DP and investigated the trade-off between problem complexity and optimality. Other studies using DP to solve ED-OCP include [5, 6, 7]. While DP provides globally optimal solutions which serve as a benchmark, the "curse of dimensionality" leading to an increased computational burden, is a hurdle to real-time implementation. Efforts such as approximate DP [8] and GPU parallelization [9] try to overcome this drawback.

In a direct method, the OCP is discretized and transcribed into a finite-dimensional non-linear programming problem and solved using well-known optimization techniques. The direct method is predominantly used in the Model Predictive Control (MPC) framework. A reference velocity computed a priori, using DP, for a given route is tracked using MPC in [10], for ACC. Using direct methods, different collaborative levels in platoons and their influence on energy consumption and platoon length are studied in [11]. Other efforts include [12, 13]. While direct methods allow for complex problem formulation, non-linearity and non-convexity make it challenging to find an optimum properly.

An indirect method converts the optimization problem to a set of differential equations, required to satisfy conditions at its boundaries through applying Pontryagin's Minimum Principle (PMP) [14]. Such equations are referred to as

Boundary Value Problems (BVP). The optimal solution is found by solving for the system of differential equations that satisfies boundary and/or interior-point conditions. PMP facilitates analytical solutions that help understand theoretical mechanisms and provide explicable results if BVP is solvable. However, non-linearity and non-convexity remain a hurdle in solving them, and numerical methods, such as multiple shooting, collocation, etc., are often employed. Reference [15], proposed a Non-Cooperative EcoACC algorithm, where an ACC is formulated as an OCP (a running cost for the cruising mode and another for the following mode). The solutions are obtained numerically using an Iterative Pontryagin's Minimum Principle (iPMP) algorithm described in [15]. The authors extend their work in [16] using the same algorithm to Cooperative-EcoACC.

The authors in [17, 18] formulate an ED-OCP for an EV with non-linear vehicle dynamics and a detailed battery model. The control inputs are chosen as the powertrain traction u_p and the friction braking u_b force. The limits on u_p (i.e. $u_{p,max}$ and $u_{p,min}$) result from maximum and minimum (braking) motor torques, $T_{m,max}$ and $T_{m,min}$, respectively. Similarly, the maximum and minimum limits on u_b are given by $u_{b,max}$ and 0, respectively. The OCP is solved using PMP, and the optimal control input consists of six modes, namely,

- Maximal traction ($u_p = u_{p,max}$, $u_b = 0$)
- Optimal traction ($u_p = u_p^+$, $u_b = 0$)
- Coasting ($u_p = 0$, $u_b = 0$)
- Optimal powertrain braking ($u_p = u_p^-$, $u_b = 0$)
- Maximal powertrain braking ($u_p = u_{p,min}$, $u_b = u_0$)
- Maximal braking ($u_p = u_{p,min}$, $u_b = u_{b,max}$)

where u_p^+ and u_p^- are functions of the states and co-states. The switching between the modes is determined by the conditions on the co-states. The optimal velocity consists of up to six modes with different possible sequences of the control input determined by the boundary conditions. However, for a given set of boundary conditions, knowing the number of modes and the optimal sequence of these modes, a priori, is not trivial. Hence, numerical methods are used to obtain the optimal solution. Even assuming a mode sequence (e.g. a full six modes in the above order), it is generally impossible to obtain a closed-form solution. To facilitate BVP treatment, the OCP is simplified to obtain closed-form solutions [19, 18], that are fast to compute and real-time implementable. The authors extend their simplified formulation to include a lead vehicle (i.e., car-following) as a pure state-inequality constraint and present closed-form analytical solutions in [20].

Chapter Outline This chapter reviews the works of [18, 20, 17], where analytical closed-form solutions are presented. Sect. 2.2 describes the ED-OCP formulation, its solution using PMP, and its implementation. The assumptions made

to obtain the closed-form analytical solutions are also stated. Sect. 2.3 reviews the NC-ED car-following scenario presented in [20]. The addition of a lead vehicle as a state-inequality constraint to the ED-OCP in Sect. 2.2 is described. The solution to the constrained ED-OCP and its implementation are presented in Sect. 2.3.2 and Sect. 2.3.3, respectively. Sect. 2.5 presents concluding remarks. The solutions presented in this chapter form the basis for the rest of this thesis.

2.2 . Unconstrained - EDOC

This section aims to find the velocity profile that minimizes the battery energy consumption of an electric CCAV, going from velocity v_0 to V_f over a time T_f and a distance D_f.

2.2.1 . OCP Formulation

The formulation of an optimal control problem requires [21]: (i) a mathematical model describing the process to be controlled (ii) specification of the performance criterion or the objective function and (iii) the physical constraints.

2.2.1.1 . Vehicle Model

The longitudinal motion of the vehicle is captured by a simple model given by Newton's second law,

$$\begin{aligned} \dot{x} &= v, \\ m\dot{v} &= F_t - (F_a + F_r + F_g) - F_b, \\ &= F_t - \frac{1}{2}\rho_a c_d A_f v^2 - mgc_r - mg\sin(\alpha(x)) - F_b \ , \\ &= (F_t - F_R - F_b)/m \ , \end{aligned} \tag{2.1}$$

where F_t, F_a, F_r, F_g, and F_b are the traction force given by the powertrain at the wheels, the aerodynamic resistance, rolling resistance, resistance due to gravity and the mechanical breaking force, respectively. The states of the system, v and x, represent the velocity and position of the vehicle, respectively. m is the mass of the vehicle and $a = \dot{v}$ is the acceleration. Considering single-gear transmissions only, the inertial mass is constant and incorporated into m. The parameters that contribute to the aerodynamic drag are ρ_a, c_d, A_f, denoting the external air density, aerodynamic drag coefficient, and vehicle frontal area, respectively. The parameters contributing to the rolling and gravity resistances are c_r, the rolling resistance coefficient, g, the gravitational constant, and α, the road slope as a function of the position x. F_R represents the collective drag forces.

To facilitate closed-form analytical solutions, the non-linear vehicle model is linearised under the following assumptions:

- The resistive forces F_R/m are modelled as a constant h. This is generally a strong assumption. However, considering an electric city car traveling at low

speeds and low aerodynamic drags compared to a truck, the error introduced may be limited.

- Only regenerative braking is possible with the mechanical friction brakes absent (i.e. $F_b = 0$)
- The magnitude of the maximum and minimum acceleration is equal (i.e. $a_{max} = -a_{min}$)

Following the assumptions, the control input u is chosen as the net force produced by the powertrain per unit mass minus h, i.e., the acceleration a. The linearised vehicle model (state dynamics, f) reads:

$$\begin{aligned} \dot{x} &= v(t), \\ \dot{v} &= a(t) = F/m - h. \end{aligned} \tag{2.2}$$

2.2.1.2 . Objective Function

With the main goal to minimize battery energy consumption, the objective function/performance criterion J, is taken as the integral of the battery power $P_b(t)$ over the trip. A quadratic, physics-based, DC motor model [22] is given by

$$P_m = k_{m,0} + k_{m,1}\omega_m + k_{m,2}\omega_m^2 + k_{m,3}T_m\omega_m + k_{m,4}T_m^2 \tag{2.3}$$

where $k_{m,\{0,1,2,3,4\}}$ represent motor modelling parameters. The motor torque T_m and speed ω_m are related to v and a by

$$T_m = \frac{m(a+h)r_w}{\gamma_m \eta_t}, \quad \omega_m = \frac{\gamma_m v}{r_w}. \tag{2.4}$$

γ_m and r_w represent the transmission ratio and the wheel radius respectively. Assuming a constant efficiency battery model and no power link losses, the battery power P_b is related to a and v by

$$P_b(t) = \begin{cases} \frac{1}{\eta_b}\left(k_{m,0} + k_{m,1}\frac{\gamma_m v(t)}{r_w} + k_{m,2}\frac{\gamma_m^2 v^2(t)}{r_w^2} + k_{m,3}\frac{m(a(t)+h)v(t)}{\eta_t} + \right. \\ \left. \quad + k_{m,4}\frac{m^2 r_w^2 (a(t)+h)^2}{\gamma_m^2 \eta_t^2}\right), \quad a \geq 0 \\ \eta_b\left(k_{m,0} + k_{m,1}\frac{\gamma_m v(t)}{r_w} + k_{m,2}\frac{\gamma_m^2 v^2(t)}{r_w^2} + \right. \\ \left. \quad + k_{m,3} m(a(t)+h)v(t)\eta_t + k_{m,4}\frac{\eta_t^2 m^2 r_w^2 (a(t)+h)^2}{\gamma_m^2}\right), \quad a \leqslant 0 \end{cases} \tag{2.5}$$

The detailed battery power model is simplified (to facilitate analytical solutions) under the following assumptions:

- No transmission and battery loses, $\eta_t = \eta_b = 1$
- $k_{m,0} = k_{m,1} = k_{m,2} = 0$ and $k_{m,3} = 1$

to yield

$$P_b(t) = m(a(t) + h)v(t) + b(a(t) + h)^2, \tag{2.6}$$

where $b = k_{m,4}m^2r_w^2\gamma_m^{-2}$. With the running cost $P_b(t)$ defined, the objective function J over a trip is written as

$$J = \int_0^{T_f} m(a(t) + h)v(t) + b(a(t) + h)^2 \, dt. \tag{2.7}$$

2.2.1.3 . Constraints

Both control and state variables can be subject to constraints of the type, $g(a, \ldots) \leq 0$ and $g(x, v) \leq 0$, respectively. They are based on physical actuation limits, route features such as minimum and maximum speed limits or collision avoidance constraints such as rear-end and lateral collision. The control limits $a_{min} \leq a(t) \leq a_{max}$, result from the minimal and maximal (braking) motor torques, $T_{m,min}$ and $T_{m,max}$. The limits on the control input is relaxed to $a_{max} = -a_{min} \to \infty$ and, the state variables remains unconstrained.

2.2.1.4 . Problem

With simplified models (2.2), (2.6) and no constraints on the state and control variables, the eco-driving optimal control problem formulated in time domain reads:

$$\begin{aligned}
&\underset{a(t)}{\text{minimize}} \quad J = \int_0^{T_f} m(a(t) + h)v(t) + b(a(t) + h)^2 \, dt, \\
&\text{state dynamics} \\
&\qquad \dot{x} = v(t), \\
&\qquad \dot{v} = a(t), \\
&\text{boundary conditions } \mathcal{BC}: \\
&\qquad \{x(0) = 0, v(0) = v_0, x(T_f) = D_f, v(T_f) = V_f\}.
\end{aligned} \tag{2.8}$$

2.2.2 . Solution

The formulated optimal control problem (2.8) is solved using Pontryagin's Minimum Principle (PMP) [14] (see Appendix A.1).
Following PMP, the Hamiltonian H is formed as:

$$H = m(a(t) + h)v(t) + b(a(t) + h)^2 + \lambda(t)a(t) + \mu(t)v(t). \tag{2.9}$$

The variables $\lambda(t)$ and $\mu(t)$ are the two costates and have the following dynamics:

$$\begin{aligned}
\dot{\mu}(t) &= -\frac{\partial H}{\partial x} = 0 \Rightarrow \mu = \text{constant} \\
\dot{\lambda}(t) &= -\frac{\partial H}{\partial v} = m(a(t) + h) + \mu.
\end{aligned} \tag{2.10}$$

Boundary conditions for both λ and μ are free, since both the states are fixed at their boundaries. The optimal control input should minimize H and therefore

$$\begin{aligned} &\frac{\partial H}{\partial a} = mv(t) + 2b(a(t)+h) + \lambda(t) = 0, \\ &a(t) = -\frac{1}{2b}\left(mv(t) + \lambda(t)\right) - h. \end{aligned} \tag{2.11}$$

The optimal solution is obtained by solving the following Two-Point-Boundary-Value-Problem (TPBVP)

$$\begin{cases} \dot{x} = v(t), \\ \dot{v} = a(t), \\ \mathcal{BC} : \{x(0) = 0, v(0) = v_0, x(T_f) = D_f, v(T_f) = V_f\} \\ \dot{\mu} = 0, \quad \mu(0) = \mu_0, \\ \dot{\lambda} = -m(a(t)+h) - \mu, \quad \lambda(0) = \lambda_0, \\ a(t) = -\frac{1}{2b}\left(mv(t) + \lambda(t)\right) - h. \end{cases} \tag{2.12}$$

The optimal control trajectory $a(t)$ is explicitly obtained as and, it is an affine function of time,

$$a(t) = \left(\frac{4v_0}{T_f} - \frac{2V_f}{T_f} + \frac{6D_f}{T_f^2}\right) + \left(\frac{6v_0}{T_f^2} + \frac{6V_f}{T_f^2} - \frac{12D_f}{T_f^3}\right) t, \tag{2.13}$$

while the optimal trajectory $v(t)$, see Fig. 2.1, is a quadratic function of time [23, 24],

$$v(t) = v_0 + \left(-\frac{4v_0}{T_f} - \frac{2V_f}{T_f} + \frac{6D_f}{T_f^2}\right) t + \left(\frac{3v_0}{T_f^2} - \frac{6D_f}{T_f^3} + \frac{3V_f}{T_f^2}\right) t^2. \tag{2.14}$$

The associated energy consumption of the trip E_b, a function of vehicle parameters and boundary conditions, is given by

$$\begin{aligned} E_b = mhD_f + m\frac{V_f^2 - v_0^2}{2} + bh^2T_f + 2bh\left(V_f - v_0\right) + \\ +4b\left(\frac{3D_f^2}{T_f^3} - \frac{3D_f\left(v_0 + V_f\right)}{T_f^2} + \frac{v_0^2 + v_0V_f + V_f^2}{T_f}\right). \end{aligned} \tag{2.15}$$

Equation (2.14) represents a parabola and an admissible speed profile only for certain combinations of the boundary conditions. In particular, conditions of the type $F(D_f, T_f) \geq 0$ for specific v_0 and V_f define the domain of validity of the parabolic speed profile. These conditions impose that the speed is always positive, that its maximum does not exceed a given limit v_{max}, or that the control input does not exceed the limit a_{max}. The conditions on the domain of feasibility of the solution is detailed in [18]. When the solution (2.14), for a given v_0 and V_f, violates any of the above-specified conditions (constraints), the final boundary conditions D_f and T_f must be adjusted such that $F(D_f, T_f) \geq 0$.

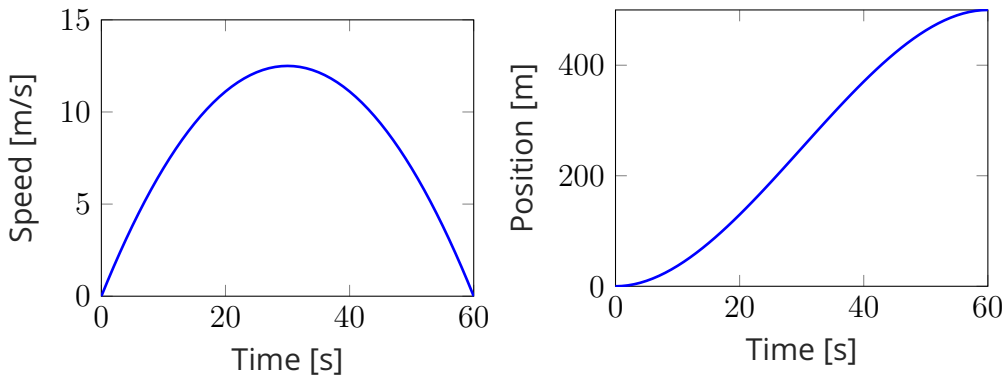

(a) (b)

Figure 2.1: Unconstrained Scenario: the parabolic speed profile (a) and the cubic position profile (b) for $v_0 = 0\ m/s, V_f = 0\ m/s, D_f = 500\ m$ and $T_f = 60\ s$.

2.2.3 . Implementation

The Eco-Driving-Optimal-Controller (EDOC) solution is embodied in a Model Predictive Control (MPC) framework to account for modeling uncertainties and closed-loop feedback. MPC is an iterative process where at each time t, based on the current measured system states and its surroundings (i.e. lead vehicles, traffic lights, etc.), an optimization over a finite horizon of length T and distance D is performed. Only the first value of the control input $a(0)$, from the resulting optimal control trajectory, $a(k),\ \forall k = 0, 1, \ldots, T$, is applied. At the next instance of t, the states are sampled again. The process is repeated but with updated boundary conditions, $\mathcal{BC} : \{0, , v(t), D = D_f - x(t), V = V_f\}$ and a shorter optimization horizon $T = T_f - t$. This fashion of MPC implementation, where the prediction horizon gets smaller as we move forward, is termed Shrinking Horizon Model Predictive Control. Figure 2.2 shows an example of MPC implementation. The blue parabola represents the predicted velocity over the horizon T, and the predicted acceleration at $k = 0$ is the applied optimal control input. Using (2.14), the equation of the predicted velocity following the boundary conditions in the MPC framework is given as,

$$v(k) = v(t) + \left(-\frac{4v(t)}{T} - \frac{2V}{T} + \frac{6D}{T^2}\right)k + \left(\frac{3v(t)}{T^2} - \frac{6D}{T^3} + \frac{3V}{T^2}\right)k^2, \quad k \in [0, T). \tag{2.16}$$

2.3 . Car-following: Non-Cooperative EDOC

A car-following scenario involves one vehicle closely following another while maintaining a safe inter-vehicular gap. In such a driving scenario, while the primary goal of the following vehicle is to maintain a safe distance to avoid a rear-end

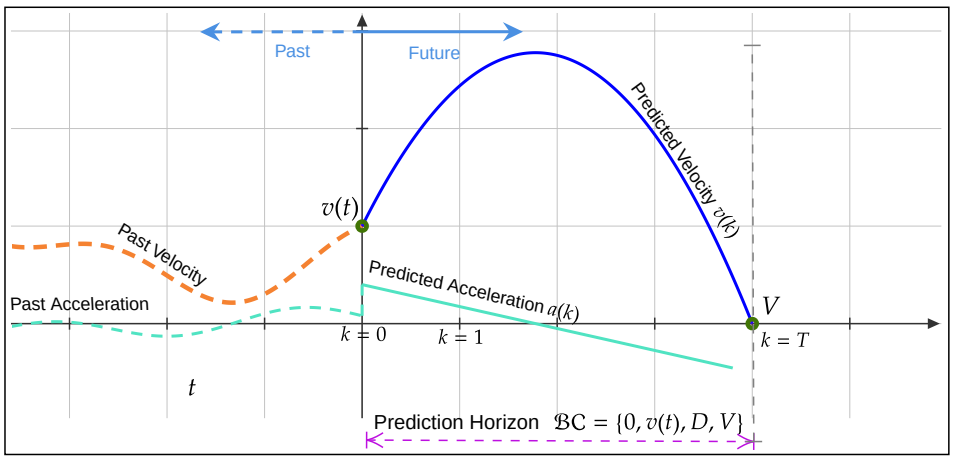

Figure 2.2: Model Predictive Control

collision, the inter-vehicle gap can be used as a degree of freedom to abrupt slow-downs [25] and increase the energy efficiency of the following vehicle.

2.3.1 . OCP Formulation

In this scenario, the following vehicle is a CCAV that is controlled, called the ego vehicle. The vehicle immediately ahead is called the lead vehicle, denoted by superscript l. The spacing gap, see Fig. 2.3, between the ego and lead vehicle, is defined as

$$\begin{aligned} \xi(t) &= x^l(t) - x(t) - L - s_{i,l}(t) \ , \\ \dot{\xi}(t) &= v^l(t) - v(t) \ , \end{aligned} \tag{2.17}$$

where $s_{i,l}$ is the minimum safe inter-vehicle distance, which can either be a constant, s_{min} (as in the case of 2.17), or resulting from a constant-time headway, $v(t)H$. In this scenario, the ego vehicle tries to avoid a rear-end collision with the lead vehicle, whose motion is predicted under constant acceleration assumption, given by,

$$x^l(t) = x_0^l + v_0^l t + \frac{1}{2} a^l t^2. \tag{2.18}$$

where the lead vehicle's initial velocity, position, and acceleration are represented by v_0^l, x_0^l and a^l, respectively. This imposes state inequality constraints $\xi(t) \geq 0$, of the type,

$$x(t) \leq x_0^l + v_0^l t + \frac{1}{2} a^l t^2, \quad t \in [0, T_f]. \tag{2.19}$$

Note that s_{min} and L are lumped in x_0^l.

2.3.2 . Solution

The optimal eco-driving speed profile in the presence of a lead vehicle is obtained by solving the optimal control problem (2.8), along with the constraint (2.19). To handle the state-inequality constraint, the indirect adjoining method

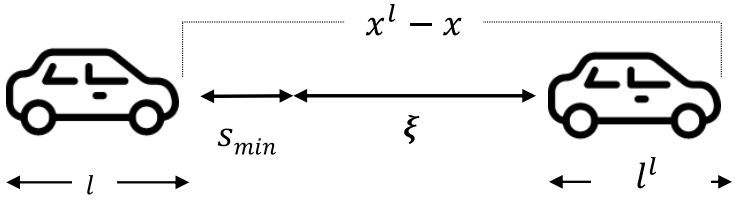

Figure 2.3: Car-Following scenario showing the spacing gap $\xi(t)$

[26] is used in this work (see Appendix A.2). The position constraint is rewritten in the form

$$\xi(t) = x(t) - (x_0^l + v_0^l t + a^l t^2/2) \leq 0. \tag{2.20}$$

and is of second order $(p = 2)$, where

$$\begin{aligned} \xi^{(1)} &= \dot{\xi} = v(t) - \left(v_0^l + a_0^l t\right), \\ \xi^{(2)} &= \ddot{\xi} = a(t) - a_0^l. \end{aligned} \tag{2.21}$$

The resulting tangency conditions are:

$$\left[\begin{array}{c} x(\theta) - (x_0^l + v_0^l \theta + a^l \theta^2/2) \\ v(\theta) - (v_0^l + a^l \theta) \end{array} \right] = 0, \tag{2.22}$$

where $\theta \in [0, T_f]$ represents the junction time. The position constraint can be active on a boundary interval or at a contact point. Here only the case of the contact point θ is considered. The Hamiltonian is adjoined with the term $\xi^{(2)}$ and multiplier η to form the Lagrangian,

$$L = H + \eta(a(t) - a^l), \tag{2.23}$$

where $\eta = 0$ if $\xi \leq 0$, $\eta \geq 0$ if $\xi = 0$. Additionally, we have $\frac{\partial \xi}{\partial v} = 0, \frac{\partial \xi^{(1)}}{\partial v} = 1$, $\frac{\partial \xi}{\partial x} = 1$ and $\frac{\partial \xi^{(1)}}{\partial x} = 0$. Therefore, the system of equations, along with (2.22), that needs to be solved reads,

$$\left\{ \begin{array}{l} \dot{x} = v(t), \\ \dot{v} = a(t), \\ \mathcal{BC} : \{x(0) = 0, v(0) = v_0, x(T_f) = X_f, v(T_f) = V_f\} \\ \dot{\lambda} = -m(a(t) + h) - \mu, \quad \lambda(0) = \lambda_0, \\ \dot{\mu} = 0, \quad \mu(0) = \mu_0, \\ a(t) = -\frac{1}{2b}(\lambda(t) + mv(t) + \eta(t)) - h, \\ \eta(t)\xi(x(t), t) = 0, \quad \eta(t) \geq 0, \quad \dot{\eta} \leq 0, \quad \ddot{\eta} \geq 0, \\ \lambda\left(\theta^-\right) = \lambda\left(\theta^+\right) + \pi_1, \\ \mu\left(\theta^-\right) = \mu\left(\theta^+\right) + \pi_0, \\ \pi_0 \geq 0, \quad \pi_1 \geq 0, \quad \pi_0 \xi(x(t), t) = 0, \quad \pi_1 \xi(x(t), t) = 0, \\ H\left(\theta^-\right) = H\left(\theta^+\right) + \pi_0(v_0^l + a^l \theta) + \pi_1 a^l \end{array} \right. \tag{2.24}$$

The constrained-optimal speed profile upon solving (2.24) is thus made up of two parabolic phases separated by θ, see Fig. 2.4. Explicitly, it reads

$$v(t) = \begin{cases} v_0 + \left(a^l + \dfrac{4\dot{\xi}_0}{\theta} + \dfrac{6\xi_0}{\theta^2}\right) t - \\ \quad - \left(\dfrac{6\xi_0}{\theta^3} + \dfrac{3\dot{\xi}_0}{\theta^2}\right) t^2, \quad t \in [0, \theta) \\ v_0^l + a^l\theta + \left(a^l - \dfrac{6\xi_0}{\theta^2} - \dfrac{2\dot{\xi}_0}{\theta}\right)(t-\theta) + \\ \quad + \left(V_f - 3v_0^l + 2v_0 - 6\dfrac{\xi_0}{\theta} - a_0^l T_f + 6\xi_0\dfrac{T_f}{\theta^2} + \right. \\ \quad \left. + 2\dot{\xi}_0\dfrac{T_f}{\theta}\right)\dfrac{(t-\theta)^2}{(T_f-\theta)^2}. \quad t \in [\theta, T_f] \end{cases} \tag{2.25}$$

where ξ_0 denotes ξ evaluated at $t = 0$. The contact time θ, that is, where the constraint is met ($\xi = 0$), is found by imposing the overall distance, which results in a cubic equation

$$\begin{aligned} &\left(v_0 - V_f + a^l T_f\right)\theta^3 + \left(4v_0^l T_f + V_f T_f - 2v_0 T_f + a^l T_f^2/2\right. \\ &\left. -3D_f\right)\theta^2 + \left(6\xi_0 T_f + v_0 T_f^2 - v_0^l T_f^2\right)\theta - \left(3\xi_0 T_f^2\right) = 0. \end{aligned} \tag{2.26}$$

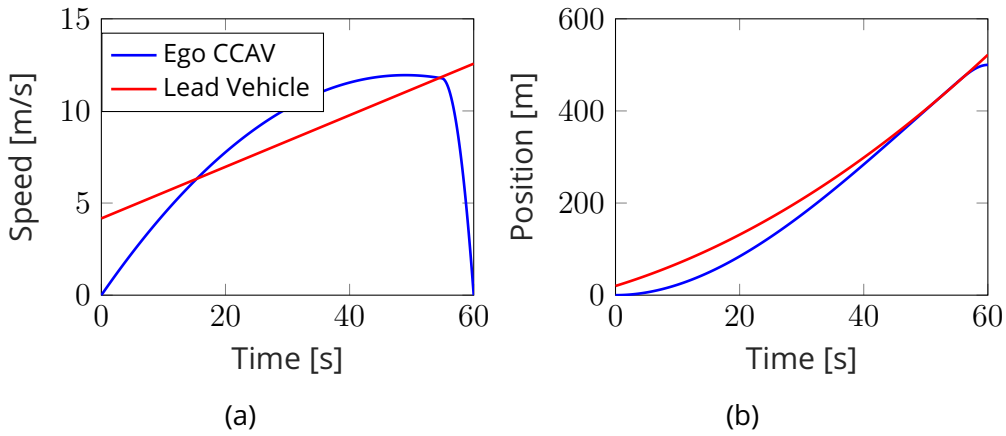

Figure 2.4: Car-Following Scenario: The speed (a) and position (b) profile of ego and lead vehicle. Boundary conditions: for $v_0 = 0\ m/s, V_f = 0\ m/s, D_f = 500\ m, T_f = 60\ s, x_0^l = 20\ m, v_0^l = 4.16\ m/s$ and $a^l = 0.14\ m/s^2$.

2.3.3 . Implementation

The lead vehicle's speed and acceleration are generally varying in time. Instead of using the initial measured states of the lead vehicle and performing a

single optimization at the start of the trip, the solutions are implemented in a shrinking horizon MPC. A new optimization is performed using the re-measured lead vehicle states at every single time step. The lead vehicle's initial states and acceleration become $x_0^l = x^l(t)$, $v_0^l = v^l(t)$ and $a^l = a^l(t)$. Figure 2.5 shows a flowchart illustrating the concept. The lead vehicle is detected using sensors, and its motion is predicted under constant acceleration. The $\mathcal{BC}$, obtained as explained in Sect. 2.2.3, along with lead vehicle constraint, is then passed to the optimal controller to obtain the optimal control input. Following the CCAV's motion, the actual position and speed serve as the feedback input to update the boundary conditions for the new iteration after each time step. With only the current/instantaneous information used in predicting the lead vehicle, we refer to this as the NC-ED car-following strategy.

Note that if the position trajectory of the lead vehicle does not intersect with the unconstrained position trajectory of the ego vehicle, the optimal solution given by (2.14) is used to obtain $a^*(t)$ in the EDOC block. On the other hand, if the lead vehicle's position trajectory intersects with the ego vehicle's unconstrained position trajectory, the optimal solution given by (2.25) is used.

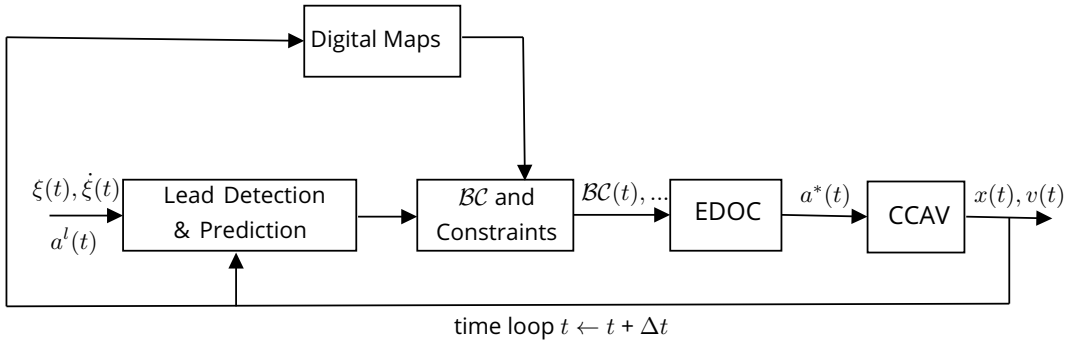

Figure 2.5: Conceptual sketch of a car-following EDOC

The first phase of position-constrained speed profile (2.25) with $\mathcal{BC}$ under MPC implementation is explicitly written as:

$$v(k) = v(t) + \left(a^l(t) + \frac{4}{\theta}\dot{\xi}(t) + \frac{6}{\theta^2}\xi(t)\right)k - \left(\frac{6}{\theta^3}\xi(t) + \frac{3}{\theta^2}\dot{\xi}(t)\right)k^2, \quad k \in [0, \theta), \quad (2.27)$$

and the contact point θ, (from 2.26), is given by

$$\begin{aligned}\Big(v(t)\ -V + a^l(t)T\Big)\,\theta^3 + \\ \Big(4v^l(t)T + VT - 2v(t)T + a^l(t)T^2/2 - 3D\Big)\,\theta^2 + \\ \Big(6\xi(t)T + v(t)T^2 - v^l(t)T^2\Big)\,\theta - 3\xi(t)T^2 = 0 \quad (2.28)\end{aligned}$$

Figure 2.6 shows an example of the NC-ED car-following strategy implemented using shrinking horizon MPC. Fig. 2.6a shows the lead vehicle and the CCAV's speed computed using the NC-EDOC. Fig. 2.6 shows the speed profile (blue) computed at every step and how the final speed is an envelope of its initial values.

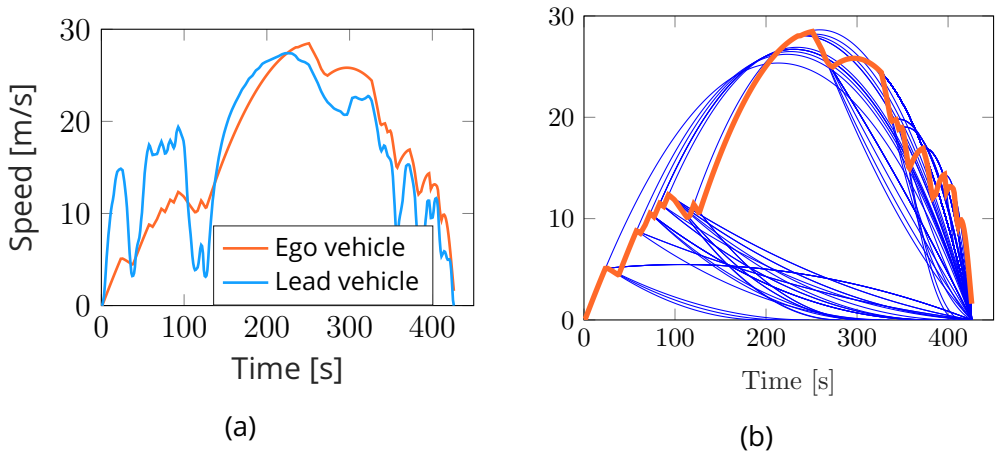

Figure 2.6: An example of the MPC implementation

2.4 . Energy Assessment Model

While the vehicle model is linearised (2.2) to facilitate closed-form analytical solutions, the performance of the algorithm are evaluated using a detailed non-linear backward vehicle model. This section describes the vehicle model in [11], that is subsequently used in Chap. (4), (5) and (6) to assess the energy consumption of the CCAVs. A Nissan Leaf is modeled using publicly available data where the motor speed ω_m and torque T_m are computed from the vehicle states, looking up the requisite motor power P_m, combining with auxiliary loads, and computing the total current to assess resistance losses.

The vehicle traction force F_t is computed from Newton's second law given by

$$F_t = ma + a_v + c_v v^2 \tag{2.29}$$

where the terms a_v and c_v represent the resistance force coefficients of the vehicle states in (2.1). A brake split model then apportions part of the total traction force F_t to the front-wheel-drive motor subject to vehicle dynamics constraints. The regeneration capacity of the front-wheel-drive is split based on the ratio given by

$$F_f = \begin{cases} F_t & \frac{F_t}{\underline{F}_t(v)} \leq 0.04 \\ 0.73F_t + 0.0108\underline{F}_t(v) & \frac{F_t}{\underline{F}_t(v)} > 0.04 \end{cases} \tag{2.30}$$

where $\underline{F}_t(v)$ is the maximum braking force (minimum traction force) that weakly depends on velocity. All $F_t < F_f$ is assumed to lost to mechanical friction brakes.

Assuming a constant drivetrain efficiency of 0.95, the motor torque and speed are computed using (2.4). A lookup table $P_m = f(\omega_m, T_m)$ maps the motor's speed and torque to its total power consumption, including motor and inverter losses, using data from [27]. Losses in the battery with resistance R_b and open-circuit voltage V_0 are then computed via the battery current i_b. The analysis models the power electrical system as a combined motor and auxiliary power sink of value P_l in parallel with the battery. Only one of the two possible solutions to (2.31) satisfies the battery current limit.

$$\begin{aligned} i_b &= \frac{V_0(SOC) \pm \sqrt{V_0^2(SOC) - 4R_b P_l}}{2R_b} \\ P_T &= P_l + i_b^2 R_b = V_0(SOC) i_b \end{aligned} \tag{2.31}$$

The total power P_T is then integrated to find the SOC and the cumulative energy consumption.

2.5 . Conclusion

This chapter reviewed the works in [18, 20, 17], where analytical closed-from solutions for eco-driving were obtained for an electric CCAV in an unconstrained and NC-ED car-following scenario. This work is considered the baseline NC-ED strategy in this thesis. The NC-ED car-following presented here predicted the lead vehicle's motion under constant acceleration to facilitate analytical closed-form solutions. The optimality of the EDOC iterative scheme in Fig. 2.5 is strongly affected by the quality of prediction of the preceding/lead vehicle. The next chapter focuses on predicting the lead vehicle's motion.

Bibliography

[1] Anil Rao. Trajectory optimization: A survey. Lecture Notes in Control and Information Sciences, 455:3–21, 03 2014.

[2] Richard Bellman. Dynamic programming. Science, 153(3731):34–37, 1966.

[3] Xiangrui Zeng and Junmin Wang. Globally energy-optimal speed planning for road vehicles on a given route. Transportation Research Part C: Emerging Technologies, 93:148–160, 2018.

[4] D. Maamria, K. Gillet, G. Colin, Y. Chamaillard, and C. Nouillant. Computation of eco-driving cycles for hybrid electric vehicles: Comparative analysis. Control Engineering Practice, 71:44–52, 2018.

[5] Felicitas Mensing, Eric Bideaux, Rochdi Trigui, and Helene Tattegrain. Trajectory optimization for eco-driving taking into account traffic constraints. Transportation Research Part D: Transport and Environment, 18:55–61, 2013.

[6] Sebastian van de Hoef, Karl H. Johansson, and Dimos V. Dimarogonas. Efficient dynamic programming solution to a platoon coordination merge problem with stochastic travel times 1 1this work was supported by the companion eu project, the knut and alice wallenberg foundation, the swedish research council, and the swedish strategic research foundation. IFAC-PapersOnLine, 50(1):4228–4233, 2017.

[7] Matteo Spano, Alessia Musa, Pier Giuseppe Anselma, Daniela Anna Misul, and Giovanni Belingardi. Battery electric vehicles platooning: Assessing capability of energy saving and passenger comfort improvement. In 2021 AEIT International Conference on Electrical and Electronic Technologies for Automotive (AEIT AUTOMOTIVE), pages 1–6, 2021.

[8] Shreshta Rajakumar Deshpande, Shobhit Gupta, Abhishek Gupta, and Marcello Canova. Real-Time Ecodriving Control in Electrified Connected and Autonomous Vehicles Using Approximate Dynamic Programing. Journal of Dynamic Systems, Measurement, and Control, 144(1), 01 2022. 011111.

[9] Zhaoxuan Zhu, Shobhit Gupta, Nicola Pivaro, Shreshta Rajakumar Deshpande, and Marcello Canova. A gpu implementation of a look-ahead optimal controller for eco-driving based on dynamic programming. In 2021 European Control Conference (ECC), pages 899–904, 2021.

[10] Sangjae Bae, Yeojun Kim, Jacopo Guanetti, Francesco Borrelli, and Scott Moura. Design and implementation of ecological adaptive cruise control for autonomous driving with communication to traffic lights. In 2019 American Control Conference (ACC), pages 4628–4634, 2019.

[11] R. Austin Dollar, Antonio Sciarretta, and Ardalan Vahidi. Information and collaboration levels in vehicular strings: A comparative study. IFAC-PapersOnLine, 53(2):13822–13829, 2020.

[12] Mahyar Vajedi and Nasser L. Azad. Ecological adaptive cruise controller for plug-in hybrid electric vehicles using nonlinear model predictive control. IEEE Transactions on Intelligent Transportation Systems, 17(1):113–122, 2016.

[13] Bart van Arem, Cornelie J. G. van Driel, and Ruben Visser. The impact of cooperative adaptive cruise control on traffic-flow characteristics. IEEE Transactions on Intelligent Transportation Systems, 7(4):429–436, 2006.

[14] Gamkrelidze L.S., Pontryagin; V.G. Boltyanskii; R.V. and Mishchenko E.F. The Mathematical Theory of Optimal Processes. Interscience Publishers, New York, 1962.

[15] Meng Wang, Winnie Daamen, Serge P. Hoogendoorn, and Bart van Arem. Rolling horizon control framework for driver assistance systems. part i: Mathematical formulation and non-cooperative systems. Transportation Research Part C: Emerging Technologies, 40:271–289, 2014.

[16] Meng Wang, Winnie Daamen, Serge P. Hoogendoorn, and Bart van Arem. Rolling horizon control framework for driver assistance systems. part ii: Cooperative sensing and cooperative control. Transportation Research Part C: Emerging Technologies, 40:290–311, 2014.

[17] Jihun Han, Ardalan Vahidi, and Antonio Sciarretta. Fundamentals of energy efficient driving for combustion engine and electric vehicles: An optimal control perspective. Automatica, 103:558–572, 2019.

[18] Antonio Sciarretta and Ardalan Vahidi. Energy-Efficient Driving of Road Vehicles. Springer, 2020.

[19] Antonio Sciarretta, Giovanni De Nunzio, and Luis Leon Ojeda. Optimal eco-driving control: Energy-efficient driving of road vehicles as an optimal control problem. IEEE Control Systems Magazine, 35(5):71–90, 2015.

[20] Jihun Han, Antonio Sciarretta, Luis Leon Ojeda, Giovanni De Nunzio, and Laurent Thibault. Safe- and eco-driving control for connected and automated electric vehicles using analytical state-constrained optimal solution. IEEE Transactions on Intelligent Vehicles, 3(2):163–172, 2018.

[21] Donald Kirk E. Optimal Control Theory:An Introduction. Dover Publications, New York, 2004.

[22] W. Dib, L. Serrao, and A. Sciarretta. Optimal control to minimize trip time and energy consumption in electric vehicles. In 2011 IEEE Vehicle Power and Propulsion Conference, pages 1–8, 2011.

[23] Wissam Dib, Alexandre Chasse, Philippe Moulin, Antonio Sciarretta, and Gilles Corde. Optimal energy management for an electric vehicle in eco-driving applications. Control Engineering Practice, 29:299–307, 2014.

[24] Nicolas Petit and Antonio Sciarretta. Optimal drive of electric vehicles using an inversion-based trajectory generation approach. IFAC Proceedings Volumes, 44(1):14519–14526, 2011. 18th IFAC World Congress.

[25] Md. Abdus Samad Kamal, Jun-ichi Imura, Tomohisa Hayakawa, Akira Ohata, and Kazuyuki Aihara. Smart driving of a vehicle using model predictive control for improving traffic flow. IEEE Transactions on Intelligent Transportation Systems, 15(2):878–888, 2014.

[26] Richard F. Hartl, Suresh P. Sethi, and Raymond G. Vickson. A survey of the maximum principles for optimal control problems with state constraints. SIAM Review, 37(2):181–218, 1995.

[27] T Burress. Benchmarking state-of-the-art technologies. in oak ridge national laboratory, 2013 us doe hydrogen fuel cells program vehicle technologies program annual merit review peer evaluation meet- ing., 2013.

3 - Lead Vehicle Prediction

This chapter discusses predicting lead vehicle velocity trajectories.

3.1 . State-of-the-Art

Advancements in navigation systems and Vehicle-to-Everything (V2X) communication have given access to a wealth of information from the environment and infrastructure, such as traffic density, location, and velocity of surrounding vehicles, upcoming road topology, grade, speed limits, etc. CCAVs can access such information to improve safety and comfort and employ it in their ED control strategies [1, 2, 3, 4]. Despite the energy efficiency improvements and other benefits demonstrated by these technologies, uncertainties in the traffic environment can limit the ability of eco-driving controllers to smoothen the velocity profile. They might eventually lead to a decline in energy savings [5]. For the real-time implementation of EDOC with consistent energy savings, it becomes necessary to include the dynamics of the traffic, especially the estimated future lead vehicle velocity into the ED's trajectory planning process.

Considering a car-following scenario with two vehicles, the lead vehicle here refers to the immediately preceding vehicle to the ego CCAV. Predicting a lead vehicle's speed trajectory is vital in improving the safety and energy consumption of CCAVs. In fact, inaccurate prediction, irrespective of the powertrain, may lead to an overreaction of the ego CCAV, causing unwanted accelerations/decelerations and ultimately worse energy consumption than a purely reactive control strategy [5, 6].

Predicting a vehicle's speed is highly dependent on the amount of information on that vehicle and its surroundings, and the used prediction method. A comprehensive overview of the existing prediction methods using model-based and data-driven techniques can be found in [7]. The ego CCAV can obtain information on the lead vehicle and its surroundings using either sensor, as in NC-ED, and/or V2X communication, as in C-ED. The methods found in the literature for predicting speed trajectories can be broadly classified as data-driven or model-based.

Data-driven time-series prediction methods such as Long-Short-Term-Memory (LSTM) [1, 11], or gated recurrent network [12], have been extensively used to perform mid-long length speed predictions. However, these methods require the availability of extensive training data and/or V2V communication.

Model-based approaches include simple models such as constant velocity and Constant Acceleration (CA). The constant velocity predicts the lead vehicle to maintain the current speed over the future prediction horizon, while the CA assumes the vehicle's future speed to move with the same acceleration until it stops or exceeds a maximum velocity. However, these models lack adaptability to variations in

driving styles and, in certain cases, are unrealistic. More sophisticated microscopic car-following models such as the Intelligent Driver Model [8], the Line-Of-Sight-based Enhanced Driver Model (EDM-LOS) [9], or Gipps' model [10], which are, in principle, used to model driver behavior, could also be used to predict the lead vehicle's velocity. Such microscopic models include parameters for driving style calibration, allowing to capture of various driver behaviors. While model-based methods lose accuracy over long-term prediction, they perform reasonably well in the short-term horizon, which is the main focus of this chapter.

This chapter compares two methods to predict the lead vehicle velocity over a short-term horizon in the absence of connectivity (V2V/V2X) or under data-restricted cases. In such scenarios, the prediction must rely only on the lead vehicle's measured position and relative velocity at the current time, as in the Non-Cooperative eco-driving (NC-ED). Two methods are considered in this study, namely, a Constant Acceleration (CA) model and a Line-of-Sight based Enhanced Driver Model (EDM-LOS). The CA uses the lead vehicle's current measured velocity and acceleration vehicle to forecast the future velocity for short instances of time. However, when approaching a fixed obstacle such as a traffic light or an intersection, the CA model prediction may become inaccurate, resulting in the inability to correctly stop the ego vehicle at the intersection correctly. On the other hand, the EDM-LOS model, without the information about the vehicle preceding the lead vehicle, fails to predict braking events during car-following.

This work was conducted during a research exchange semester at the Center for Automotive Research (CAR) at The Ohio State University, and its contributions are as follows. Two lead vehicle velocity predictors are developed: Constant Acceleration-Average Braking (CA-AB) and EDM-LOS based Predictor (EDM-LOSP). The CA-AB is an improved model over CA in predicting decelerations to a stop in the presence of an obstacle. The EDM-LOSP is an improved model over EDM-LOS to identify and predict braking events during car-following. The proposed prediction strategies are applied to a dynamic programming-based EDOC for a mild Hybrid Electric Vehicle (mHEV) developed at CAR [13]. A DP-based EDOC allows the implementation of non-linear prediction models like the EDM-LOSP. The performance of the proposed predictors is evaluated for energy efficiency and travel time in a simulation-based environment using real-world driving profiles. They are compared against CA as a baseline and an ideal scenario with perfect velocity prediction (wait-and-see) as a benchmark.

Chapter Outline Section 3.2 describes the two methods, CA-AB and EDM-LOSP, developed for leader velocity prediction. The following section describes the application of the developed predictors to an EDOC for an mHEV. The formulation, solution method, and implementation are presented in the section. The simulation results in Sect. 3.3.4 discuss evaluating the predictors' performance using real-world drive cycles. Concluding remarks are given in Sect. 3.4.

3.2 . Lead Vehicle Velocity Prediction

The two models considered in this work to predict the lead vehicle velocities are the CA-AB and the EDM-LOSP. These models result from improvements made to the CA, and EDM proposed in literature [2, 3, 9]. This section describes the CA and EDM-LOS models, their drawbacks, and the improvements made leading to the CA-AB and EDM-LOSP. Note that all predictions over a horizon length N_H, are denoted using $\hat{(.)}$, and observed/measured signals are represented using $(.)_0$.

3.2.1 . Constant Acceleration-Average Braking (CA-AB)

The CA model predicts the future velocity of the lead vehicle to have a constant acceleration until it stops or reaches the speed limit [16]:

$$\hat{a}^l(t) = \begin{cases} a_0, & \hat{v}^l(t) < v_{lim} \\ 0, & \hat{v}^l(t) \geq v_{lim} \vee \hat{v}^l(t) = 0 \end{cases} \tag{3.1}$$

where a_0^l represents the lead vehicle's acceleration measured at the start of prediction (i.e. $t = 0$) and $\hat{a}^l$ represents the predicted acceleration. The speed limit of the route is given by v_{lim}. However, the CA model cannot correctly predict where the lead vehicle will stop when approaching an obstacle, such as a traffic light or a stop sign. The prediction could result in the lead vehicle stopping either before or after the obstacle. To overcome this drawback, the measured acceleration a_0^l is here replaced with an average braking acceleration $\tilde{a}$, defined as:

$$\tilde{a} = \frac{{v_0^l}^2}{2(D_{TL} - x_0^l)} \tag{3.2}$$

where D_{TL} represents the position of the traffic light, x_0^l and v_0^l represent the lead vehicle's position and velocity measured at $t = 0$. Note that this model formulation implies that the ego CCAV has access to V2I information, namely road grade, speed limits and location of stop signs and traffic signals within the N_H prediction horizon. Equation (3.2) represents the minimum kinematic deceleration required by the lead vehicle to come to a stop at the obstacle. The modes of the CA-AB can be summarized as follows:

$$\hat{a}^l(t) = \begin{cases} a_0, & \hat{v}^l(t) < v_{lim} & (FD) \\ 0, & \hat{v}^l(t) \geq v_{lim} \vee \hat{v}^l(t) = 0 & (FD) \\ \tilde{a}, & & (S). \end{cases} \tag{3.3}$$

FD and *S* stand for freeway driving and stop mode, respectively. The stop mode is activated in the presence of either a stop sign or a traffic light with a red signal phase within N_H.

3.2.2 . Enhanced-Driver-Model with Line-of-Sight based Predictor (EDM-

LOSP)

The existing EDM-LOS is a deterministic velocity predictor representing various levels of driver aggressiveness, [4]. The EDM-LOS includes three distinct operating modes, namely, Car-Following *(CF)*, Freeway Driving *(FD)* and Stop Mode *(S)*. The different operating modes are represented by the following equations:

$$\hat{a}^l(t) = \begin{cases} a_{max}\left(1 - \left(\frac{\hat{v}^l(t)}{v_{lim} - \theta_0}\right)^{\delta}\right), & v_0^l \leq v_{lim}, \quad (FD) \\ a_{max}\left(1 - \left(\frac{\hat{v}^l(t)}{\hat{v}^{l-1}(t)}\right)^{\delta} - \left(\frac{\Delta x^*\left(\hat{v}^l, \Delta v\right)}{\Delta x^l(t)}\right)^2\right), & (CF) \\ -\frac{1}{b}\left(\frac{\hat{v}^l(t)^2}{2\Delta x^l(t)}\right)^2, & (S) \end{cases} \tag{3.4}$$

where

$$\begin{aligned} \Delta x^l(t) &= \hat{x}^{l-1}(t) - \hat{x}^l(t) - l^{l-1} \\ \Delta x^*\left(\hat{v}^l, \Delta v\right) &= s_{min} + \frac{\hat{v}^l(t)\left(\hat{v}^{l-1}(t) - \hat{v}^l(t)\right)}{2\sqrt{a_{max} b}} \\ s_{brake}(t) &= \left(1 + \frac{c_1}{\delta}\right)\left(\frac{\hat{v}^{l^2}(t)}{2b}\right). \end{aligned} \tag{3.5}$$

The terms $\hat{v}^l(t)$ and $\hat{x}^l(t)$ represent the lead vehicle velocity and position, respectively. $[a_{max}, \delta, b, c_1, \theta_0]$ are the set of EDM-LOS calibration parameters. Freeway driving represents the transition to the route speed limit without any vehicle preceding the lead vehicle. The degree of aggressiveness is further characterized by a calibration term θ_0, which determines the offset from the route speed limit. As per this formulation, a relatively relaxed driver would drive slightly below the speed limit. The maximum acceleration, a_{max}, and driver aggressiveness, δ, controls how quickly the desired speed is achieved. Regarding the car-following mode, $\hat{x}^{l-1}(t)$ and $\hat{v}^{l-1}(t)$ represent the predicted position and speed of the vehicle preceding the lead vehicle. The terms $\Delta x^l(t)$ and Δx^* represents the current and the desired gap between the lead and the vehicle preceding the lead vehicle, respectively. The term b in the Stop mode represents the comfortable deceleration. When approaching an obstacle, such as a traffic light, the deceleration usually does not exceed b and is dynamically self-regulating towards a situation in which the kinematic deceleration equals b [3]. The driver's aggressiveness in braking distance is captured by s_{brake}, which is dependent on a calibration term c_1/δ.

The Line-Of-Sight (LOS) scheme in the EDM is used to realistically model the driver response when approaching a traffic light. The LOS is a distance parameter below which, in the presence of a traffic light, the driver can preview the signal phase of the upcoming traffic light. The presence of a traffic light at D_{TL} sets the flag $TL = 1$, when $D_{TL} - x_0^l \leq$ min(LOS,N_H). The driver performs a stopping maneuver (S) under two conditions, namely either if the previewed signal phase is

red or, the signal phase is yellow and $x_0^l > s_{brake}$. The term $\Delta x^l(t)$ now becomes

$$\Delta x^l(t) = D_{TL} - \hat{x}^l(t). \tag{3.6}$$

Therefore, stop mode is activated when:

$$S = \begin{cases} 1, & TL = 1, \text{Red Light}, x_0^l \leq \text{LOS} \\ 1, & TL = 1, \text{Yellow Light}, s_{brake}(t) < x_0^l \leq \text{LOS}. \end{cases} \tag{3.7}$$

A detailed rule-based logic using LOS in the presence of a stop sign or traffic light is described in [15].

In the CF mode, the absence of V2V communication makes the information on $\hat{x}^{l-1}(t)$ and $\hat{v}^{l-1}(t)$ unavailable for the ego vehicle to predict the car-following behavior, in particular deceleration events, of the lead vehicle. To overcome this, a modification of the freeway driving and stop mode equations are developed here (EDM-LOSP). The prediction of the lead vehicle's transition to the desired speed in the FD mode uses only the current velocity, which is obtained by setting $\hat{v}^l(0) = v_0^l$ in (3.4). Given the availability of the current acceleration a_0^l, it is possible to replace a_{max} with:

$$a_m = \frac{a_0^l}{1 - \left(\frac{v_0^l}{v_{lim} - \theta_0}\right)^{\delta}}. \tag{3.8}$$

Along with initial condition $\hat{v}^l(0) = v_0^l$, replacing a_{max} with a_m ensures that the first predicted acceleration $\hat{a}^l(0) = a_0^l$. Ideally, this results in a perfect prediction for the first step, as in the case of a constant acceleration assumption. In addition, EDM-LOS is sensitive to the calibration parameters, in particular a_{max} and δ. The set of EDM parameters about the lead vehicle are generally unknown to the ego CCAV. When modelling driver behavior using EDM-LOS, these parameters are either calibrated offline from recorded driving data [16] or using online estimation techniques [17]. Replacing a_{max} with the available current acceleration a_0^l reduces some of the sensitivity. While the other parameters δ and θ_0 still allow to capture different driver aggressiveness. The FD mode is employed when the current acceleration a_0^l is non-negative. When a_0^l is negative and there is no traffic light within N_H, the lead vehicle is assumed to brake because of the vehicle in front of the lead vehicle. Since the car-following mode in EDM-LOS cannot be employed, the stop mode is modified to predict the braking behavior. The comfortable deceleration b is replaced by the current acceleration a_0^l and $x^{l-1}(t)$ term in $\Delta x^l(t)$ is replaced by assuming the lead vehicle is decelerating to a fixed obstacle at a position given by

$$\frac{{v_0^l}^2}{2|a_0^l|}. \tag{3.9}$$

One can observe that doing the above modifications to the stop mode results in converting to a constant acceleration model, as shown in Appendix A.3. Incorpo-

rating the current acceleration a_0^l of the lead vehicle, the equations of EDM-LOSP is summarized as:

$$\hat{a}^l(t) = \begin{cases} a_m \left(1 - \left(\frac{\hat{v}^l(t)}{v_{lim} - \theta_0}\right)^{\delta}\right), & v_0^l \leq v_{lim}, a_0^l \geq 0 \\ \left(\frac{1}{a_0^l}\right) \left(\frac{\hat{v}^{l^2}(t)}{2\left(\frac{v_0^{l^2}}{2|a_0^l|} - x^l(t)\right)}\right)^2, & a_0^l < 0 \\ -\left(\frac{1}{b}\right) \left(\frac{\hat{v}^{l^2}(t)}{2\left(D_{TL} - x^l(t)\right)}\right)^2, & S = 1 \end{cases} \tag{3.10}$$

3.2.3 . Comparison of Predictor Performance

To highlight and compare the performance of the proposed predictors, a short driving profile was experimentally collected and used as reference for the lead vehicle velocity. The speed prediction performance was quantified by computing the Root-Mean-Square-Error (RMSE) between the actual and predicted speed. Prediction horizon lengths of 5, 10 and 15 seconds are evaluated for each predictor. The results are summarized in Table 3.1, showing the CA-AB and EDM-LOSP performing better over their counterparts. Figure 3.1 provides a visual description of how each velocity predictor performs (10 s prediction horizon) during a portion of the driving profile. The difference between CA and CA-AB can be mostly appreciated when the lead vehicle speed goes to zero in the presence of red phase traffic light (e.g. around 80 s). The CA does not predict the velocity to stop at the traffic light, as seen from the red dashed lines close to 80 s. Indeed, a longer prediction horizon causes the velocity to pass the traffic light. The proposed CA-AB uses $\tilde{a}$ in the place of a_0^l, hence predicting the lead vehicle stop at the traffic light. Summarizing, the advantages of using CA-AB over CA can be appreciated more in urban routes, due to the high traffic light and stops density. The portions of decreasing velocities of the lead vehicle, apart from the traffic light, for instance at 10 s, 25 s and 50 s are due the presence of vehicles preceding the lead vehicle. This behavior, given the availability of information on the vehicle preceding the lead, is predicted using the CF mode in EDM-LOS. However, without that information, this predictor assumes the lead vehicle to always be in FD mode forecasting its velocity to reach a desired speed. The proposed EDM-LOSP overcomes this by identifying ($a_0^l < 0$) and predicting decelerations using the second mode above mentioned in (3.10).

3.3 . Application to NC-EDOC for a mild-Hybrid Electric Vehicle

This section describes the application of the prediction models, CA-AB and EDM-LOSP, to a mild HEV (mHEV) ego CCAV in a car-following scenario. The

Table 3.1: RMSE of different speed predictors for 5 s, 10 s and 15 s prediction horizon

Prediction Horizon, s	CA	CA-AB	EDM-LOS	EDM-LOSP
5	1.00	0.97	1.80	0.81
10	2.63	2.40	2.70	2.24
15	3.67	3.45	3.47	3.15

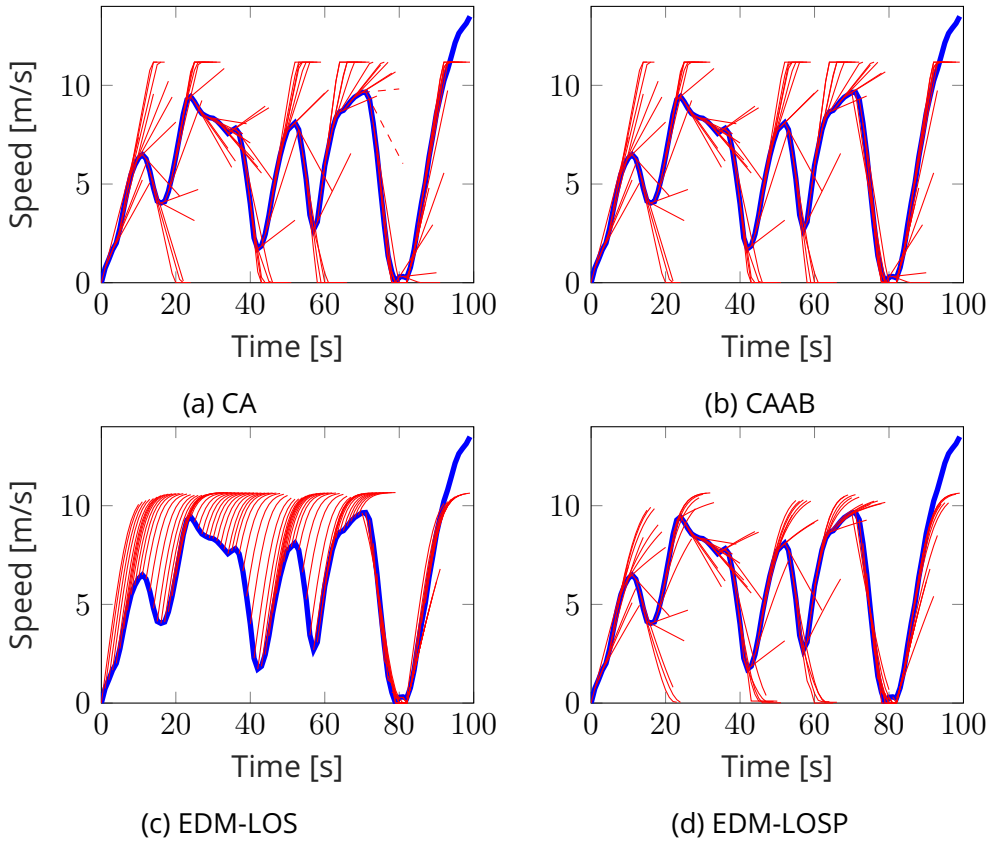

(a) CA (b) CAAB

(c) EDM-LOS (d) EDM-LOSP

Figure 3.1: Speed predictions of the different for a 10 s prediction window. In red, the velocities forecasted at each time step while in blue the actual lead vehicle speed

ego CCAV is equipped with a DP based EDOC developed in [13]. The various subsections,3.3.1 to 3.3.3, describe the OCP formulation, solution method and implementation of EDOC. Section 3.3.4 presents the simulation results.

3.3.1 . OCP Formulation

The main objective of the ego CCAV is to minimize the fuel consumption and travel time of the CCAV over an entire itinerary. The ED-OCP presented here is

formulated in a discrete spatial domain.

3.3.1.1 . Vehicle Model

A forward-looking model of a P0 parallel mild-hybrid electric vehicle, see Fig. 3.2, is adopted in this work to predict the longitudinal dynamics and energy consumption, [13]. A Belted Starter Generator (BSG) is connected to a 1.8 L turbocharged gasoline engine and a 48 V battery pack. The vehicle is modeled considering only the longitudinal dynamics given by the time-continuous counterpart in (2.1). The powertrain components of the mHEV, such as the engine (fuel maps), BSG (torque limit and efficiency maps), torque converter, and transmission, are modeled using maps as a quasi-static representation. The battery is modeled using a zeroth order equivalent circuit comprising an ideal voltage source and a resistor. The detailed equations of the powertrain component's model and the validation are described in [13].

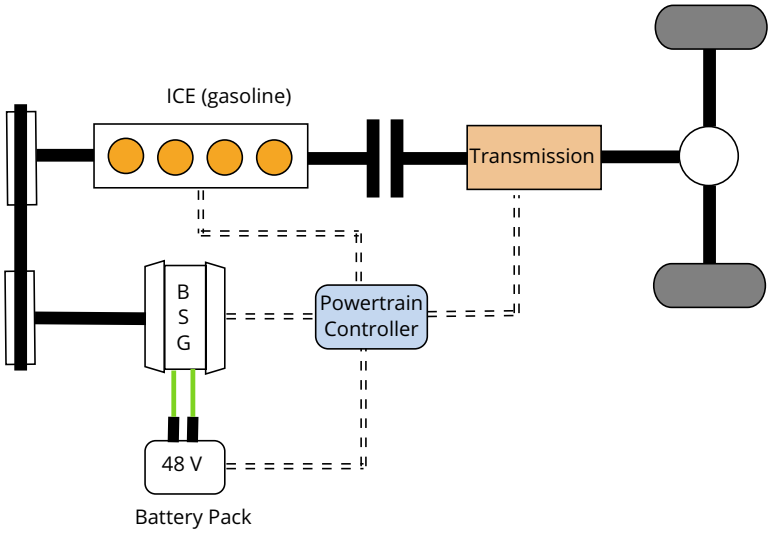

Figure 3.2: Schematic of a P0 parallel mild Hybrid Vehicle

The state variables are chosen as the vehicle velocity, battery state of charge (SoC), and travel time: $\mathcal{X}_x = [v_x, \mathcal{E}_x, t_x]^T$. The engine torque and BSG torque are chosen as the control variables: $u_x = [T_{eng}, T_{bsg}]^T$. The discretized state dynamic equations, collectively represented by f, in the spatial domain is given as

$$\begin{aligned} v_{x+1}^2 &= v_x^2 + 2\Delta d_x \frac{(F_{t,x}(\mathcal{X}_x, u_x) - F_{R,x}(v_x) - F_b)}{m} \\ \mathcal{E}_{x+1} &= \mathcal{E}_x - \frac{\Delta d_x}{\bar{v}_x} \frac{\bar{I}_{batt,x}(\mathcal{E}_x, T_{bsg,x})}{C_{nom}} \\ t_{x+1} &= t_x + \frac{\Delta d_x}{\bar{v}_x} \end{aligned} \tag{3.11}$$

where Δd_x is the distance over one step, i.e. $\Delta d_x = d_{x+1} - d_x$, and d_x is the distance traveled along the route at position x. The average velocity over one step

is given by $\bar{v}_x(=\frac{v_x+v_{x+1}}{2})$. The battery current at x, along with the auxiliary loads current, is represented as $\bar{I}_{batt,x}$, and C_{nom} represents the nominal capacity of the battery.

3.3.1.2 . Objective Function

The objective of the OCP is to minimize the fuel consumption and travel time of a CCAV over a given trip. The controller aims at minimizing a cost, given by:

$$J(\mathcal{M}) = c_{N_x}(x_{N_x}) + \sum_{x=1}^{N_x-1} c_x(\mathcal{X}_x, u_x) \tag{3.12}$$

where c_{N_x} and N_x denote the terminal and the number of steps in the given route. The per stage cost, c_x, represents the weighted average of fuel consumption and travel time and is given by,

$$c_x(\mathcal{X}_x, u_x) = \left(\gamma \frac{\dot{m}_{f,x}(\mathcal{X}_x, u_x)}{\dot{m}_{f,norm}} + (1-\gamma)\right) \Delta t_x \tag{3.13}$$

where $\gamma \in (0,1)$ is the trade-off, $\dot{m}_{f,x}$ is the fuel flow rate, $\dot{m}_{f,norm}$ is the normalizing factor, and Δt_x is the travel time per step. A control map $\mu_x(\mathcal{X}_x)$ at position x, is a set of admissible control inputs satisfying the constraints mentioned in Sect. 3.3.1.3. The collection of admissible maps for $x = 1, ..., N_x$ is referred as the policy of the controller, denoted by $\mathcal{M} := \mu_0, ..., \mu_{N_x}$.

3.3.1.3 . Constraints

Both the state and control variables are subject to constraints such as

$$\begin{aligned}
v_x &\in \left[v_x^{\min}, v_x^{\max}\right], \quad \forall x = 1, \ldots, N_x \\
\mathcal{E}_x &\in \left[\xi_x^{\min}, \mathcal{E}_x^{\max}\right], \quad \forall x = 1, \ldots, N_x \\
t_x &\in [0, t_N], \quad \forall x = 1, \ldots, N_x \\
v_0 &= v_0^{\min}, \quad \xi_0 \in \left[\xi^{\min}, \xi^{\max}\right] \\
a_x &\in \left[a^{\min}, a^{\max}\right], \quad \forall x = 1, \ldots, N_x \\
T_{eng,x} &\in \left[T_{eng,x}^{\min}, T_{eng,x}^{\max}\right], \quad \forall x = 0, \ldots, N_x \\
T_{bsg,x} &\in \left[T_{bsg,x}^{\min}, T_{bsg,x}^{\max}\right], \quad \forall x = 0, \ldots, N_x
\end{aligned} \tag{3.14}$$

where v_x^{min}, v_x^{max} refers to the minimum and maximum speed limit; $\mathcal{E}_x^{min}$, $\mathcal{E}_x^{max}$ refer to the minimum and maximum SoC limits; a^{min}, a^{max} refer to the vehicle acceleration for comfort; $T_{eng,x}^{min}, T_{eng,x}^{max}$ refer to the engine torque limits; $T_{bsg,x}^{min}, T_{bsg,x}^{max}$ refer to the BSG torque limits respectively. t_N refers to the maximum travel time limit imposed at the end of the route, which can be estimated using the time taken to complete the historical trips. To ensure charge-sustenance, $\mathcal{E}_0 = \mathcal{E}_{N_x}$. The above constraints are formulated as a result of either physical actuation limits or route characteristics. To include V2I information and in the presence of a traffic light, additional constraints are imposed on the time such that it lies in the feasible set of travel time for passing at green at a signalized intersection, $t_x \in \Gamma_{G,x}$ [14].

3.3.1.4 . Problem

With state dynamics (3.11), the objective function (3.13) and constraints (3.14) on the state and control variables, the ED-OCP formulated in discrete spatial domain reads:

$$\underset{\mathcal{M}}{\text{minimize}} \quad J(\mathcal{M}) = c_{N_x}(\mathcal{X}_{N_x}) + \sum_{x=1}^{N_x-1} \left(\gamma \frac{\dot{m}_{f,x}(\mathcal{X}_x, u_x)}{\dot{m}_{f,norm}} + (1-\gamma) \right) \Delta t_x$$

state dynamics

$$\begin{aligned} v_{x+1}^2 &= v_x^2 + 2\Delta d_x \frac{(F_{t,x}(\mathcal{X}_x, u_x) - F_{R,x}(v_x) - F_b)}{m} \\ \mathcal{E}_{x+1} &= \mathcal{E}_x - \frac{\Delta d_x}{\bar{v}_x} \frac{\bar{I}_{batt,x}(\mathcal{E}_x, T_{bsg,x})}{C_{nom}} \\ t_{x+1} &= t_x + \frac{\Delta d_x}{\bar{v}_x} \end{aligned}$$

boundary conditions $\mathcal{BC}$:

$$\{v(0) = v_0, \mathcal{E}(0) = \mathcal{E}_0, t(0) = 0, v(N_x) = \text{free}, \mathcal{E}(N_x) = \mathcal{E}_0, t(N_x) = \text{free}\}. \tag{3.15}$$

The ED-OCP formulated in (3.15) is hereafter referred to as the long-term optimization.

3.3.2 . Solution

The formulated long-term ED-OCP is solved using DP assuming all green phase traffic lights. The algorithm used for DP is developed in-house at the Center for Automotive Research, The Ohio State University. The procedure first initializes the cost-to-go function J, which represents the minimal cost to reach an admissible terminal state from a state $\mathcal{X}$ at step x. Then the algorithm proceeds backward from position N_x to 1, updating J taking advantage of Bellman's principle of optimality,

$$\begin{aligned} & J_{N_x} = c_{N_x}(\mathcal{X}_{N_x}), \\ \underset{\mu_x(\mathcal{X}_x)}{\text{minimize}} \quad & J_x(\mathcal{X}_x) = J_{x+1}(f_x(\mathcal{X}_x, \mu_x(\mathcal{X}_s))) + c_x(\mathcal{X}_x, \mu_x(\mathcal{X}_x)), \\ & \forall x = 1, \ldots, N_x - 1. \end{aligned} \tag{3.16}$$

The policy $\mathcal{M}^* = (\mu_1^*, \ldots, \mu_{N_x}^*)$ is optimal if for each $\mathcal{X}_x$ and x, $\mu_x^*(\mathcal{X}_x)$ minimizes right hand side of (3.16).

3.3.3 . Implementation

At the start of a trip, given the speed limit and the route length, the long-term optimization is solved using DP, and the results are stored in an offline memory. Information on traffic light SPaT is generally unknown, a priori, over an entire route. If the real-time route conditions, such as varying SPaT information or a lead vehicle, vary from the assumptions made at the trip's start, the above long-term

optimization has to be re-run to reflect those changes. With limited computational resources on vehicles and the computationally expensive nature of DP, it becomes unfeasible to periodically recompute the optimization problem (3.16) for the horizon N_x. To overcome this an MPC framework (short-term), the receding horizon approach, is used. The MPC truncates the long-term optimization of N_x steps to N_H, such that $N_H < N_x$. The short-term optimization problem reads,

$$\begin{aligned} \underset{\hat{\mathcal{M}}}{\text{minimize}} \quad & J_x(\hat{\mathcal{M}}) = c_{x+N_H}(\mathcal{X}_x + N_H) + \sum_{k=x}^{x+N_H-1} + c_k(\mathcal{X}_k, \mu_k(\mathcal{X}_k)), \\ & \forall x = 1, \ldots, N - N_H + 1. \end{aligned} \tag{3.17}$$

where $\hat{\mathcal{M}}$ represents the collection of admissible control input maps for $k = x, \ldots, x + N_H - 1$. A key challenge in (3.17) is the definition of the terminal cost and/or terminal state constraint that approximate the optimal solution provided by DP in a full-information scenario. Care has to be taken while imposing the terminal cost for the MPC – a charge-sustaining constraint on the battery SoC over each horizon results in an overly conservative torque split strategy, while a greedy heuristic can lead to violation of SoC-neutrality over the entire trip. Therefore, a terminal cost (or equivalently, the cost to complete the remaining route) approximation strategy based on the use of Approximate Dynamic Programming (ADP) is introduced such that the terminal cost of short-term optimization is approximated from the stored offline solution of the long-term optimization under partial route information [13]. Under the ADP framework, the following OCP is solved backward from $k + N_H - 1$ to k, $\forall k = 1, \ldots, N_X - N_H + 1$:

$$\begin{aligned} & \tilde{J}_{k+N_H}(\mathcal{X}_{k+N_H}) = c_{k+N_H}(\mathcal{X}_{k+N_H}), \\ \underset{\hat{\mu}_x(\mathcal{X}_x)}{\text{minimize}} \quad & \tilde{J}_x(\mathcal{X}_x) = \tilde{J}_{x+1}(\mathcal{X}_x, \hat{\mu}_x(\mathcal{X}_x)) + c_x(\mathcal{X}_x, \hat{\mu}_x(\mathcal{X}_x)), \\ & \forall x = k, \ldots, k + N_H - 1. \end{aligned} \tag{3.18}$$

where $\tilde{J}_{k+N_H}$ is the approximated terminal cost. It should be noted that the vehicle model, the stage cost, and the constraints in the long-term optimization remain the same in the short-term optimization.

However, in the presence of a lead vehicle, an additional rear-end collision avoidance constraint is formulated on the time state variable. At a position, x, the lead vehicle acceleration $\hat{a}^l_k$ is predicted as described in Sect. 3.2. The time-continuous formulation presented in Sect. 3.2 is converted to the discrete spatial domain and can be used to forecast the lead vehicle velocity $\hat{v}^l_k$ and arrival time $\hat{t}^l_k$, in the short-term optimization, for $k = x, \ldots, x + N_H - 1$:

$$\hat{v}^l_{k+1} = \sqrt{\hat{v}^{l^2}_k + 2\hat{a}^l_k \Delta d_k} \tag{3.19}$$

$$\hat{t}^l_{k+1} = \hat{t}^l_k + \frac{2\Delta d_k}{\hat{v}^l_{k+1} + \hat{v}^l_k} \tag{3.20}$$

The constraint on the time t is affected by imposing a time-gap constraint between the ego CCAV and lead vehicle as:

$$t_k \geq \hat{t}_k^l + t_{gap} \tag{3.21}$$

where t_{gap} represents the safety gap to the leader in time.

3.3.4 . Simulation Results

This section provides an application of the aforementioned lead vehicle velocity prediction methods. The different predictors, CA-AB and EDM-LOSP, are implemented in the above-described EDOC, particularly in equation (3.20). The performance of the proposed predictors is evaluated in terms of energy efficiency and travel time using real-world driving profiles and compared against CA as a baseline and an ideal scenario with perfect velocity prediction (wait-and-see) as a benchmark. For this analysis, different driving scenarios and routes were considered to demonstrate the utility of the speed predictors in the eco-driving problem. Six different routes were selected and divided between urban and mixed scenarios. The route data were obtained using GPS information extracted from different vehicles driven along the designated routes. The location of traffic lights along the route was known. However, Signal Phasing and Timing (SPaT) were not available. A realistic SPaT was manually generated by leveraging the time spent at stops by the lead vehicle. Additional information on the routes on traffic light density and average speed limits is provided in Table 3.2. The speed limits, lead vehicle velocity, and traffic light locations for the different routes are found in Appendix A.4 as a function of distance traveled.

Table 3.2: Routes information for urban and mixed driving scenarios

Route Name	Traffic light density (1/km)	Average speed limits (m/s)
Urban Route 1	3.0	12.5
Urban Route 2	1.2	17.8
Urban Route 3	2.3	14.7
Mixed Route 1	0.5	26.3
Mixed Route 2	0.7	22.3
Mixed Route 3	0.4	26.3

The results obtained, in terms of total fuel consumed and travel time, and the different speed predictors are shown in Fig. 3.3. The optimization problem aims to minimize both fuel and time with an equal trade-off (i.e., $\gamma = 0.5$). It is worth noting that all the strategies implemented result in charge sustaining, i.e., the initial and final SOC is approximately equal to 50 %. The benchmark solution provided in these results corresponds to a perfect knowledge of the lead vehicle velocity in the prediction horizon (i.e., 200 m).

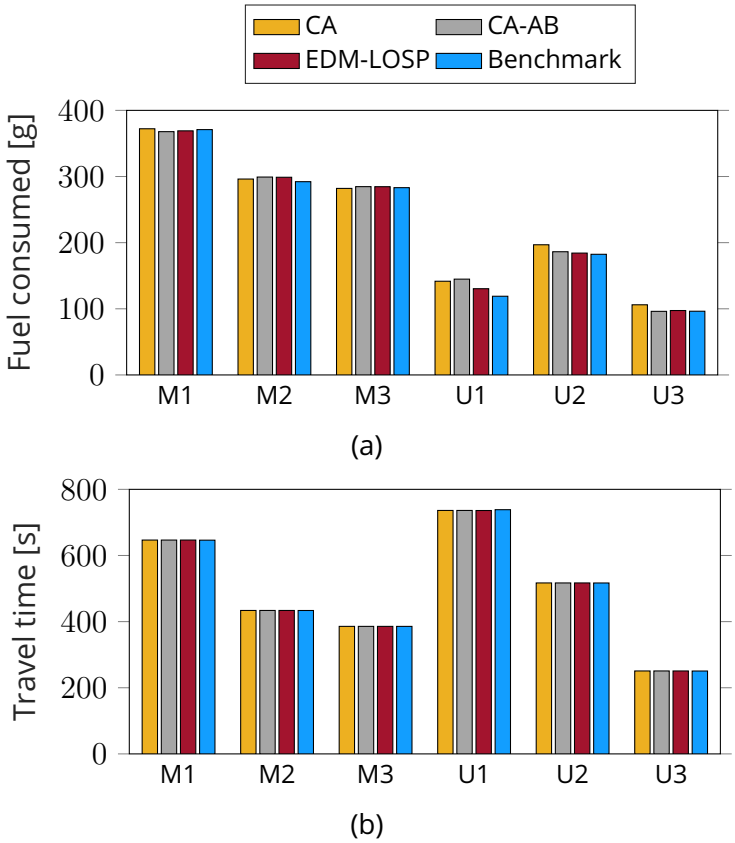

Figure 3.3: Bar plots for fuel consumed (a) and travel time (b) of the ego vehicle using the four predictors on six different routes (M for mixed and U for Urban).

The bar plot in Fig. 3.3b shows travel time to remain practically unchanged among the different speed predictors, whereas in Fig. 3.3a the fuel consumed varies considerably. The highest differences are found in urban routes, where ego vehicle using EDM-LOSP and CA-AB predictors, perform better than the CA and are much closer to the Benchmark. Table 3.3 shows the percentage gain in fuel consumed for CA, CA-AB and EDM-LOSP with respect to the Benchmark. Note that the Benchmark predictor (i.e., having perfect prediction) doesn't necessarily give the least energy consumption. The negative values in Table 3.3 indicates a lower energy consumption than the Benchmark. This is mainly because some speed fluctuations in the lead vehicle profile is smoothed in the prediction horizon allowing for less variations in the ego vehicle speed.

The energy gains in urban routes are further analyzed in terms of the ego vehicle's acceleration Root-Mean-Square (RMS). The ego vehicle using CA predictor has the highest average RMS of 0.52 m/s^2 and, when using CA-AB and EDM predictors, the RMS is given as 0.51 m/s^2 and 0.50 m/s^2 respectively. The increased acceleration RMS of the ego vehicle using CA, indicates more frequent variations

Table 3.3: Percentage of fuel consumed w.r.t. the Benchmark predictor

Predictor	M1	M2	M3	U1	U2	U3
CA	0.34	1.37	-0.40	19.07	7.89	10.11
CA-AB	-0.84	2.39	0.54	21.73	2.12	-0.18
EDM-LOSP	-0.51	2.29	0.52	9.58	1.00	1.11

in acceleration, leading to higher fuel consumption. No substantial changes are observed in mixed routes when applying the different predictors. This is mainly because the lead vehicle, for a substantial portion of the route, is at a constant speed where the different predictors perform similarly.

An example of how the eco-driving solution approaches the traffic lights is shown in Fig. 3.4 and is most visible in the zoomed window that highlights two close traffic lights. It can be noticed how the prediction of lead vehicle speed, along with the signal phase knowledge, allows the ego vehicle to not stop at traffic lights when it is feasible, thus avoiding inefficient deceleration to null speed and subsequent acceleration. Analyzing further the zoomed window, it can be seen that the benchmark solution starts decelerating long before the first traffic light and accelerates only towards the end of the green phase, just enough to avoid stopping. Further differences can also be seen in the behavior of the CA eco-driving approach (in yellow in Fig. 3.4) that accelerates right after the lead vehicle leaves the traffic light and then decelerates when the gap is low.

Figure 3.5, illustrates the eco-driving solutions with the different speed predictors implemented on Mixed Route 2. Generally, no visible differences are found among the different predictors' solutions. This is mainly because the lead vehicle in a mixed route maintains a constant speed for majority of the route, see Fig. A.1e, and all predictors perform well in such situations. However, all demonstrate smoother velocities for the ego vehicle with respect to the lead vehicle avoiding unnecessary slowdowns (see Fig. 3.5 around 840 m and 2815 m), thus improving overall energy efficiency.

The fact that the travel time does not vary as noticeably as the fuel consumption is attributable to the need to comply with traffic light phases and the constraint imposed to stay behind the lead vehicle. Two simulations are performed with different weights between fuel consumed and travel time to support this statement. Even when orienting the cost function to penalize the travel time (i.e., lower γ) more than the fuel consumption, no substantial variations are found, as seen in Fig. 3.6. It is worth noting that the y-axis in Fig. 3.6 is magnified for the sake of clarity and that the differences between $\gamma = 0.5$ and $\gamma = 0.2$, are in the orders of seconds, hence confirming that the constraints posed by the lead vehicle and the traffic lights do not allow room for travel time variation.

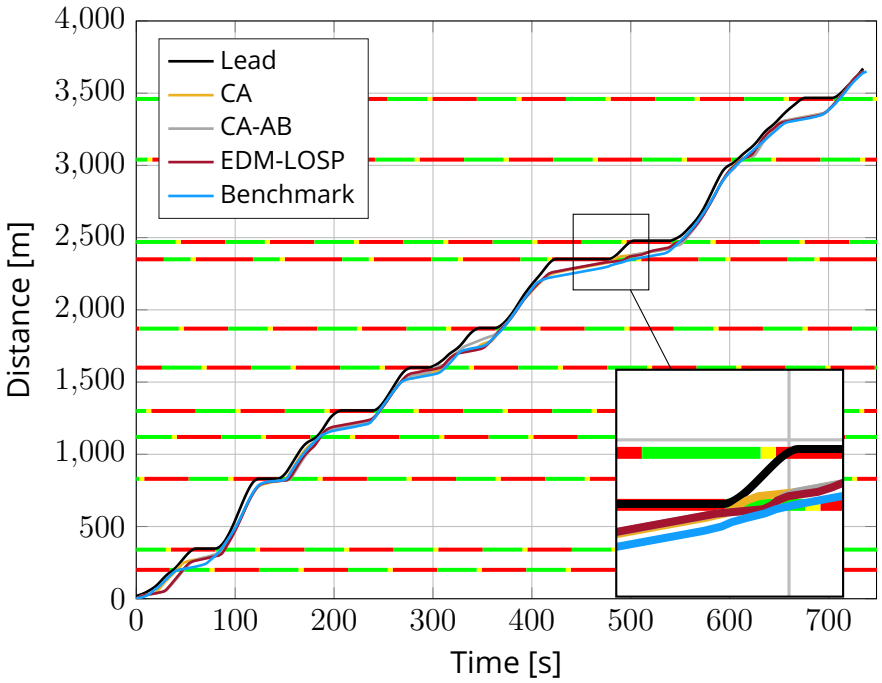

Figure 3.4: Traffic lights SPaT and trajectories of the lead vehicle and ego vehicle using different predictors

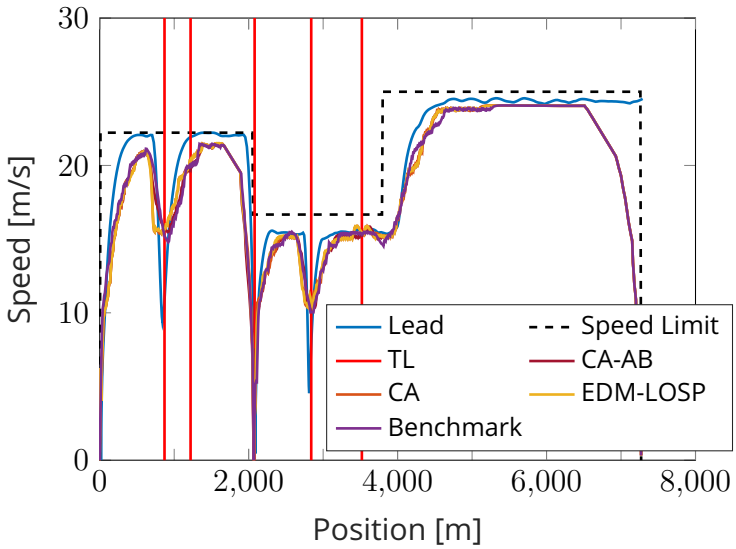

Figure 3.5: Velocity traces of ego vehicle using the different speed predictors in Mixed Route 2, as a function of distance

3.4 . Conclusion

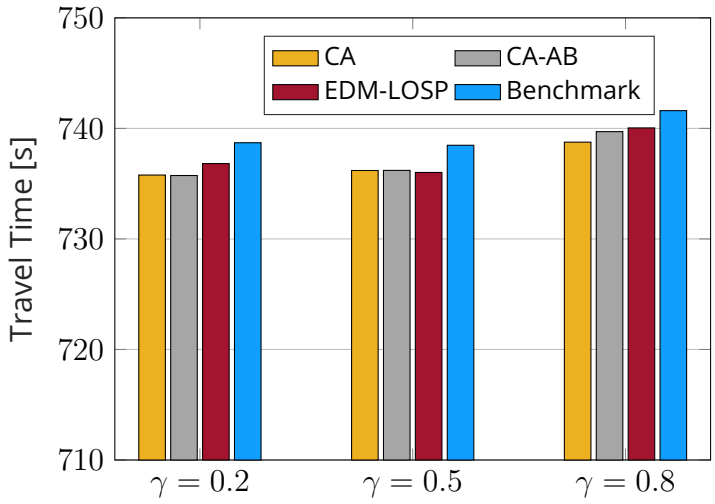

Figure 3.6: Bar plots graph of the travel times obtained using different speed predictors and different weights in the cost function for Urban Route 1

The prediction accuracy of lead vehicle velocity increases with increase availability of information, especially via V2V communication. However, in the absence of V2V communication or in a data-restricted environment, the prediction accuracy decreases. To mitigate this, two predictors, namely CA-AB and EDM-LOSP, were developed in this chapter to predict lead vehicle velocity using only the current measured information (NC-ED). First, a CA predictor was modified to incorporate an average deceleration part while slowing down or stopping. Second, the EDM-LOS was modified to incorporate current acceleration information in capturing lead vehicle decelerations during car-following. A comparative study was conducted to analyze the prediction accuracy of the developed predictors over different prediction horizons. A time-gap based constraint was formulated in the EDOC for mHEV leveraging the predicted lead vehicle velocity. Simulations were performed over 6 real-world routes representing urban and mixed driving scenarios with the developed predictors. Results show energy savings for CA-AB over CA and EDM-LOSP performing better over CA-AB, especially in urban scenarios with high traffic light or stop sign density.

Bibliography

[1] Z. D. Asher, D. A. Baker, and T. H. Bradley, "Prediction Error Applied to Hybrid Electric Vehicle Optimal Fuel Economy," IEEE Transactions on Control Systems Technology, pp. vol. 26, no. 6, pp. 2121-2134, 2018.

[2] E Hyeon, Y Kim, N Prakash, and AG Stefanopoulou, "Influence of Speed Forecasting on the Performance of Ecological Adaptive Cruise Control," in Dynamic Systems and Control Conference, Utah, 2019.

[3] Martin Treiber and Arne Krestig, "Car-Following Models Based on Driving Strategies," in Traffic Flow Dynamics: Data, Models and Simulation. Berlin,Heidelberg: Springer Berlin Heidelberg, 2013, pp. 181-204.

[4] Gupta Shobhit, R.Deshpande Shreshta, Tulpule Punit, Canova Marcello, and Rizzoni Giorgio, "An Enhanced Driver Model for Evaluating Fuel Economy on Real-World Routes," in Advances in Autonomotive Control , Orleans, 2019, pp. Pages 574-579.

[5] Brackstone Mark and McDonald Mike, "Car-following: a historical review," Transportation Research Part F: Traffic Psychology and Behaviour, vol. 2, no. 4, pp. 181-196, Decemeber 1999.

[6] Eunjeong Hyeon, "Speed Forecasting Strategies for the Energy-Optimal Car-Following of Connected and Automated Vehicles". Michigan: Doctoral Thesis, 2022.

[7] Deshpande Shreshta Rajakumar, Gupta Shobhit, Kibalama Dennis, Pivaro Nicola, and Canova Marcello, "Benchmarking fuel economy of connected and automated vehicles in real world driving conditions via monte carlo simulation," in ASME Dynamic Systems and Control Conference, Pittsburgh,PA, 2020.

[8] Bharatkumar Hegde, Michael O'Keefe, Steven Muldoon, Jeffery Gonder, and Chen-Fang Change, "Real-World Driving Features for Identifying Intelligent Driver Model: Preprint.," in SAE WCX World Congress Experience Digital Summit, 2021, pp. NREL/CP-5400-78817.

[9] Monteil Julien, O'Hara Niall, Cahill Vinny, and Bouroche Melanie, "Real-time estimation of drivers' behaviour," in International Conference on Intelligent Transportation Systems, 2015.

[10] Gupta Shobhit and Canova Marcello, "Eco-Driving of Connected and Autonomous Vehicles with Sequence-to-Sequence Prediction of Target Vehicle Velocity," in IFAC, Tokyo, Japan, 2021, pp. Volume 54, Issue 10, Pages 430-436.

[11] Zhu, Zhaoxuan, Shobhit Gupta, Nicola Pivaro, Shreshta Rajakumar Deshpande, and Marcello Canova. "A gpu implementation of a look-ahead optimal controller for eco-driving based on dynamic programming." In 2021 European Control Conference (ECC), pp. 899-904. IEEE, 2021.

[12] Gupta, S. (2019). "Look-Ahead Optimization of a Connected and Automated 48V Mild-Hybrid Electric Vehicle" (Masters Thesis, The Ohio State University).

[13] Deshpande, Shreshta Rajakumar, Shobhit Gupta, Abhishek Gupta, and Marcello Canova. "Real-Time Ecodriving Control in Electrified Connected and Autonomous Vehicles Using Approximate Dynamic Programing." Journal of Dynamic Systems, Measurement, and Control 144, no. 1 (2022): 011111.

[14] Gupta, Shobhit, Shreshta Rajakumar Deshpande, Daniela Tufano, Marcello Canova, Giorgio Rizzoni, Karim Aggoune, Pete Olin, and John Kirwan. "Estimation of fuel economy on real-world routes for next-generation connected and automated hybrid powertrains". No. 2020-01-0593 . 2020.

[15] Olin, Pete, Karim Aggoune, Li Tang, Keith Confer, John Kirwan, Shreshta Rajakumar Deshpande, Shobhit Gupta, Punit Tulpule, Marcello Canova, and Giorgio Rizzoni. "Reducing fuel consumption by using information from connected and automated vehicle modules to optimize propulsion system control". No. 2019-01-1213. SAE Technical Paper, 2019.

[16] Sciarretta, Antonio, and Ardalan Vahidi. "Energy saving potentials of CCAVs." In Energy-Efficient Driving of Road Vehicles, pp. 1-31. Springer, Cham, 2020.

[17] Yufang, Li, Chen Mingnuo, and Zhao Wanzhong. "Investigating long-term vehicle speed prediction based on BP-LSTM algorithms." IET Intelligent Transport Systems 13, no. 8 (2019): 1281-1290.

[18] Jacome, Olivia, Shobhit Gupta, Stephanie Stockar, and Marcello Canova. "Data-driven Driver Model for Speed Advisory Systems in Partially Automated Vehicles." arXiv preprint arXiv:2205.08445 (2022).

4 - Platooning

This chapter discusses eco-driving of a platoon of electric CCAVs.

4.1 . State-of-the-Art

Platooning, an extension of car-following, is a scenario where more than two vehicles closely follow each other while maintaining a safe gap from the preceding one. Such vehicular platoons often referred to as strings, can suffer from string instability when the spacing gaps between vehicles amplify upstream along the string.

Some relevant characteristics must be considered to study the dynamics of vehicular platoons. A comprehensive overview of platoon characteristics is mentioned in [1]. In terms of composition, a platoon can be homogeneous or heterogeneous. A homogeneous platoon assumes the same dynamics for all the vehicles; its string stability properties have been studied in [2, 3, 4, 5, 6]. On the other hand, a heterogeneous platoon assumes that vehicles in the platoon can have different dynamics, see [7, 8, 9].

Secondly, the communication topology amongst the vehicles in the platoon must also be considered. Communication with only the nearest preceding vehicle is called predecessor following [8, 3]. Communication policies such as bidirectional following [2] which involves communication with the preceding and following vehicle, [10] or predecessor-leader [4] are also employed.

The third characteristic to be considered is the car-following strategy (control law) used by the vehicles in the platoon. Among various car-following strategies in literature, the most extensively studied is the linear-time invariant Adaptive Cruise Control (ACC). With ACC, the control law is based only on the measurements from onboard sensors, such as radar, lidar, or a camera setup. They measure the relative speed and distance with the preceding vehicle that is then fed as input to the controller. The acceleration is then determined to follow a desired spacing policy. With a constant spacing policy, a constant safe distance is tracked, see [4, 2]. With a constant-time headway policy, the desired gap is velocity-dependent, see [8, 3]. Nonlinear spacing policies have also been proposed; see [11]. Studies such as [4, 8, 5] have shown that ACC with a constant spacing strategy exhibits string instability, whose mitigation requires adopting a constant-time headway policy with a certain minimum headway time [8, 3]. Besides the above strategies, there exist car-following models used to simulate individual driving behavior. Such models, more prominent in the field of traffic flow dynamics, include the Optimal Velocity Model, Newell's car-following model, Gipp's Model, Intelligent Driver Model (IDM), etc [12].

The evolution of communication and automated technology enables the inclu-

sion of additional information from other vehicles in the control law. As stated in Chap. 1, there are three types of cooperation based on the amount of information shared and motivation for the common good. In the NC-ED strategy, each vehicle optimizes for itself and shares only its instantaneous control action with its neighbors. ACC, with the additional functionality to communicate with the preceding vehicle to receive its current acceleration, is traditionally called as Cooperative ACC (CACC). The authors in [13, 8] have shown that a CACC platoon can be string stable using a constant headway policy but with a smaller minimum headway time compared to an ACC using the same policy. However, this strategy of sharing the current acceleration, according to the classification used in this thesis falls under the Non-Cooperative strategy. Optimal control formulations, employing the MPC framework, is also used in the design of ACC and CACC controllers to allow multiple design criteria and constraints on state and control variables [14, 15, 16]. The authors in [17] have described the use of NC-EDOC[1], in a CCAV platoon. The authors assessed the energy efficiency and string compactness of this algorithm. They showed that the NC-EDOC saves energy for the first followers but is string unstable and thus displays larger overall energy consumption for the string, indicating more complex ED hierarchical schemes are necessary to improve both aspects.

In the C-ED, each vehicle still optimizes for itself but shares its future intentions with the neighboring vehicles. We assume that each vehicle shares the result of its eco-driving optimization, i.e., its intended accelerations over the near future, with its following vehicle. The drawbacks of the NC-EDOC in platoons, demonstrated by [17], is taken as the main motivation for the C-EDOC. The idea of sharing future intentions with the neighboring vehicle has been proposed in [18, 19] for vehicle formations and stabilization, and [17, 20] for energy efficiency and comfort and has been implemented in a numerical approach. The Cooperative eco-driving algorithm presented here differs by implementing the shared intentions analytically.

In the CC-ED, the control action of each vehicle is such that it optimizes for the entire group [21, 16]. The Centralized Cooperative EcoACC algorithm, in [22] is proposed as an extension of their work in [16]. The formulated optimal control problem is solved using an indirect numerical method and does not provide a closed-form solution.

The main goal of this chapter is to present the three levels of cooperation applied to a ED platoon of electric CCAVs and evaluate the performance of the algorithms in terms of energy efficiency and string compactness. A standard ACC is chosen as the baseline for evaluation. A theoretical analysis of the string stability of the three algorithms is also presented.

Chapter Outline The organization of this chapter is as follows. Sect. 4.2, in-

[1]Referred to as Position-Constrained Shrinking Horizon Control (PCSHC) in that paper.

troduces vehicle and platoon model. The OCP formulation, solution and the implementation for the NC-ED, C-ED and CC-ED are presented in Sect. 4.3, Sect. 4.4, and Sect. 4.5, respectively. Sect. 4.6, gives a theoretical analysis on the string stability of the three EDOCs and Sect. 4.7 presents the simulation results of the algorithms. Concluding remarks are presented in Sect. 4.8.

4.2 . Platoon and Vehicle Model

Consider a platoon consisting of $N+1$ CCAVs, where each CCAV is indexed i from 1 to N. The first vehicle or the leader in the platoon is indexed $i=0$, which acts as the reference trajectory for the platoon. The index of the vehicles increases going upstream in the platoon. For example, the vehicle preceding the i-th vehicle is denoted as $i-1$ and the vehicle following as $i+1$. As shown in Fig. 4.1, the platoon uses predecessor–following communication topology where each vehicle communicates only with the nearest preceding vehicle. All vehicles in the platoon have the same plant dynamics (homogeneous platoon) and use constant spacing policy. The spacing gap, between the CCAV i and $i-1$ is defined as

$$\xi_i(t) = x_{i-1}(t) - x_i(t) - l_{i-1} - s_{min}. \tag{4.1}$$

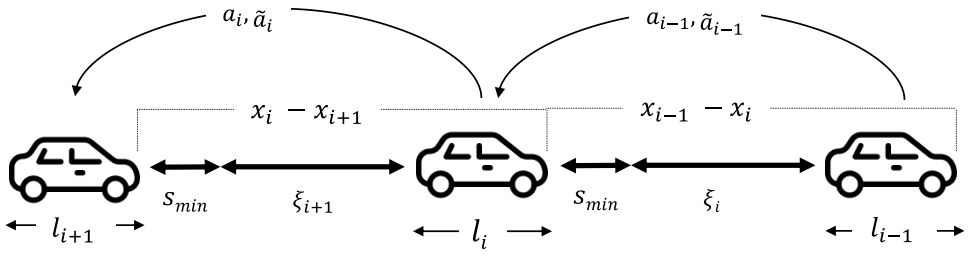

Figure 4.1: Platooning scenario

The platooning scenario considered here involves only a single lane, thereby excluding any lane change possibility. The motion of each CCAV in the platoon is therefore only longitudinal, and its dynamics are captured by the linearised model given by (2.2). Under similar assumptions as in Sect. 2.2.1.1, the linearised longitudinal vehicle model for a CCAV i, $\forall i = 1, \ldots, N$ is given as

$$\begin{aligned} \dot{x}_i &= v_i(t), \\ \dot{v}_i &= a_i(t) = F/m - h. \end{aligned} \tag{4.2}$$

In a standard ACC, the feedback control law is of the form $a_i(v_i, \xi_i, \dot{\xi}_i)$, and is given by

$$a_i(t) = k_p \xi_i(t) + k_v \dot{\xi}_i(t) \ , \quad \forall i = 1, \ldots, N, \tag{4.3}$$

where k_p and k_v denote gains. The main goal of ACC is to follow the preceding vehicle with the desired safe distance. However, we aim at deriving a car-following feedback control law, of the form, $a_i(v_i, \xi_i, \dot{\xi}_i, ...)$, such that each vehicle not only follows its predecessor, but does it in an energy-efficient way.

4.3 . Non-Cooperative EDOC

As previously described, in the Non-Cooperative strategy each vehicle optimises for itself and shares only its instantaneous information with the other vehicles. Therefore, in a platoon, each CCAV i using sensors measures the current states, $x_{i-1}, v_{i-1}, a_{i-1}$, of the preceding CCAV $i-1$. As in the case of a car-following scenario, CCAV i tries to avoid a rear-end collision with CCAV $i-1$ which imposes a state inequality constraint $\xi_i(t) \geq 0$. The motion of CCAV $i-1$ over the optimization horizon is predicted under a constant acceleration assumption,

$$x_{i-1}(t) = x_{i-1,0} + v_{i-1,0}t + \frac{a_{i-1}t^2}{2}, \quad t \in [0, T_{i,f}]. \tag{4.4}$$

where $x_{i-1,0}, v_{i-1,0}, a_{i-1}$ are the initial position, velocity and acceleration.

4.3.1 . OCP Formulation

Under similar assumptions on vehicle model, objective function and constraints as in Sect. 2.3, each CCAV i obtains its eco-driving speed profile by solving the following optimization problem,

$$\begin{aligned}
&\underset{a_i(t)}{\text{minimize}} \quad J_i = \int_0^{T_{i,f}} m(a_i(t)+h)v_i(t) + b(a_i(t)+h)^2 \, dt, \\
&\text{state dynamics} \\
&\qquad \dot{x}_i = v_i(t), \\
&\qquad \dot{v}_i = a_i(t), \\
&\text{boundary conditions } \mathcal{BC}: \\
&\qquad \{x_i(0) = 0, v_i(0) = v_{i,0}, x_i(T_{i,f}) = D_{i,f}, v(T_{i,f}) = V_{i,f}\}, \\
&\text{constraints} \\
&\qquad x_i(t) \leq x_{i-i,0} + v_{i-1,0}t + \frac{1}{2}a_{i-1}t^2, \quad t \in [0, T_{i,f}].
\end{aligned} \tag{4.5}$$

4.3.2 . Solution

The OCP (4.5) for each CCAV i, $\forall i \in [1, N]$, is solved using PMP following similar steps detailed in Sect. 2.3. In the absence of the constraint from CCAV $i-1$, the optimal solution is given by

$$v_i(t) = v_{i,0} + \left(-\frac{4v_{i,0}}{T_{i,f}} - \frac{2V_{i,f}}{T_{i,f}} + \frac{6D_{i,f}}{T_{i,f}^2}\right) t + \left(\frac{3v_{i,0}}{T_{i,f}^2} - \frac{6D_{i,f}}{T_{i,f}^3} + \frac{3V_{i,f}}{T_{i,f}^2}\right) t^2.$$
$$t \in [0, T_{i,f}], \quad \forall i \in [1, N]. \quad (4.6)$$

and in the presence of the preceding vehicle constraint $\xi_i(t) \geq 0$, the optimal solution yields two parabolic speed profiles joined at it's contact point θ_i.

$$v_i(t) = \begin{cases} v_{i,0} + \left(a_{i-1} + \frac{4\dot{\xi}_{i,0}}{\theta_i} + \frac{6\xi_{i,0}}{\theta_i^2}\right) t - \\ \quad - \left(\frac{6\xi_{i,0}}{\theta_i^3} + \frac{3\dot{\xi}_{i,0}}{\theta_i^2}\right) t^2, \quad t \in [0, \theta_i) \\ v_{i-1,0} + a_{i-1}\theta_i + \left(a_{i-1} - \frac{6\xi_{i,0}}{\theta_i^2} - \frac{2\dot{\xi}_{i,0}}{\theta_i}\right)(t - \theta_i) + \\ \quad + \left(V_{i,f} - 3v_{i-1,0} + 2v_{i,0} - 6\frac{\xi_{i,0}}{\theta_i} - a_{i-1}T_{i,f} + 6\xi_{i,0}\frac{T_{i,f}}{\theta_i^2} + \right. \\ \quad \left. + 2\dot{\xi}_{i,0}\frac{T_{i,f}}{\theta_i}\right) \frac{(t-\theta_i)^2}{(T_{i,f} - \theta_i)^2}. \quad t \in [\theta_i, T_{i,f}], \quad \forall i \in [1, N]. \end{cases} \quad (4.7)$$

The contact time θ_i, that is, where the constraint is met ($\xi_i = 0$), is given by

$$\begin{aligned}(v_{i,0} - V_{i,f} + a_{i-1}T_{i,f})\,\theta_i^3 + \left(4v_{i-1,0}T_{i,f} + V_{i,f}T_{i,f} - 2v_{i,0}T_{i,f} + a_{i-1}T_{i,f}^2/2\right. \\ \left. -3D_{i,f}\right)\theta_i^2 + \left(6\xi_{i,0}T_{i,f} + v_{i,0}T_{i,f}^2 - v_{i-1,0}T_{i,f}^2\right)\theta_i - \left(3\xi_{i,0}T_{i,f}^2\right) = 0.\end{aligned} \quad (4.8)$$

4.3.3 . Implementation

The preceding vehicle's velocity and acceleration are generally varying in time and hence the above solutions are implemented in a shrinking horizon MPC fashion, as described in Sect. 2.3.3. This section explicitly states the optimal control input applied by a CCAV i in the EDOC.

If the position trajectory of the CCAV $i-1$ (i.e. $x_{i-1}(k)$) does not intersect with the unconstrained position trajectory of the CCAV i, that is, if F_{cf} given by

$$\begin{aligned}F_{cf} = \left(x_i(t) + v_i(t)k + \left(-\frac{2v_i(t)}{T_i} - \frac{V_i}{T_i} + \frac{3D_i}{T_i^2}\right)k^2 + \right. \\ \left. \left(\frac{v_i(t)}{T_i^2} - \frac{2D_i}{T_i^3} + \frac{V_i}{T_i^2}\right)k^3\right) - \left(x_{i-1}(t) + v_{i-1}(t)k + \frac{a_{i-1}(t)k^2}{2}\right) = 0\end{aligned} \quad (4.9)$$

has no real positive root in k, then the optimal solution given by

$$v_i(k) = v_i(t) + \left(-\frac{4v_i(t)}{T_i} - \frac{2V_i}{T_i} + \frac{6D_i}{T_i^2}\right)k + \left(\frac{3v_i(t)}{T_i^2} - \frac{6D_i}{T_i^3} + \frac{3V_i}{T_i^2}\right)k^2,$$
$$k \in [0, T_i), \quad \forall i \in [1, N]. \quad (4.10)$$

and the optimal acceleration, $a_i(k)$ with $k = 0$, given by

$$a_i(t) = -\frac{4}{T_i} v_i(t) - \frac{2}{T_i} V_i + \frac{6}{T_i^2} D_i \ . \tag{4.11}$$

is used. If F_{cf} has a positive real root, then optimal velocity given by

$$v_i(k) = v_i(t) + \left(a_{i-1}(t) + \frac{4}{\theta_i} \dot{\xi}_i(t) + \frac{6}{\theta_i^2} \xi_i(t) \right) k - \left(\frac{6}{\theta_i^3} \xi_i(t) + \frac{3}{\theta_i^2} \dot{\xi}(t) \right) k^2, \\ k \in [0, \theta_i), \quad \forall i \in [1, N], \tag{4.12}$$

and the optimal acceleration, $a_i(k)$ with $k = 0$, given by

$$a_i(t) = a_{i-1}(t) + \frac{4}{\theta_i} \dot{\xi}_i(t) + \frac{6}{\theta_i^2} \xi_i(t) \ . \tag{4.13}$$

is used. The control law (4.13) is structurally similar to that of ACC, however, it also depends on the acceleration of the preceding vehicle.

The assumption of a constant acceleration for the CCAV $i-1$ could render the controllers (4.11)–(4.13) infeasible in certain situations. For instance, when acceleration a_{i-1} is negative, it is possible that CCAV $i-1$ stops at a time $t_{stop} = v_{i-1}/|a_{i-1}| < T_i$, hindering the CCAV i from reaching its final position D_i. In this situation the boundary conditions of the CCAV i are updated to that of $i-1$

$$V_i = 0 \ , \qquad D_i = \xi_i(t) + \frac{v_{i-1}(t)^2}{2|a_{i-1}(t)|} \ . \tag{4.14}$$

Substituting these boundary conditions in (4.11), the control input is modified as

$$a_i(t) = -\frac{4}{T_i} v_i(t) + \frac{6}{T_i^2} \xi_i(t) + \frac{3}{T_i^2} \frac{v_{i-1}(t)^2}{|a_{i-1}(t)|} \ . \tag{4.15}$$

Another scenario that could render (eqs. (4.11) and (4.13)) infeasible during deceleration of CCAV $i-1$, is when it stops at a time $t_{stop} > T_i$ but at a position lower than D_i. The updated boundary conditions are therefore given by:

$$\begin{aligned} V_i &= v_{i-1}(t) + a_{i-1}(t) T_i \ , \\ D_i &= x_{i-1}(T_i) = \xi_i(t) + v_{i-1}(t) T_i + \frac{a_{i-1}(t) T_i^2}{2} \ . \end{aligned} \tag{4.16}$$

Substituting these boundary conditions in (4.11), the control input is obtained as

$$a_i(t) = a_{i-1}(t) + \frac{4}{T_i} \dot{\xi}_i(t) + \frac{6}{T_i^2} \xi_i(t) \ . \tag{4.17}$$

4.4 . Cooperative EDOC

In C-ED scenario, cooperation is introduced in the platoon as the ability to share intentions over a certain horizon. Each CCAV i still optimizes for itself but shares its future intentions with the following vehicle, i.e., CCAV $i+1$. Differing from the NC-ED scenario, where CCAV i measures the instantaneous acceleration of CCAV $i-1$, in the C-ED scenario, CCAV i solves its own OCP and sends its solution to the following CCAV. Thus CCAV i receives from CCAV $i-1$. To use this vector of shared accelerations in the eco-driving control of a CCAV i, this is lumped into one "future mean value" $\tilde{a}_{i-1}$, evaluated over a preview window length L, as

$$\tilde{a}_{i-1} = \frac{1}{L}\int_{t}^{t+L} a_{i-1}(\tau)d\tau \ . \tag{4.18}$$

This future mean preceding vehicle's acceleration $\tilde{a}_{i-1}$ replaces the measured acceleration a_{i-1} in all equations of the previous section. The preview window length L is chosen based on sensitivity analysis for minimum energy consumption.

4.4.1 . OCP Formulation

Each CCAV i, $\forall i \in [1, N]$, solves the same OCP formulated in (4.5), with the exception that the state-inequality constraint becomes,

$$x_i(t) \leq x_{i-i,0} + v_{i-1,0}t + \frac{1}{2}\tilde{a}_{i-1}t^2, \quad t \in [0, T_{i,f}]. \tag{4.19}$$

4.4.2 . Solution

The optimal trajectory in the absence of the constraint (4.19), $\forall i \in [0, N]$, is given by (4.6) and in the presence of the constraint is given by,

$$v_i(t) = \begin{cases} v_{i,0} + \left(\tilde{a}_{i-1} + \dfrac{4\dot{\xi}_{i,0}}{\theta_i} + \dfrac{6\xi_{i,0}}{\theta_i^2}\right)t - \\ \quad - \left(\dfrac{6\xi_{i,0}}{\theta_i^3} + \dfrac{3\dot{\xi}_{i,0}}{\theta_i^2}\right)t^2, \quad t \in [0, \theta_i) \\ v_{i-1,0} + \tilde{a}_{i-1}\theta_i + \left(\tilde{a}_{i-1} - \dfrac{6\xi_{i,0}}{\theta_i^2} - \dfrac{2\dot{\xi}_{i,0}}{\theta_i}\right)(t-\theta_i) + \\ \quad + \left(V_{i,f} - 3v_{i-1,0} + 2v_{i,0} - 6\dfrac{\xi_{i,0}}{\theta_i} - \tilde{a}_{i-1,0}T_{i,f} + 6\xi_{i,0}\dfrac{T_{i,f}}{\theta_i^2} + \right. \\ \quad \left. + 2\dot{\xi}_{i,0}\dfrac{T_{i,f}}{\theta_i}\right)\dfrac{(t-\theta_i)^2}{(T_{i,f}-\theta_i)^2}. \quad t \in [\theta_i, T_{i,f}], \quad \forall i \in [1, N]. \end{cases} \tag{4.20}$$

The contact time θ_i, that is, where the constraint is met ($\xi_i = 0$), is given by

$$\begin{aligned} &(v_{i,0} - V_{i,f} + \tilde{a}_{i-1}T_{i,f})\,\theta_i^3 + \left(4v_{i-1,0}T_{i,f} + V_{i,f}T_{i,f} - 2v_{i,0}T_{i,f} + \tilde{a}_{i-1}T_{i,f}^2/2\right. \\ &\left. -3D_{i,f}\right)\theta_i^2 + \left(6\xi_{i,0}T_{i,f} + v_{i,0}T_{i,f}^2 - v_{i-1,0}T_{i,f}^2\right)\theta_i - \left(3\xi_{i,0}T_{i,f}^2\right) = 0. \end{aligned} \tag{4.21}$$

4.4.3 . Implementation

With the solutions being implemented in shrinking horizon MPC, the term $a_{i-1}(t)$ in equations (4.9),(4.12),(4.13),(4.15) and (4.17) is replaced by $\tilde{a}_{i-1}(t)$.

4.5 . Centralized Cooperative EDOC

In Centralized Cooperative strategy, the objective is to minimise the energy consumption of the entire platoon.

4.5.1 . OCP Formulation

Two different OCP are formulated considering the entire platoon as a single system. The first formulation considers no preceding vehicle to the platoon (i.e., absence of vehicle $i = 0$) and the second formulation considers a preceding vehicle (i.e., presence of vehicle $i = 0$). The trajectory of vehicle $i = 0$ is imposed and it acts as a leader to the platoon.

Absence of vehicle $i = 0$**:** Under similar assumptions as in Chap. 2, the cost functional is now formulated as the sum of battery energy (2.6) of all N CCAVs in the platoon. In the *absence* of a preceding vehicle $i = 0$ to the platoon, the first optimal control problem can be formulated as

$$\underset{a_i(t)}{\text{minimize}} \quad J = \int_0^{T_{i,f}} \sum_{i=1}^{N} \left(m\left(a_i(t) + h\right) v_i(t) + b\left(a_i(t) + h\right)^2 \right] dt,$$

state dynamics and $\mathcal{BC}$ for $i = 1$

$$\begin{aligned} &\dot{x_i} = v_i(t), \\ &\dot{v_i} = a_i(t), \\ &\mathcal{BC} : \{x_1(0) = 0, v_1(0) = v_{1,0}, x_1(T_{1,f}) = D_{1,f}, v_1(T_{1,f}) = V_{1,f}\}, \end{aligned}$$

state dynamics and $\mathcal{BC}$ for $i \in [2, N]$

$$\begin{aligned} &\dot{\xi}_i(t) = w_i(t) = v_{i-1}(t) - v_i(t), \\ &\dot{w}_i(t) = a_{i-1}(t) - a_i(t), \\ &\mathcal{BC} : \{\xi_i(0) = \xi_{i,0}, w_i(0) = w_{i,0}, \xi_i(T_{i,f}) = \xi_{i,f}, w_i(T_{i,f}) = 0\}. \end{aligned} \tag{4.22}$$

where $\xi_i(t)$ and $w_i(t)$ represent relative position and velocity, respectively.

Since there is no preceding vehicle to CCAV 1, it remains unconstrained. However, CCAVs $2 \leq i \leq N$ is imposed with a state-inequality constraint of the form

$$\xi_i(t) \geq 0, \quad \forall i \in [2, N] \tag{4.23}$$

to avoid colliding with each other.

Presence of vehicle $i = 0$**:** In the *presence* of a preceding vehicle $i = 0$,

CCAV 1 avoids a rear-end collision with a position-inequality constraint of the form

$$x_1(t) \leq x_{0,0} + v_{0,0}t + \frac{1}{2}\tilde{a}_0 t^2, \quad t \in [0, T_{i,f}]. \tag{4.24}$$

We assume that CCAV 0 shares its future intentions, $\tilde{a}_0$, with CCAV i. The second OCP is formulated by appending (4.24) to the set of equations in (4.22) and (4.23).

4.5.2 . Solution

The solution is obtained using PMP analysis.

Absence of vehicle $i = 0$: The Hamiltonian is formed as,

$$\begin{aligned} H = m(a_1(t)+h)v_1(t) + b(a_1(t)+h)^2 + \lambda_1 a_1(t) + \mu_1 v_1(t) \\ + \sum_{i=2}^{N} m(a_i(t)+h)(v_1(t) - \sum_{n=2}^{i} w_n(t)) + b(a_i(t)+h)^2 \\ + \lambda_i(a_{i-1}(t) - a_i(t)) + \mu_i w_i(t). \end{aligned} \tag{4.25}$$

The co-state dynamics, for $i = 1$, are given as

$$\begin{aligned} \dot{\mu_1}(t) &= -\frac{\partial H}{\partial x_1} = 0 \\ \dot{\lambda_1}(t) &= -\frac{\partial H}{\partial v_1} = \sum_{i=1}^{N} m(a_i(t)+h) + \mu_1, \end{aligned} \tag{4.26}$$

and for the rest $N-1$ and $\forall\ i \in [2, N]$ are given as

$$\begin{aligned} \dot{\mu_i}(t) &= -\frac{\partial H}{\partial \xi_i} = 0 \\ \dot{\lambda_i}(t) &= -\frac{\partial H}{\partial w_i} = -m(a_i(t)+h) + \mu_i. \end{aligned} \tag{4.27}$$

The control input $a(t)$ for $i = 1$ is given by

$$\begin{aligned} \frac{\partial H}{\partial a_1} &= m v_1(t) + 2b(a_1(t)+h) + \lambda_1(t) + \lambda_2(t) = 0, \\ a_1(t) &= -\frac{1}{2b}\left(m v_1(t) + \lambda_1(t) + \lambda_2(t)\right) - h. \end{aligned} \tag{4.28}$$

and for all $i \in [2, N]$

$$\begin{aligned} \frac{\partial H}{\partial a_i} &= m(v_1(t) - \sum_{n=2}^{N} w_n(t)) + 2b(a_i(t)+h) - \lambda_i(t) + \mathbb{1}_A \lambda_{i+1}(t) = 0, \\ a_i(t) &= -\frac{1}{2b}\left(m(v_1(t) - \sum_{n=2}^{N} w_n(t))) + \lambda_i(t) - \mathbb{1}_A \lambda_{i+1}(t)\right) - h \end{aligned} \tag{4.29}$$

where $\mathbb{1}$ is an indicator function of subset $A = [2, N-1]$.

For $i = 1$, the necessary condition $\partial H/\partial a_1 = 0$ depends on the adjoint states to its own speed and relative speed to the follower. However, when solving for the optimal solution $v_1(t)$, one would find the same solution as in (4.6) with $i = 1$, indicating that the first follower is not affected by the cooperation of the platoon. For the rest $N - 1$ vehicles, the optimal solution for relative velocity is given by

$$w_i(t) = w_{i,0} - \left(\frac{4w_{i,0}}{T_{i,f}} - \frac{6\xi_{i,f}}{T_{i,f}^2} + \frac{6\xi_{i,0}}{T_{i,f}^2}\right) t - \left(\frac{6\xi_{i,f}}{T_{i,f}^3} - \frac{6\xi_{i,0}}{T_{i,f}^3} - \frac{3w_{i,0}}{T_{i,f}^2}\right) t^2, \\ t \in [0, T_{i,f}), \;\; i \in [2, N] \quad (4.30)$$

and the velocity of vehicles $2 \leq i \leq N$ is given by

$$v_i(t) = v_1(t) - \sum_{n=2}^{i} w_n(t). \quad (4.31)$$

Thus, the optimal velocity of vehicles $2 \leq i \leq N$, depends on $v_1(t)$ and relative speed of preceding vehicles, as per the relation (4.31), indicating the cooperative nature of the Centralized strategy. The optimal solution of the relative position (spacing gap) is given by

$$\xi_i(t) = \xi_{i,0} + w_{i,0}t - \left(\frac{2w_{i,0}}{T_{i,f}} - \frac{3\xi_{i,f}}{T_{i,f}^2} + \frac{3\xi_{i,0}}{T_{i,f}^2}\right) t^2 \\ - \left(\frac{2\xi_{i,f}}{T_{i,f}^3} - \frac{2\xi_{i,0}}{T_{i,f}^3} - \frac{w_{i,0}}{T_{i,f}^2}\right) t^3, \; t \in [0, T_{i,f}), \; i \in [2, N]. \quad (4.32)$$

It can be proven that $\xi_i(t)$ given by (4.32) will always be greater than or equal to zero provided the final relative position $\xi_{i,f} \geq 0$ and certain conditions are satisfied. Thus the solution (4.30) for CCAVs $2 \leq i \leq N$ is sufficient to remain collision free. The conditions under which $\xi_i(t) \geq 0$ are discussed in Sect. 4.6.3.

Presence of vehicle $i = 0$**:** In the *presence* of a preceding vehicle $i = 0$ in front of the platoon, the optimal solution for the vehicle $i = 1$ is the same as in the Cooperative EDOC, given by the Eqn.(4.20). The solution for the rest $N - 1$ vehicles remains unchanged.

4.5.3 . Implementation

Similar to the NC-EDOC and C-EDOC, the optimal solutions are implemented in a MPC framework. The optimal solution is rewritten, using (4.30), with boundary conditions in the MPC horizon as, $\mathcal{BC} : \{\xi_{i,0} = \xi_i(t), w_i(0) = w_i(t), \xi_i(T_i) = \xi_{i,f}, w_i(T_i) = 0\}$, as

$$w_i(k) = w_i(t) - \left(\frac{4w_i(t)}{T_i} - \frac{6\xi_{i,f}}{T_i^2} + \frac{6\xi_i(t)}{T_i^2}\right) k - \\ \left(\frac{6\xi_{i,f}}{T_i^3} - \frac{6\xi_i(t)}{T_i^3} - \frac{3w_i(t)}{T_i^2}\right) k^2, \;\; k \in [0, T_i) \quad (4.33)$$

For the Centralized Cooperative case, the explicit control inputs evaluated at $k = 0$ for CCAV $i = 1$ are the same as given in Sect. 4.4.3 and for CCAVs $2 \leq i \leq N$, it is obtained from (4.31). For vehicle $i > 1$, the control input a_i, in the *absence* of a vehicle $i = 0$, is given by

$$a_i(t) = \left(-\frac{4}{T_1}v_1(t) - \frac{2}{T_1}V_1 + \frac{6}{T_1^2}D_1\right) - \sum_{n=2}^{i}\left(\frac{4w_n(t)}{T_n} - \frac{6\xi_{n,f}}{T_n^2} + \frac{6\xi_n(t)}{T_n^2}\right),\ 2 \leq i \leq N \quad (4.34)$$

and in the *presence* of a vehicle $i = 0$, is given by

$$a_i(t) = \left(a_0(t) + \frac{4}{\theta_1}\dot{\xi}_1(t) + \frac{6}{\theta_1^2}\xi_1(t)\right) - \sum_{n=2}^{i}\left(\frac{4w_n(t)}{T_n} - \frac{6\xi_{n,f}}{T_n^2} + \frac{6\xi_n(t)}{T_n^2}\right),\ 2 \leq i \leq N \quad (4.35)$$

where $a_0(t)$ is the current acceleration of the vehicle leading the Centralized platoon.

4.6 . String stability

This section verifies if the car-following feedback control law obtained, for the NC-EDOC, C-EDOC and CC-EDOC are string stable. As previously stated, a tight formation platoon can experience "string instability" where the disturbance of the system states are amplified along the string. Various definitions and analysis methods have been proposed in literature to study string stability [1]. In this study, we employ the definition of a "strong frequency domain string stability" sufficient condition [8] which states that, a platoon with linear control law and predecessor following topology is string stable, if the transfer function between of the outputs between CCAV i and CCAV $i-1$, denoted by $\mathcal{G}$, is such that

$$||\mathcal{G}(s)||_\infty \leq 1. \quad (4.36)$$

$s \to j\omega$ denotes the Laplace variable, and $||.||_\infty$ denotes the maximum amplitude for all $\omega > 0$. Disturbance of various system states, such as velocity, gap and position are often considered in literature. However, for a homogeneous platoon the transfer function for these signals are identical. Focusing on preventing collisions, the error between the desired and the actual inter vehicle distances, given by ξ_i, is often considered. If ξ_i denotes the signal of interest, the string stability transfer function $\mathcal{G}_i(j\omega)$, for a CCAV i is written as

$$\mathcal{G}_i(j\omega) = \frac{\xi_i(j\omega)}{\xi_{i-1}(j\omega)}, \quad \forall i \in [1, N]. \quad (4.37)$$

The platoon is said to be string stable if

$$||\mathcal{G}_i(j\omega)||_\infty \leq 1, \quad \forall i \in [1, N], \;\; \omega > 0. \tag{4.38}$$

In the case $||\mathcal{G}_i(j\omega)||_\infty = 1$, this condition is called marginally string stable.

4.6.1 . Non-Cooperative EDOC

To study the string stability of a platoon it is convenient to define the system states that couples the dynamics of CCAV i and its predecessor CCAV $i-1$. Here, the system states are defined as $z = (\xi_i, \dot{\xi}_i, v_i, a_{i-1})$. The non-linear control law $a_i(t)$ for a NC-EDOC under nominal conditions (i.e. without infeasibilities) is given by (4.13), and is stated below:

$$a_i(t) = a_{i-1}(t) + \frac{4}{\theta_i}\dot{\xi}_i(t) + \frac{6}{\theta_i^2}\xi_i(t). \tag{4.39}$$

The term $\theta_i = f(z_i, D_i, T_i, V_i)$ is given by

$$a\theta_i^3 + b\theta_i^2 + c\theta_i + d = 0, \tag{4.40}$$

where

$$\begin{aligned} a &= v_i - V_i + a_{i-1}T_i \\ b &= 2T_i(2\dot{\xi}_i + v_i) + V_iT_i + a_{i-1}T_i^2/2 - 3D_i \\ c &= 6\xi_iT_i - \dot{\xi}_iT_i^2 \\ d &= -3\xi_iT_i^2. \end{aligned}$$

To make the analysis simpler, a receding horizon approach is assumed where D_i, T_i and V_i, are considered constants. An explicit solution for θ_i is obtained by solving for the root of the cubic equation (4.40), given by

$$\theta_i = \left(q + \left(q^2 + (r - p^2)^3\right)^{1/2}\right)^{1/3} + \left(q - \left(q^2 + (r - p^2)^3\right)^{1/2}\right)^{1/3} + p, \tag{4.41}$$

where

$$p = -b/(3a), \;\; q = p^3 + (bc - 3ad)/(6a^2), \;\; r = c/(3a).$$

4.6.1.1 . String Stability Transfer Function, $\mathcal{G}_{i,NC}$

To obtain the string stability transfer function $\mathcal{G}_{i,NC}(j\omega)$, the non-linear control law given by (4.39) is linearised around the equilibrium with a positive θ_i[2]. An equilibrium condition for a non-stationary platoon is given by $a_i(z_i) = 0, \forall i \in [1, N]$, where $z_i = (0, 0, v^*, 0)$. This indicates that all the CCAVs drive at the same speed v^*. The linearised control law around equilibrium is obtained as

$$\bar{a_i} = f_\xi\bar{\xi}_i + f_{\dot{\xi}}\dot{\bar{\xi}}_i + f_v\bar{v_i} + f_a\bar{a}_{i-1}, \tag{4.42}$$

[2]A positive θ_i at equilibrium exists under the conditions $V_i < v_i$ and $D_i/T_i > (2v_i + V_i)/3$

where $\bar{\xi}_i = \xi_i - \xi_{i,e}, \dot{\bar{\xi}}_i = \dot{\xi}_i - \dot{\xi}_{i,e}, \bar{v}_i = v_i - v_{i,e}$ and, $\bar{a}_{i-1} = a_{i-1} - a_{i-1,e}$ denote the perturbations and subscript e denotes the states at equilibrium. The terms $f_\xi = \frac{\partial a_i}{\partial \xi_i}, f_{\dot{\xi}} = \frac{\partial a_i}{\partial \dot{\xi}_i}, f_v = \frac{\partial a_i}{\partial v_i}, f_a = \frac{\partial a_i}{\partial a_{i-1}}$ denote the partial derivatives of (4.39) explicitly evaluated as

$$f_\xi = \frac{6}{\theta_i^2} - \frac{4\dot{\xi}_i \frac{\partial \theta_i}{\partial \xi_i}}{\theta_i^2} - \frac{12\xi_i \frac{\partial \theta_i}{\partial \xi_i}}{\theta_i^3}, \tag{4.43a}$$

$$f_{\dot{\xi}} = \frac{4}{\theta_i} - \frac{4\dot{\xi}_i \frac{\partial \theta_i}{\partial \dot{\xi}_i}}{\theta_i^2} - \frac{12\xi_i \frac{\partial \theta_i}{\partial \dot{\xi}_i}}{\theta_i^3}, \tag{4.43b}$$

$$f_v = -\left(\frac{4\dot{\xi}_i \frac{\partial \theta_i}{\partial v_i}}{\theta_i^2} + \frac{12\xi_i \frac{\partial \theta_i}{\partial v_i}}{\theta_i^3} \right), \tag{4.43c}$$

$$f_a = 1 - \left(\frac{4\dot{\xi}_i \frac{\partial \theta_i}{\partial a_{i-1}}}{\theta_i^2} + \frac{12\xi_i \frac{\partial \theta_i}{\partial a_{i-1}}}{\theta_i^3} \right). \tag{4.43d}$$

The dependency of the states on time and for θ_i on z are dropped for readability. The dynamics of the spacing error are given by

$$\begin{aligned} \bar{\xi}_i &= \bar{x}_{i-1} - \bar{x}_i \\ \dot{\bar{\xi}}_i &= \bar{v}_{i-1} - \bar{v}_i, \\ \ddot{\bar{\xi}}_i &= \bar{a}_{i-1} - \bar{a}_i, \end{aligned} \tag{4.44}$$

Substituting for $\bar{a}_{i-1}$ and $\bar{a}_i$ using (4.42) yields

$$\ddot{\bar{\xi}}_i = f_\xi(\bar{\xi}_{i-1} - \bar{\xi}_i) + f_{\dot{\xi}}(\dot{\bar{\xi}}_{i-1} - \dot{\bar{\xi}}_i) + f_v(\bar{v}_{i-1} - \bar{v}_i) + f_a(\bar{a}_{i-1} - \bar{a}_{i-2}). \tag{4.45}$$

Replacing $\dot{\bar{\xi}}_i = (\bar{v}_{i-1} - \bar{v}_i)$ and $\ddot{\bar{\xi}}_{i-1} = (\bar{a}_{i-1} - \bar{a}_{i-2})$, the last equation is rearranged to yield

$$\ddot{\bar{\xi}}_i + (f_{\dot{\xi}} - f_v)\dot{\bar{\xi}}_i + f_\xi \bar{\xi}_i = f_a \ddot{\bar{\xi}}_{i-1} + f_{\dot{\xi}} \dot{\bar{\xi}}_{i-1} + f_\xi \bar{\xi}_{i-1}. \tag{4.46}$$

With the bar on the variables dropped for readability, assuming zero initial conditions and taking Laplace transform of Eqn. (4.46), the string stability transfer function $\mathcal{G}_{i,NC}(s)$ of ξ_i is given as

$$\mathcal{G}_{i,NC}(s) = \frac{\xi_i}{\xi_{i-1}} = \frac{f_a s^2 + f_{\dot{\xi}} s + f_\xi}{s^2 + (f_{\dot{\xi}} - f_v)s + f_\xi}. \tag{4.47}$$

Inserting $s \to j\omega$

$$\mathcal{G}_{i,NC}(j\omega) = \frac{UP}{LP} = \frac{-f_a \omega^2 + f_{\dot{\xi}} j\omega + f_\xi}{-\omega^2 + (f_{\dot{\xi}} - f_v)j\omega + f_\xi}. \tag{4.48}$$

4.6.1.2 . String Stability Criteria

String stability requires $|\frac{UP}{LP}| \leq 1$, which is equivalent to [23]:

$$||UP||_2 \leq ||LP||_2. \tag{4.49}$$

Taking magnitude of UP yields

$$\begin{aligned} |UP| &= (f_\xi - f_a\omega^2)^2 + (f_{\dot{\xi}}\omega)^2, \\ &= f_a^2\omega^4 + (f_{\dot{\xi}}^2 - 2f_\xi f_a)\omega^2 + f_\xi^2. \end{aligned} \tag{4.50}$$

Similarly, the magnitude of LP is given by

$$\begin{aligned} |LP| &= (f_\xi - \omega^2)^2 + (f_{\dot{\xi}} - f_v)^2\omega^2, \\ &= \omega^4 + (f_{\dot{\xi}}^2 + f_v^2 - 2f_{\dot{\xi}}f_v - 2f_\xi)\omega^2 + f_\xi^2. \end{aligned} \tag{4.51}$$

Thus the condition $|\frac{UP}{LP}| \leq 1$ simplifies as:

$$||\mathcal{G}_i(\omega)||_\infty = \frac{f_a^2\omega^4 + (f_{\dot{\xi}}^2 - 2f_\xi f_a)\omega^2 + f_\xi^2}{\omega^4 + (f_{\dot{\xi}}^2 + f_v^2 - 2f_{\dot{\xi}}f_v - 2f_\xi)\omega^2 + f_\xi^2} \leq 1. \tag{4.52}$$

String stability requires $||\mathcal{G}_i(\omega)||_\infty \leq 1$, which is unconditionally satisfied if the coefficients of the LP are greater than the UP. Therefore, the first sufficient condition for string stability is given by

$$f_a^2 \leq 1, \tag{4.53a}$$

$$f_v(2f_{\dot{\xi}} - f_v) - 2f_\xi(f_a - 1) \leq 0. \tag{4.53b}$$

In the event of the coefficients of the LP are not greater than the UP, the second condition for string stability is obtained by maximizing for the polynomial

$$\underset{\omega>0}{max}\ Y_1(\omega) = (f_a^2 - 1)\omega^2 + (2f_{\dot{\xi}}f_v - f_v^2 + 2f_\xi - 2f_\xi f_a) \leq 0 \tag{4.54}$$

The polynomial (4.54) is obtained by rearranging the fraction (4.52) as shown below:

$$f_a^2\omega^4 + (f_{\dot{\xi}}^2 - 2f_\xi f_a)\omega^2 + f_\xi^2 \leq \omega^4 + (f_{\dot{\xi}}^2 + f_v^2 - 2f_{\dot{\xi}}f_v - 2f_\xi)\omega^2 + f_\xi^2, \tag{4.55}$$

$$(f_a^2 - 1)\omega^4 + (2f_{\dot{\xi}}f_v - f_v^2 + 2f_\xi - 2f_\xi f_a)\omega^2 \leq 0. \tag{4.56}$$

After solving for the critical point ω^* by setting $\partial Y_1/\partial\omega = 0$ and inserting it into Y_1, we obtain the second sufficient condition for string stability as,

$$F_{nc,1} = f_a^2 \leq 1, \tag{4.57a}$$

$$F_{nc,2} = f_v(2f_{\dot{\xi}} - f_v) - 2f_\xi(f_a - 1) \leq 0. \tag{4.57b}$$

It can be noticed that both conditions, (4.53) and (4.57) are identical.

4.6.1.3 . String Stability at Equilibrium Point

Evaluating the partial derivatives $f_a, f_v, f_\xi, f_{\dot{\xi}}$ at equilibrium, we obtain

$$f_a = 1, \quad f_v = 0, \quad f_\xi = \frac{6}{\theta_i^2}, \quad f_{\dot{\xi}} = \frac{4}{\theta_i}. \tag{4.58}$$

Substituting these values in (4.52), the magnitude of the transfer function $||\mathcal{G}_i(\omega)||_\infty = 1$, and the inequalities in (4.57) becomes equalities, indicating that the equilibrium point of Non-Cooperative EDOC is only marginally string stable. This is also consistent with literature [8], where a platoon with using constant spacing policy and the acceleration of the preceding vehicle is marginally string stable.

4.6.2 . Cooperative EDOC

This section extends our analysis to the Cooperative-EDOC. The control law of the C-EDOC is identical to that of the Non-Cooperative, with the exception of the instantaneous preceding vehicle's acceleration, $a_{i-1}(t)$, replaced by $\tilde{a}_{i-1}(t)$. The control law reads

$$a_i(t) = \tilde{a}_{i-1}(t) + + \frac{4}{\theta_i}\dot{\xi}_i(t) + \frac{6}{\theta_i^2}\xi_i(t), \tag{4.59}$$

where θ_i is given by (4.41), with $\tilde{a}_{i-1}(t)$ replacing $a_i(t)$ where necessary. In a similar fashion to the NC-EDOC, the C-EDOC is linearised around equilibrium to yield

$$\bar{a_i} = f_\xi \bar{\xi_i} + f_{\dot{\xi}}\dot{\bar{\xi}}_i + f_v \bar{v_i} + f_a \bar{\tilde{a}}_{i-1}, \tag{4.60}$$

with partial derivatives as in (4.43) with $\tilde{a}_{i-1}(t)$ replacing $a_i(t)$ where necessary. The spacing error dynamics equation is obtained as

$$\ddot{\bar{\xi}}_i + (f_{\dot{\xi}} - f_v)\dot{\bar{\xi}}_i + f_\xi \bar{\xi}_i = f_a \ddot{\bar{\xi}}_{i-1} + f_{\dot{\xi}}\dot{\bar{\xi}}_{i-1} + f_\xi \bar{\xi}_{i-1} \tag{4.61}$$

4.6.2.1 . String Stability Transfer Function, $\mathcal{G}_{i,C}$

With the bar on the variables dropped for readability, assuming zero initial conditions and taking Laplace transform of Eqn. (A.17), the string stability transfer function (see Appendix A.5 for derivation) for the C-EDOC $\mathcal{G}_{i,c}(s)$ is given as

$$\mathcal{G}_{i,c}(s) = \frac{\xi_i}{\xi_{i-1}} = \frac{(f_a/L(e^{(sL)} - 1) + f_{\dot{\xi}})s + f_\xi}{s^2 + (f_{\dot{\xi}} - f_v)s + f_\xi}. \tag{4.62}$$

Inserting $s \to j\omega$, we get

$$\mathcal{G}_c(\omega) = \frac{UP}{LP} = \frac{(f_a/L(e^{(j\omega L)} - 1) + f_{\dot{\xi}})j\omega + f_\xi}{-\omega^2 + (f_{\dot{\xi}} - f_v)j\omega + f_\xi}. \tag{4.63}$$

Using the identity $e^{j\omega L} = \cos(\omega L) + j\sin(\omega L)$ and rearranging the UP, we get

$$UP = \left(f_\xi - \frac{f_a\omega}{L}\sin(\omega L)\right) + j\left(\frac{f_a\omega}{L}\cos(\omega L) - \frac{f_a\omega}{L} + f_{\dot{\xi}}\omega\right). \tag{4.64}$$

Taking magnitude of UP yields

$$\begin{aligned}|UP| &= \left(f_\xi - \frac{f_a\omega}{L}\sin(\omega L)\right)^2 + \left(\frac{f_a\omega}{L}\cos(\omega L) - \frac{f_a\omega}{L} + f_{\dot{\xi}}\omega\right)^2, \\ &= \left(f_\xi^2 + \frac{f_a^2\omega^2}{L^2}\sin^2(\omega L) - \frac{2f_\xi f_a\omega}{L}\sin(\omega L)\right) + \left(f_{\dot{\xi}}^2\omega^2 + \frac{f_a^2\omega^2}{L^2} - \right. \\ &\quad \left. \frac{2f_a^2\omega^2}{L^2}\cos(\omega L) + \frac{f_a^2\omega^2}{L^2}\cos^2(\omega L) - \frac{2f_a f_{\dot{\xi}}\omega^2}{L} + \frac{2f_a f_{\dot{\xi}}\omega^2}{L}\cos(\omega L)\right).\end{aligned} \tag{4.65}$$

Using the identity $\sin^2(\omega L)+\cos^2(\omega L) = 1$ and, the Taylor's series approximation $\sin(\omega L) \leq \left(\omega L - \frac{(\omega L)^3}{6}\right)$ and $\cos(\omega L) \leq \left(1 - \frac{(\omega L)^2}{2}\right)$, we get

$$|UP| \geq \left(\frac{L^2 f_a f_\xi}{3} - L f_a f_{\dot{\xi}} + f_a^2\right)\omega^4 + \left(f_{\dot{\xi}}^2 - 2f_a f_\xi\right)\omega^2 + f_\xi^2 \tag{4.66}$$

Similarly, the magnitude of LP is given by

$$|LP| \geq \omega^4 + (f_{\dot{\xi}}^2 + f_v^2 - 2f_{\dot{\xi}} f_v - 2f_\xi)\omega^2 + f_\xi^2. \tag{4.67}$$

Thus the condition $|\frac{UP}{LP}| \leq 1$ simplifies as:

$$\frac{\left(\frac{L^2 f_a f_\xi}{3} - L f_a f_{\dot{\xi}} + f_a^2\right)\omega^4 + \left(f_{\dot{\xi}}^2 - 2f_a f_\xi\right)\omega^2 + f_\xi^2}{\omega^4 + (f_{\dot{\xi}}^2 + f_v^2 - 2f_{\dot{\xi}} f_v - 2f_\xi)\omega^2 + f_\xi^2} \leq 1. \tag{4.68}$$

4.6.2.2 . String Stability Criteria

Similar to the Non-Cooperative case, the conditions for the transfer function $\mathcal{G}_{i,C} \leq 1$ is obtained by analysing the coefficients of the fraction and finding the maximum of the function obtained from (4.68). In doing so, the conditions for Cooperative string stability are given by

$$F_{c,1} = \left(\frac{L^2 f_a f_\xi}{3} - L f_a f_{\dot{\xi}} + f_a^2\right) \leq 1, \tag{4.69a}$$

$$F_{c,2} = f_v(2f_{\dot{\xi}} - f_v) - 2f_\xi(f_a - 1) \leq 0 \tag{4.69b}$$

4.6.2.3 . String Stability at Equilibrium Point

With the partial derivatives at equilibrium obtained as, $f_a = 1, f_v = 0, f_\xi = \frac{6}{\theta_i^2}, f_{\dot{\xi}} = \frac{4}{\theta_i}$ and evaluating (4.69) at equilibrium, the condition (4.69b) is equal to zero, as in (4.57b). The condition (4.69a) is less than 1 if

$$\frac{f_\xi L^2}{3} - L f_{\dot{\xi}} < 0, \tag{4.70}$$

Evaluating θ_i at equilibrium we obtain

$$\theta_i = \frac{-b}{a} \tag{4.71}$$

where $b = 2T_i v_i + V_i T_i - 3D_i$ and $a = (v - V)$. Substituting (4.71) in f_ξ and $f_{\dot{\xi}}$, the condition (4.69a) is simplified as

$$L < 2\theta_i. \tag{4.72}$$

Expanding the terms yield a condition for Cooperative string stability in terms of its boundary conditions and the preview window length as

$$(v_i - V_i)L + 4T_i v_i + 2V_i T_i - 6D_i < 0. \tag{4.73}$$

The magnitude of the transfer function $\mathcal{G}_{i,C}$ is less than 1, if the above condition is satisfied indicating cooperation improves string stability over the Non-Cooperative EDOC where only marginal string stability could be guaranteed.

A careful analysis of the condition (4.69a), which is quadratic in L, shows that, for $L = 0$, the Cooperative condition (4.69a) reduces to the Non-Cooperative condition (4.57a), which is consistent with the definitions of the Cooperative and Non-Cooperative schemes. Furthermore, the condition (4.69a) has a minimum at θ_i and indicates instability at $L > 2\theta_i$. Graphically, this is represented in Fig. 4.2.

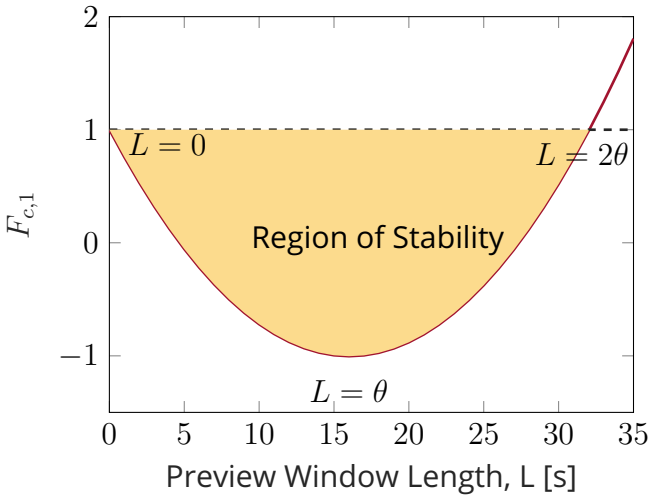

Figure 4.2: Region of Stability. The figure is plotted at equilibrium for values of $f_\xi = 0.0234$ and $f_{\dot{\xi}} = 0.25$

4.6.2.4 . Numerical Evaluation

A numerical analysis is performed to further evaluate the benefits of cooperation on string stability. The conditions obtained from the above theoretical analysis is evaluated for different boundary conditions *around* the equilibrium. For a fixed $D_i = 500$ m and $T_i = 60$ s, the other boundary conditions $\xi_i, \dot{\xi}_i, v_i, V_i, a_{i-1}$ are varied randomly around the equilibrium following a normal distribution. The distributions of the boundary conditions are given in Appendix A.6. Fig 4.3 shows

the frequency distributions for varying values of $L = 5, 10, 20$ of the conditions (4.57a) and (4.69a) when (4.57b, 4.69b) is satisfied. The distribution of values in the stability region for the C-EDOC is higher than the NC-EDOC and increases for increasing values of L, further indicating that cooperation improves the string stability of a platoon.

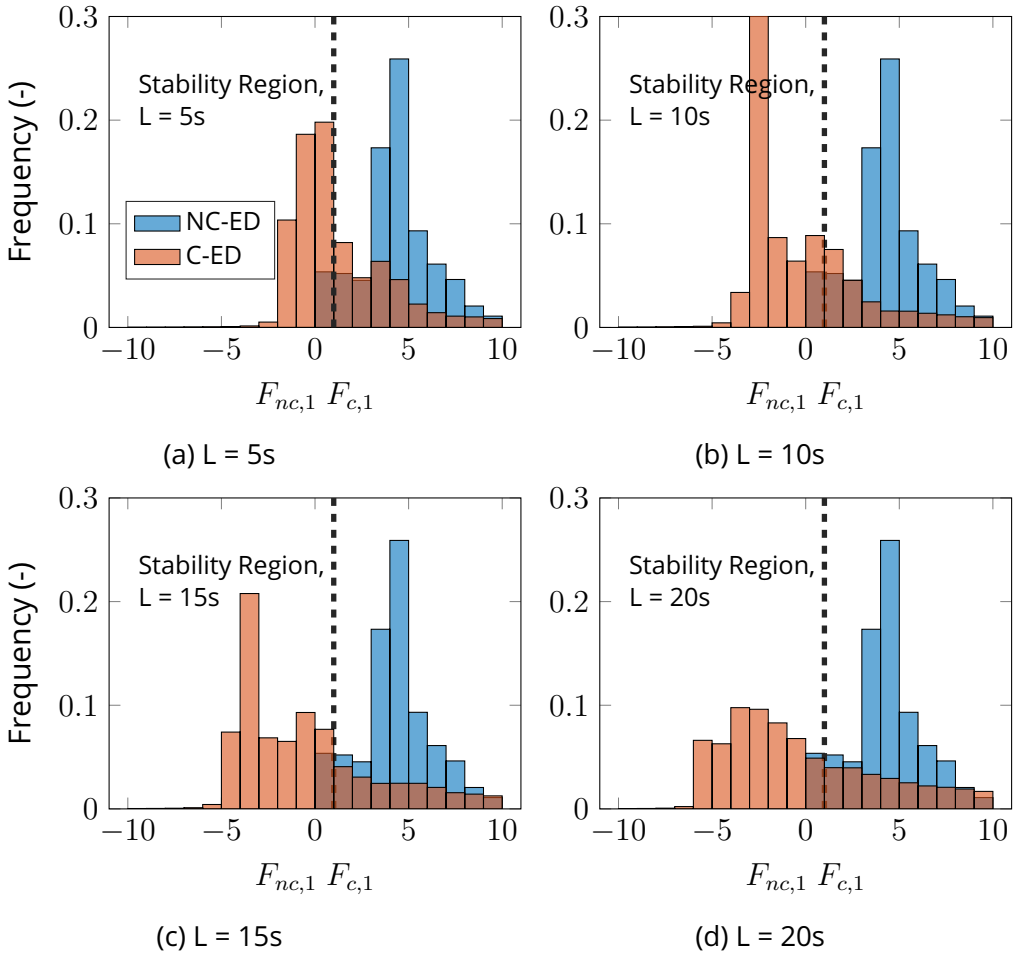

Figure 4.3: Frequency Distribution of the NC-ED ($F_{nc,1}$) and C-ED ($F_{c,1}$) stability conditions for varying values of L when ($F_{nc,2}$,$F_{c,2}$) are satisfied. The left side of the dotted line indicates stability region.

4.6.3 . Centralized Cooperative EDOC

The string stability Centralized Cooperative EDOC platoon can be studied without the use of the transfer function in frequency domain. An explicit solution for relative position (i.e. spacing error) for the CC-EDOC is given by (4.32). Assuming same boundary conditions for relative velocity and position for all CCAVs $i \in [2, N]$, the spacing gap between any CCAV i and $i-1$ has the same

dynamics given by

$$w(k) = w(t) - \left(\frac{4w(t)}{T} - \frac{6\xi_f}{T^2} + \frac{6\xi(t)}{T^2}\right)k - \left(\frac{6\xi_f}{T^3} - \frac{6\xi(t)}{T^3} - \frac{3w(t)}{T^2}\right)k^2, \quad k \in [0, T). \tag{4.74}$$

Identical relative position dynamics for all CCAVs indicate that the spacing gap does not propagate upstream the platoon, thereby maintaining string stability. An example of the relative position and velocity is shown in Fig. 4.4 for a CC-EDOC platoon.

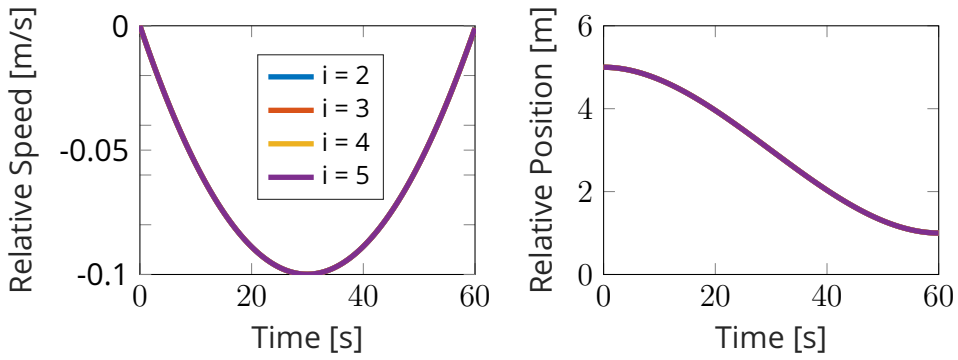

(a) (b) Relative Position $\xi_i(k)$

Figure 4.4: Relative Velocity $w_i(k)$ in (a) and Relative Position $\xi_i(k)$ in (b) for CCAVs $i \in [2, 5]$

Table 4.1: The local minimum, its critical point and the conditions for the local minimum to remain at its critical point

Cases	Local Minimum	Crit. Point	Condition
$w_i(t) \geq 0$, $\Delta\xi_i \geq 0$	$\xi_{i,f}$	$k = T_i$	-
$w_i(t) \geq 0$, $\Delta\xi_i \leq 0$	$\xi_{i,f}$	$k = T_i$	$T_i\lvert w_i(t)\rvert > 3\lvert\Delta\xi_i\rvert$
$w_i(t) \leq 0$, $\Delta\xi_i \geq 0$	$\xi_{i,f}$	$k = T_i$	$T_i\lvert w_i(t)\rvert < 3\lvert\Delta\xi_i\rvert$
$w_i(t) \leq 0$, $\Delta\xi_i \leq 0$	ξ_{min}[a]	k_1[a]	$\xi_{min} \geq 0$

[a] Refer to Appendix A.7

However, the choice of a certain set boundary conditions could render $\xi_i(k) < 0$, causing a rear-end collision. The conditions under which $\xi_i(k) \geq 0$ is ensured is discussed here. Equation (4.32), being a cubic function of time, has one local minimum and maximum and the critical point indicates where the local minimum occurs. The critical points of $\xi_i(k)$ are obtained from $w_i(k) = 0$. A local minimum

occurring within an interval with positive values at its extremities, is automatically the global minimum in that interval, for a cubic equation. Therefore, a non-negative local minimum in the interval $[0, T_i]$ guarantees $\xi_i(k) \geq 0$. Four cases are considered based on the signs of $w_i(t)$ and $\Delta\xi_i = \xi_i(t) - \xi_{i,f}$.

Table 4.1 gives the local minimum and its critical point for the four considered cases. A positive local minimum with its critical point within the prediction horizon would guarantee $\xi_i(k) \geq 0, \ \forall \ k \in [0, T_i]$. For the first three cases, the local minimum is $\xi_{i,f}$ and it occurs at T_i, ensuring $\xi_i(k) \geq 0$. However, for the last case, a negative local minimum ξ_{min} occurs at $k_1 \in [0, T_i]$. The condition $\xi_{min} \geq 0$ is enforced so that $\xi_i(k) \geq 0, \ \forall \ k \in [0, T_i]$. The equation for ξ_{min} and the proof that k_1 occurs within the horizon T_i is given in the Appendix A.7.

4.7 . Simulation results

This section discusses the simulation results of energy assessment and mean string length. The energy is computed using the model detailed in Sect. 2.4. Four homogeneous platoons, each with $N = 5$, with different algorithms are simulated. The first one is equipped with an ACC using a constant headway time of 1.2 s. The second, third and the fourth platoon are equipped with the NC-EDOC, C-EDOC and CC-EDOC respectively. The WLTC High drive cycle is used for energy assessment and the string compactness is assessed using the mean string length. The leader in the platoon $i = 0$, acting as the virtual reference trajectory, follows the WLTC cycle in open loop, with no elevation, covering a fixed distance D_i in a fixed time T_i.

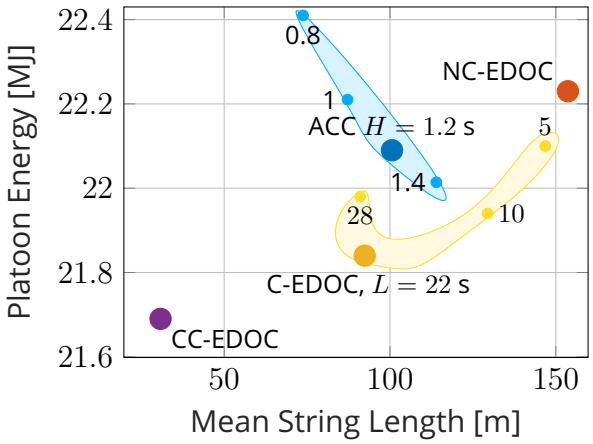

Figure 4.5: Energy vs Mean String Length of the four algorithms. ACC with $H = 1.2$ s, represents the minimum headway time for string stability for the used proportional and derivative gains and $L = 22$ s, is the preview window length for minimum energy consumption of the Cooperative strategy.

A study by [17] showed the NC-EDOC algorithm has better energy efficiency

with a single follower in comparison to the ACC but performed worse in terms of energy efficiency and string compactness when evaluated with several following vehicles. Figure 4.5, shows the energy efficiency versus mean string length, excluding the virtual reference vehicle $i = 0$, of the different algorithms. The C-EDOC, with $L = 22$ s overcomes the drawbacks of the NC-EDOC in a platoon, performing better in terms of energy efficiency and string compactness. The gain in energy efficiency is attributed to better prediction of the preceding vehicle in the C-EDOC. The NC-EDOC predicts the preceding vehicle using the constant instantaneous acceleration $a_{i-1}(t)$ over the prediction horizon T_i. However, this prediction can sometimes cause CCAV i to overreact to an instantaneous strong deceleration of CCAV $i-1$, that is likely to change its acceleration in the near future. The C-EDOC captures to an extent this change in acceleration of the preceding vehicle by using the mean of the future accelerations $\tilde{a}_{i-1}(t)$ over a window length L. The preview window length L is chosen based on a sensitivity analysis for minimum energy consumption for a given trajectory. A too small horizon length L, may not capture any preceding vehicle's change in acceleration and a too large L, could cause the ego vehicle to react to a change too far out in the future. In this simulation, with vehicle $i = 0$ following WLTC High, a too large L caused the ego vehicles to travel slower in the beginning, increasing its gap from $i = 0$, and travel faster towards the end to satisfy the enforced average speed. This opposing behavior of planning for too far in the future while having to satisfy the given average speed ($D_{i,f}/T_{i,f}$) increases the energy consumption. The CC-EDOC performs best in terms of energy efficiency and string compactness owing to the cooperative nature of CCAVs to reduce the overall energy consumption, provided vehicle $i = 1$ follows an eco-driving speed profile.

Figure 4.6, shows the velocity profiles of the vehicles in the platoon with the four different algorithms. It can be seen that NC-ED, using $a_{i-1}(t)$ smoothens out certain speed fluctuations of the reference trajectory but appears to have certain discontinuities (sharp decelerations) when the leader is decelerating aggressively (for example, between 350 s and 450 s). On the other hand, the velocity trajectories of the Cooperative eco-driving algorithm have reduced discontinuities and follow a much smoother trajectory as a result of using the average of the future accelerations $\tilde{a}_{i-1}(t)$ of the preceding vehicle. The vehicles in the Centralized Cooperative algorithm follow an almost unvaried speed profile amongst each other, indicating fewer variations in accelerations/decelerations among them. This, in turn, contributes to better overall energy efficiency as a platoon compared to the other algorithms.

Remark 1. *The implementation complexity of the three cooperative algorithms in a platoon can be two fold, i.e., computational speed and required information to obtain the ED control input. The closed-form analytical solutions obtained for the three cooperative algorithms ensure high computational efficiency. However, the information required by each algorithm increases with increasing cooperation.*

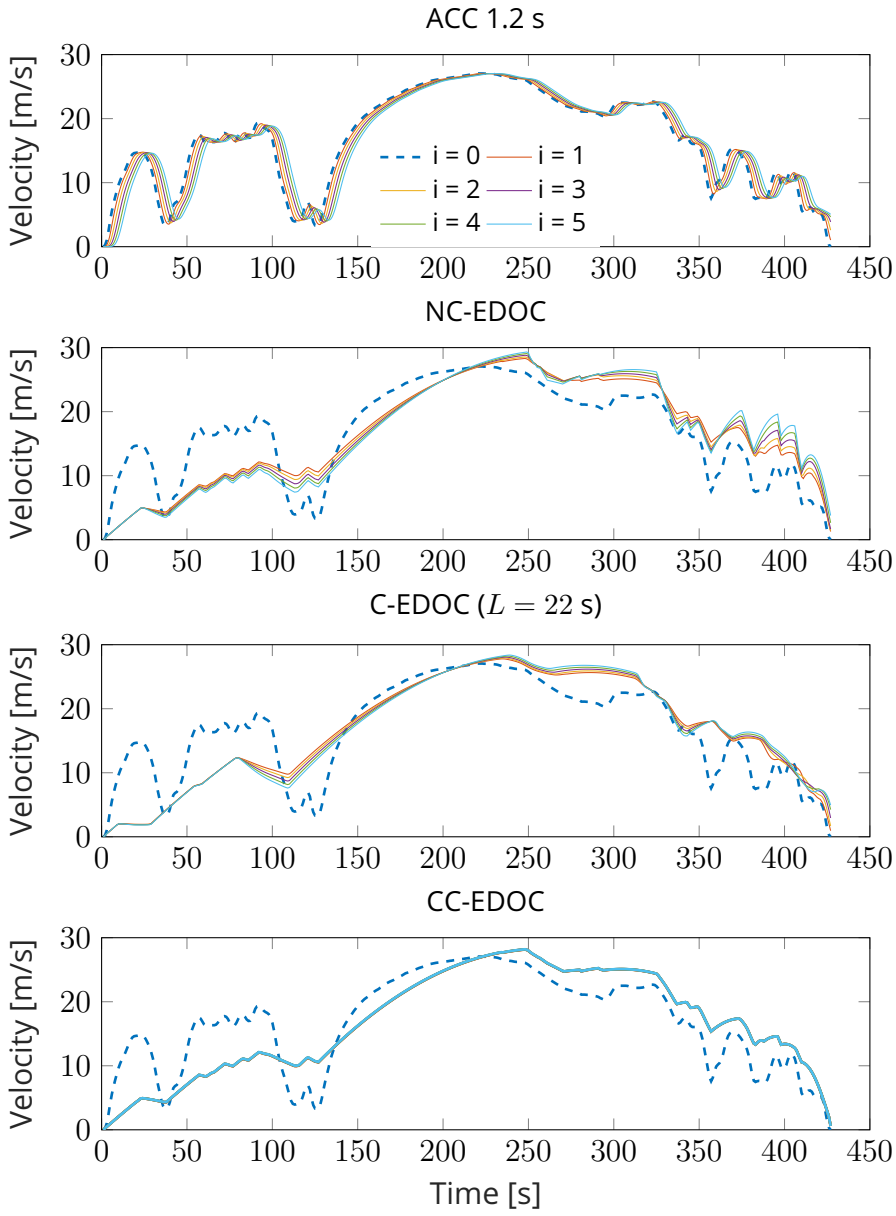

Figure 4.6: Velocity Trajectories in the WLTC High Cycle

This in turn increases the complexity in the perception/communication modules of a CCAV. The NC-ED platoon requires the instantaneous information, via sensors, of CCAV $i-1$ to obtain its control input while the C-ED platoon requires CCAV $i-1$ to share its intentions via communication. The CC-ED platoon requires all the CCAVs preceding CCAV i to share its information, making it the platoon with the highest complexity.

Specific Case Study : In this section, we detail the discontinuities observed

in the velocity trajectories of NC-EDOC in Figure 4.6. The situation simulated here shows a homogeneous platoon with $N = 10$ under a sinusoidal perturbation, for the leader $i = 0$, of frequency $\omega = 0.01$ rads/s and final time $T_{i,f} = 630$ s. The vehicles in a platoon start with the same initial velocity and a certain initial separation greater than s_{min}.

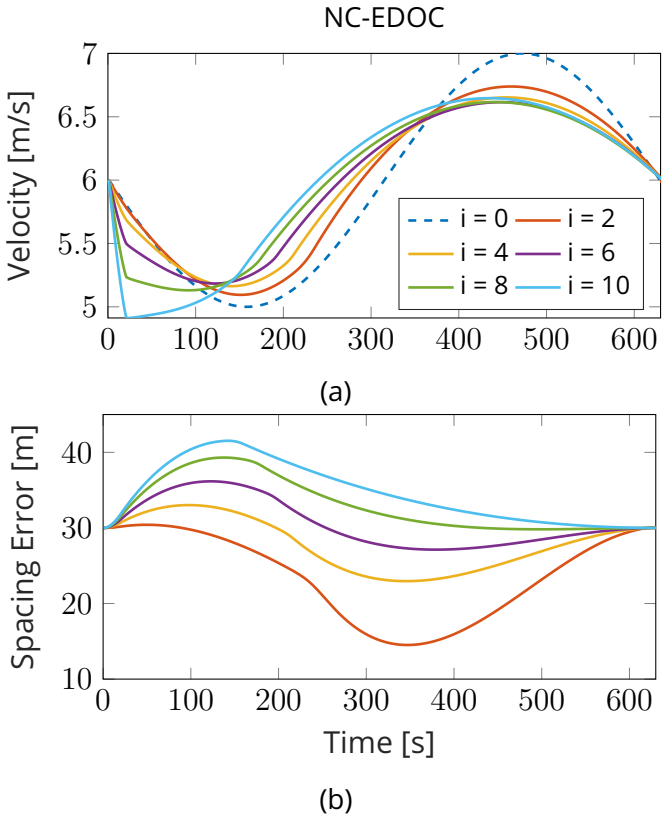

Figure 4.7: Velocity profile (Fig. 4.7a) and spacing error (Fig. 4.7b) of a NC-EDOC platoon ($N = 10$) under a sinusoidal perturbation of the leader

Figures 4.7a–4.7b show the Non-Cooperative case where the preceding vehicle shares only its current acceleration a_{i-1}. At the first time step, the ego vehicle finds its preceding vehicle decelerating and stopping at a time $t_{stop} = v_{i-1}/|a_{i-1}| = 6/0.01 = 600$ s, which is less than $T_i = 630$ s. This would obstruct the ego vehicle to reach its destination D_i. The controller, therefore based on the condition $t_{stop} < T_i$ chooses (4.15) as its control input. Since a large negative acceleration a_{i-1} is assumed to persist in the future, the controller tends to overreact to preceding vehicle's acceleration, that is likely to change after several seconds. In doing so, the acceleration of each vehicle is larger in magnitude than its preceding vehicle as we move upstream in the platoon, eventually causing them to come to a stand still. Figure 4.7a shows the velocity profile of the vehicles in the platoon and Fig. 4.7b the amplification of the spacing error during the beginning of the trip, thus making

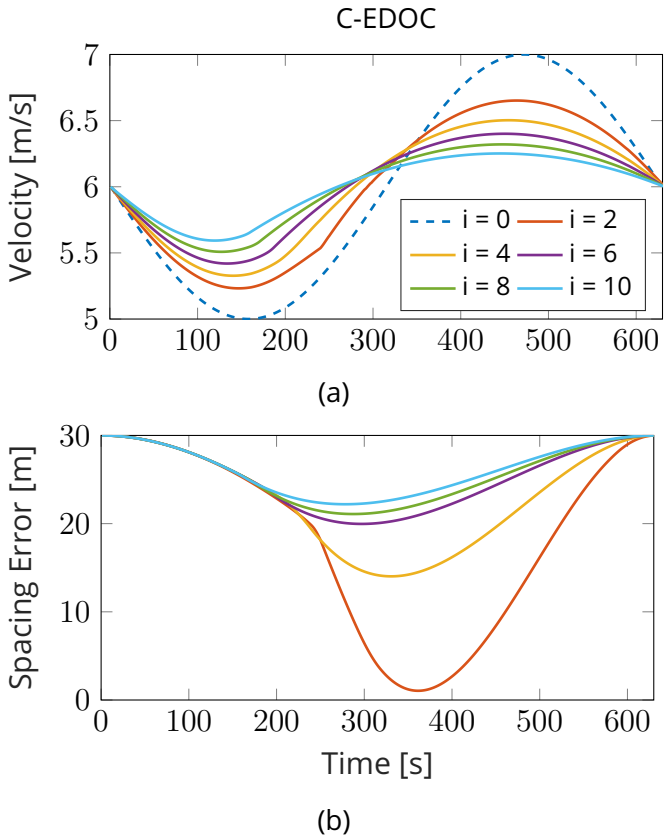

Figure 4.8: Velocity profile (Fig. 4.8a) and spacing error (Fig. 4.8b) of an C-EDOC platoon ($N = 10$) under a sinusoidal perturbation of the leader, with $L = 40$ s.

the platoon string unstable.

In the Cooperative case, Figures 4.8a–4.8b, the leader $i = 0$ following a known trajectory, now shares its vector of future acceleration over a preview window length $L = 40$ s. The following vehicle $i = 1$, solving its OCP with constant preceding vehicle acceleration, uses the mean of the acceleration vector $\tilde{a}_{i-1}$ over 40 s rather than instantaneous acceleration a_{i-1}. The mean of the shared acceleration $\tilde{a}_{i-1}$ is now lower in magnitude than the current acceleration a_{i-1}, indicating that the preceding vehicle is either going to reduce its deceleration or start accelerating in the near future. The condition $t_{stop} < T_i$ now finds the preceding vehicle to stop at a time after the final time T_i, thereby enabling the controller to use control input (4.17). Figure 4.8a shows the velocity profile of the ego vehicles in the platoon. The deceleration of each vehicle is attenuated as we go upstream the platoon, thereby preventing any propagation of spacing error.

4.8 . Conclusion

A car-following ED scenario formulated as an OCP in Chap. 2 is extended to the platoons. Three levels of cooperation (i.e., NC-ED, C-ED, and CC-ED) are applied to the platoons and evaluated for their energy efficiency and string compactness. While NC-EDOC is energy efficient with a single follower, it performs worse in energy efficiency and string compactness when evaluated in a string of several following vehicles. This is mainly attributed to the overreaction of the ego vehicle to an instantaneous strong acceleration/deceleration of the preceding vehicle. The C-EDOC, when using the average of the future acceleration of the preceding vehicle, has a better motion prediction and compensates to an extent for the overreaction of the ego vehicle. This improves energy efficiency and string compactness compared to NC-EDOC. The CC-EDOC performs best in terms of energy efficiency and string compactness. This confirms our intuitive understanding that a rigid platoon would be the target if the leading vehicle performs eco-driving.

Bibliography

[1] Shuo Feng, Yi Zhang, Shengbo Eben Li, Zhong Cao, Henry X Liu, and Li Li. String stability for vehicular platoon control: Definitions and analysis methods. Annual Reviews in Control, 47:81–97, 2019.

[2] L.E. Peppard. String stability of relative-motion pid vehicle control systems. IEEE Transactions on Automatic Control, 19(5):579–581, 1974. cited By 113.

[3] Lingyun Xiao and Feng Gao. Practical string stability of platoon of adaptive cruise control vehicles. IEEE Transactions on intelligent transportation systems, 12(4):1184–1194, 2011.

[4] D. Swaroop and J. K. Hedrick. Constant Spacing Strategies for Platooning in Automated Highway Systems. Journal of Dynamic Systems, Measurement, and Control, 121(3):462–470, 09 1999.

[5] P. Seiler, A. Pant, and K. Hedrick. Disturbance propagation in vehicle strings. IEEE Transactions on Automatic Control, 49(10):1835–1842, 2004.

[6] D. Swaroop and J. K. Hedrick. String stability of interconnected systems. IEEE Transactions on Automatic Control, 41(3):349–357, 1996.

[7] E. Shaw and J. K. Hedrick. String stability analysis for heterogeneous vehicle strings. In 2007 American Control Conference, pages 3118–3125, 2007.

[8] Gerrit JL Naus, Rene PA Vugts, Jeroen Ploeg, Marinus JG van De Molengraft, and Maarten Steinbuch. String-stable cacc design and experimental validation: A frequency-domain approach. IEEE Transactions on vehicular technology, 59(9):4268–4279, 2010.

[9] S. Sheikholeslam and C. A. Desoer. Longitudinal control of a platoon of vehicles. In 1990 American Control Conference, pages 291–296, 1990.

[10] P. Barooah and J. P. Hespanha. Error amplification and disturbance propagation in vehicle strings with decentralized linear control. In Proceedings of the 44th IEEE Conference on Decision and Control, pages 4964–4969, 2005.

[11] D. Yanakiev and I. Kanellakopoulos. Nonlinear spacing policies for automated heavy-duty vehicles. IEEE Transactions on Vehicular Technology, 47(4):1365–1377, 1998.

[12] Martin Treiber and Arne Kesting. Traffic Flow Dynamics: Data, Models and Simulation. Springer, 2013.

[13] R. Rajamani and Chunyu Zhu. Semi-autonomous adaptive cruise control systems. In Proceedings of the 1999 American Control Conference (Cat. No. 99CH36251), volume 2, pages 1491–1495 vol.2, 1999.

[14] Kai ching Chu. Decentralized control of high-speed vehicular strings. Transportation Science, 8(4):361–384, 1974.

[15] Shengbo Eben Li, Zhenzhong Jia, Keqiang Li, and Bo Cheng. Fast online computation of a model predictive controller and its application to fuel economy–oriented adaptive cruise control. IEEE Transactions on Intelligent Transportation Systems, 16(3):1199–1209, 2015.

[16] Meng Wang, Winnie Daamen, Serge P. Hoogendoorn, and Bart van Arem. Rolling horizon control framework for driver assistance systems. part i: Mathematical formulation and non-cooperative systems. Transportation Research Part C: Emerging Technologies, 40:271–289, 2014.

[17] R.A. Dollar, A. Sciarretta, and A. Vahidi. Information and collaboration levels in vehicular strings: A comparative study. IFAC World Congress 2020, 2020.

[18] William B. Dunbar and Richard M. Murray. Distributed receding horizon control for multi-vehicle formation stabilization. Automatica, 42(4):549–558, 2006.

[19] Y. Zheng, S. E. Li, K. Li, F. Borrelli, and J. K. Hedrick. Distributed model predictive control for heterogeneous vehicle platoons under unidirectional topologies. IEEE Transactions on Control Systems Technology, 25(3):899–910, 2017.

[20] R. Austin Dollar and Ardalan Vahidi. Quantifying the impact of limited information and control robustness on connected automated platoons. In 2017 IEEE 20th International Conference on Intelligent Transportation Systems (ITSC), pages 1–7, 2017.

[21] Aaron Lelouvier, Jacopo Guanetti, and Francesco Borrelli. Eco-platooning of autonomous electrical vehicles using distributed model predictive control. 2017.

[22] Meng Wang, Winnie Daamen, Serge P. Hoogendoorn, and Bart van Arem. Rolling horizon control framework for driver assistance systems. part ii: Cooperative sensing and cooperative control. Transportation Research Part C: Emerging Technologies, 40:290–311, 2014.

[23] Meng Wang, Honghai Li, Jian Gao, Zichao Huang, Bin Li, and Bart van Arem. String stability of heterogeneous platoons with non-connected automated vehicles. In 2017 IEEE 20th International Conference on Intelligent Transportation Systems (ITSC), pages 1–8, 2017.

5 - Intersection

This chapter discusses the intersection ED scenario.

5.1 . State-of-the-Art

An intersection is a junction where two or more roads meet, and is a shared resource that only a limited number of vehicles can occupy at once. Several vehicles wanting to use it simultaneously can cause conflicts leading to collisions. Therefore, intersections are controlled to resolve these conflicts, using traffic technologies such as traffic lights and stop or yield signs. In a CCAV environment, the vehicles in an intersection can coordinate and communicate to resolve conflicts with each other. This eliminates the need for additional infrastructure leading to un-signalized intersections.

In the literature on un-signalized intersections, the area within the perimeter where CCAVs can communicate with each other or the infrastructure is often called the Control Zone (CZ). The region in the center, where vehicle paths cross, is called the Intersection Zone (IZ), see Fig. 5.1a. The lane in the CZ leading to and out of the IZ is called the entry and exit lanes, respectively. An intersection being a shared resource poses two main challenges: scheduling the CCAVs in the IZ and its motion planning.

The scheduling problem determines the priority of CCAVs at the intersection. Heuristic or rule-based methods such as First Come First Serve (FCFS) [1] or First-In-First-Out (FIFO), right-before-left and nearest to the crossing point, etc., are often used in literature to schedule CCAVs crossing an intersection. Scheduling problems can also be cast as optimization problems to minimize travel time or energy consumption using tools such as Mixed Integer Linear Programming (MILP) [2, 3]. The second challenge, motion planning, involves generating paths or trajectories for the longitudinal and lateral motion of the CCAVs. The literature distinguishes a path as having a spatial component and a trajectory as having a temporal component. A path is a geometric set of points, $f(x, y, \ldots) = 0$, to go from point *a* to point *b*, and a trajectory describes the evolution of path in time, $x(t)$ [4]. Suppose a CCAV follows a predefined fixed path. In that case, the problem narrows down to finding the trajectory (i.e., velocity) concerning a certain objective while respecting constraints such as vehicle dynamics, speed limits, and safety constraints.

A rich body of literature is available for intersection scheduling and motion planning. A comprehensive overview of the various heuristic and optimization methods employed can be found in [5, 6]. Some of the works focusing on trajectory optimization for energy consumption are reviewed here. Reference [7] proposes a problem formulation to minimize the trip time and the control effort of a CCAV

crossing an intersection. Pontryagin's Minimum Principle (PMP) is used to formulate the problem. The authors state that the problem, in theory, could be solved using PMP. However, owing to the difficulty in obtaining analytical solutions, the problem is solved using numerical discrete and convex optimization. Rear-end collision in the CZ is avoided by formulating a position-inequality constraint, and lateral collision is avoided by modeling the entire IZ as a collision region. In the numerical Model Predictive Control (MPC) proposed by [8], the cost functional directly captures the energy usage of an Electric Vehicle (EV) and the travel time. The authors in [9, 10, 11] formulate a quadratic MPC to minimize the control effort and the deviation from the reference velocity. In [9], the vehicle closest to the intersection in terms of time is assigned a higher priority. Rear-end and lateral collisions are formulated as linear constraints, and the solutions are obtained numerically. Reference [10] use a predefined crossing order, and the optimization problem is solved sequentially in that order. Lateral collision is avoided by enforcing a terminal constraint in the finite horizon. The authors do not consider more than one vehicle arriving in the same lane simultaneously eliminating the rear-end collisions. The authors in [11] assign priority using the vehicle's time to react, giving priority to faster vehicles closer to the intersection. Lateral collision is avoided by modeling the collision region as a point on the vehicle's path. The dots in Fig.5.2, represents a collision point, and this modeling approach allows for more than one vehicle inside the IZ simultaneously.

While numerical methods facilitate non-linear models and complex formulations, analytical methods provide fast and explicable solutions. However, only a handful of research efforts have been made to obtain analytical closed-form solutions in the optimal control framework of CCAVs in an intersection. The authors in [12], present a bi-level optimization problem for scheduling and trajectory of CCAVs in an intersection without any turns. The upper-level optimization schedules the CCAVs by maximizing the throughput under the FIFO policy. The authors argue that the lower-level problem minimizes acceleration, which minimizes the transient engine operation and fuel consumption. With the optimization horizon of the lower-level problem only on the entry lane, the solution to this problem produces an optimal speed profile only until the start of IZ. The vehicles are restricted to a constant velocity thereafter through the intersection. In a follow-up work [13], the authors extended the problem formulation to consider left and right-turning vehicles and present a bi-level optimization solely for the trajectory of the CCAVs. Still, under FIFO policy, the upper-level problem has an optimization horizon only for the entry lane, jointly minimizing travel time and accelerations. The arrival time and velocity at the end of the entry lane are then used as inputs to the second optimization problem. The lower-level problem jointly reduces jerks and accelerations with an optimization horizon only for the IZ. The CCAVs are restricted to constant velocity on the exit lane to avoid rear-end collision. The solution to the above formulation leads to one optimal speed profile on the entry lane and a second

optimal speed profile inside the IZ followed by a constant velocity.

The main objective of this chapter is to obtain analytical solutions to the ED problem of an electric CCAV crossing an un-signalized intersection subject to safety constraints. As in the platooning ED-Scenario, the aim is then to explore the benefits of cooperation. The contributions of this chapter can be summarised as follows. We formulate a single-level optimization problem to the ED intersection scenario with an optimization horizon that includes the entry lane, the IZ and the exit lane. The analytical, objective function directly captures the energy usage in an EV, and can deal with position and speed constraints, similar to what has already been studied in [14, 15, 16] and presented in Chap. 2. Cooperation is introduced amongst the CCAVs as the ability to share intentions. Two levels of cooperation, namely the NC-ED and C-ED, are evaluated for performance in terms of energy consumption.

Chapter Outline: The organization of this chapter is as follows. Section 5.2 presents the intersection and vehicle model and its assumptions. The various conflicts in an intersection are also discussed. In Sect. 5.3 and Sect. 5.4, the OCP formulation, solution method and implementation for the NC-EDOC and C-EDOC are respectively presented. The simulation results and their discussions are presented in Sect.5.5. Concluding remarks are given in Sect. 5.6.

5.2 . Intersection and Vehicle Model

This section describes the considered un-signalized intersection and vehicle model. The various conflicts a CCAV can face in an intersection are also analyzed.

5.2.1 . Intersection Model

The intersection considered here is an isolated un-signalized four-legged intersection with flat straight roads crossing at right angles. Figure 5.1a represents the intersection model considered in this paper. Each leg of the intersection consists of two lanes with traffic flowing in opposite directions. The center of the intersection, of equal sides, where two or more paths can intersect, is called the Intersection Zone (IZ). It is within the IZ a possible lateral collision can occur. The roads leading to and away from the IZ, of length l, are called the entry lane and exit lane, respectively. The area in the vicinity of IZ where CCAVs can communicate with each other, and a coordinator is called the Control Zone (CZ). The point where the entry and exit lane meets the IZ is called the Diverging Point ($\mathcal{D}$) and Merging Point ($\mathcal{M}$), respectively.

Let $N(t) \in \mathbb{N}$ be the total number of CCAVs in the CZ, and $\mathcal{N}(t) = \{1, 2, ..., N(t)\}$ be the set of CCAVs' ID inside the CZ at time $t \in \mathbb{R}^+$. A CCAV leaving the CZ is removed from $\mathcal{N}(t)$, and the IDs' are reset starting from one. The sequence[1]

[1] Unlike a set, the order matters in a sequence

$\mathcal{CO}(t)$ is a permutation of $\mathcal{N}(t)$ that represents the crossing order according to a given criterion, whose n^{th} element is denoted as $\mathcal{CO}_n(t)$. As mentioned earlier, the criterion can be FCFS, right-before-left, or as a result of an upper-level optimizer. In this work, we assume a predefined crossing order computed and communicated to the vehicles via a coordinator present at the intersection.

For a four-way intersection with one lane in each direction, there are a total of 12 paths across the intersection. Taking a left or right turn, the path of a CCAV in the IZ is modeled as a constant radius arc with a central angle of 90°. The path of the CCAV in the entry and exit lanes is modeled as straight lines through the center of the lane. The entry lane and the direction of a CCAV determine along which of the 12 paths it travels. The lateral collision region in this work is modeled as points, called Crossing Points ($\mathcal{C}$), and are given by the intersection of the CCAVs' paths. Figure 5.2 shows the 12 paths and the 16 crossing points in the IZ.

We assume that each CCAV entering the intersection has perfect information about the geometry of the intersection and can compute the distance to the crossing points on its path. Furthermore, each CCAV receives the following information from other CCAVs with higher priority: the entry lane, heading direction, arrival time at their crossing point, and instantaneous or future control actions.

In this modeling framework, we impose further assumptions to abstract from implementation issues and focus on the fundamental aspect of motion planning: (i) all CCAVs are equipped with V2V communication capabilities. Appropriate sensors can sense local information of itself and others in proximity without losses or delays; (ii) the CCAVs are not allowed to overtake each other nor make a U-turn; (iii) no pedestrians are considered crossing the intersection; (iv) each CCAV follows a predefined path without any deviation.

To simplify the analysis and the mathematical formulation, the paths in an intersection are converted from a 2-D Cartesian coordinate to a single-dimensional coordinate system. Figure 5.1a shows the 2-D paths in OXY, and Fig 5.1b shows the path converted to 1-D in x. For example, CCAV $i \in \mathcal{N}(t)$ having initial coordinates in OXY as $\Delta_0 = \{X_0^i, Y_0^i\}$ and final coordinates as $\Delta_f = \{X_f^i, Y_f^i\}$, is mapped onto x with 0 and $D_{i,f}$ as initial and final coordinates, respectively. The length from Δ_0 to $\mathcal{D}$ in OXY is denoted using $\mathcal{D}$ in x, however, the length from Δ_0 to $\mathcal{M}$ in OXY is denoted by $\mathcal{M}_i$ in x. The subscript i in $\mathcal{M}_i$ indicates that the merging point depends on the path (i.e., left, right, and straight) taken by the CCAV i. On the other hand, the diverging point $\mathcal{D}$ is independent of the path as it occurs before the turn. Similarly, the length of the path for CCAV i from Δ_0 to $\mathcal{C}$, denoted by $\mathcal{C}_{ip}$, is different from the path for CCAV p from Δ_0 to $\mathcal{C}$, denoted by $\mathcal{C}_{pi}$. The length from $\mathcal{D}$ to $\mathcal{M}_i$ in x represents the curvilinear length of the arc $\mathcal{D}$ to $\mathcal{M}$ in OXY for CCAV i. The single-dimension reformulation is justified from the assumption that, the CCAV's path remains fixed without any deviation. In doing so, the lateral control (i.e.steering angle) is fixed, reducing the problem

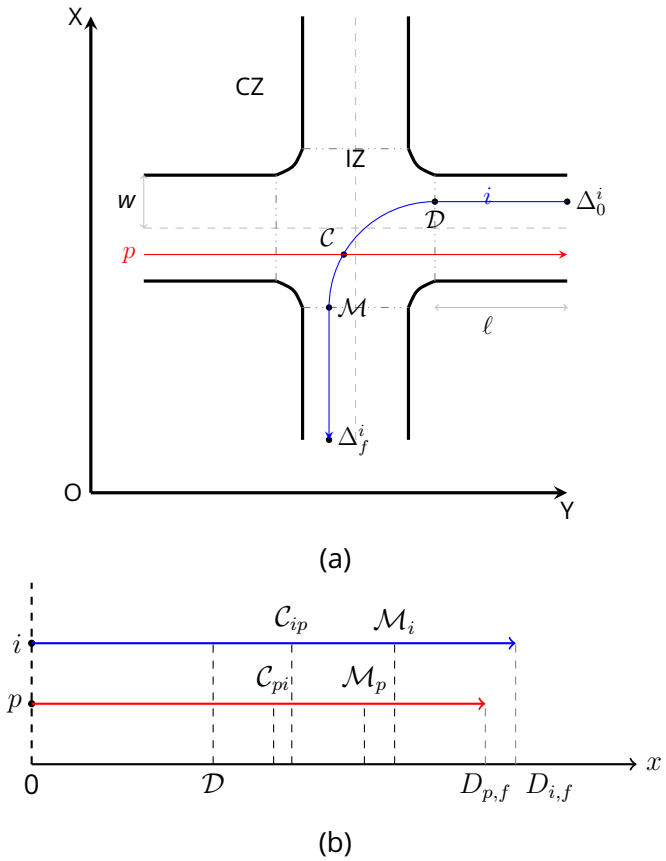

Figure 5.1: Intersection Model in (a): $\mathcal{M}, \mathcal{D}, \mathcal{C}_{i,p}$ represent the merging point, diverging point and crossing point respectively for CCAV i. ℓ and w are the exit and entry lane length and width of each lane, respectively. The 1-D transformation of the paths are shown in (b).

to finding the ED velocity along the path.

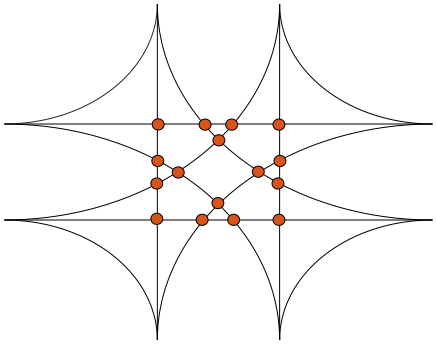

Figure 5.2: 16 Crossing Points in an intersection with 12 paths

5.2.2 . Conflicts in an Intersection

This section describes the fundamental conflicts any CCAV $i \in \mathcal{N}(t)$ can face with its higher prioritized CCAVs. The higher prioritized vehicles for a CCAV $i \in \mathcal{N}(t)$, with priority k such that $\mathcal{CO}_k(t) = i$, is given by the sub-sequence $\mathcal{H}^i(t) = (\mathcal{CO}_n(t))_{n=1}^{k-1}$. There are four types of fundamental conflicts in a traffic conflict analysis: car-following /sequential, crossing, diverging and merging conflict [17].

Car-following/Sequential Conflict: The car-following/sequential conflict, see Fig. 5.3a, occurs when CCAV $i \in \mathcal{N}(t)$ has a preceding CCAV $p \in \mathcal{H}^i(t)$ following the same path. Let $\mathcal{CF}^i(t)$ represent a sub-sequence of $\mathcal{H}^i(t)$, with all vehicles in $\mathcal{H}^i(t)$ having the same path as CCAV i.

Crossing Conflict: A crossing conflict, see Fig. 5.3b, occurs for CCAV $i \in \mathcal{N}(t)$ when its path intersects with a CCAV $c \in \mathcal{H}^i(t)$ in the IZ. Let $\mathcal{CC}^i(t)$ represent a sub-sequence of $\mathcal{H}^i(t)$, with all the vehicles in $\mathcal{H}^i(t)$ whose paths intersect with CCAV i.

Diverging Conflict: A diverging conflict, see Fig. 5.3c, occurs when CCAV $i \in \mathcal{N}(t)$ has the same entry lane with a preceding CCAV $d \in \mathcal{H}^i(t)$, but different heading directions. The conflict exists for CCAV $i \in \mathcal{N}(t)$ only until $\mathcal{D}$. Let $\mathcal{DC}^i(t)$ represent a sub-sequence of $\mathcal{H}^i(t)$, with all vehicles in $\mathcal{H}^i(t)$ having the same entry lane as CCAV $i \in \mathcal{N}(t)$ but with a different heading direction.

Merging Conflict: Merging conflict, see Fig. 5.3d, occurs when CCAV $i \in \mathcal{N}(t)$ has the same exit lane as CCAV $e \in \mathcal{H}^i(t)$ but with different entry lanes. The exit lane of a CCAV can be easily found with the knowledge of intersection geometry, entry lane, and heading direction. A merging conflict is active only in the exit lane starting from $\mathcal{M}_i$. Let $\mathcal{MC}^i(t)$ a sub-sequence of $\mathcal{H}^i(t)$, with all vehicles in $\mathcal{H}^i(t)$ having the same exit lane as CCAV i but different entry lane.

The sequences $\mathcal{DC}^i(t), \mathcal{MC}^i(t), \mathcal{CC}^i(t), \mathcal{CF}^i(t)$ are collectively referred to as the conflicting sequences in the remainder of the chapter.

5.2.3 . Turning Speed

Another important safety consideration independent of the other CCAVs in the intersection is the turning speed. We enforce a safe turning speed for CCAVs taking a turn in the intersection. The centripetal force provided by the tyre friction forces defines the safe speed of the CCAVs in turns and is given by

$$v_{safe} = \sqrt{fgR}, \tag{5.1}$$

where f, g, and R represent the tyre friction coefficient, gravitational constant, and radius of the turn. The latter is different for left and right-turning vehicles.

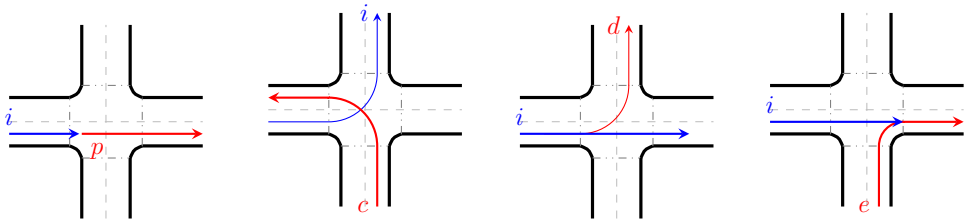

(a) Sequential (b) Crossing (c) Diverging (d) Merging

Figure 5.3: Four Basic Conflicts in an Intersection.

5.2.4 . Vehicle Model

As mentioned above, the CCAVs follow a fixed path, meaning vehicles can control only their acceleration/deceleration. This enables the decoupling of path and trajectory. A second-order longitudinal dynamics to describe each CCAV $i \in \mathcal{N}(t)$. Under similar assumptions as in Sect. 2.2.1.1, the linearised longitudinal vehicle model is given as

$$\begin{aligned} \dot{x}_i &= v_i(t), \\ \dot{v}_i &= a_i(t) = F/m - h. \end{aligned} \tag{5.2}$$

It remains to obtain the ED optimal feedback control law $a_i(t)$ for each CCAV i resolving the conflicts it can face.

5.3 . Non-Cooperative EDOC

In the NC-EDOC, each CCAV aims to minimize its energy consumption while sharing and having access to only instantaneous information from other CCAVs in $\mathcal{N}(t)$. This section describes the ED-OCP formulation for a CCAV $i \in \mathcal{N}(t)$ and the mathematical translation of the various conflicts into constraints. The solution of the ED-OCP with different constraints obtained using PMP and its implementation are detailed in this section.

5.3.1 . OCP Formulation

Consider a CCAV $i \in \mathcal{N}(t)$ crossing an intersection of distance $D_{i,f}$ in time $T_{i,f}$ with given initial and final speed $v_{i,0}$ and $V_{i,f}$ respectively. Let $t_{i,0}$ be its entry time in the CZ.

5.3.1.1 . Unconstrained-EDOC

In the event of CCAV i being the only vehicle in the intersection (i.e. $|\mathcal{N}(t)| = 1$), an unconstrained OCP is formulated as shown below. Under similar assumptions for an electric vehicle in Sect. 2.2, and employing the vehicle model (5.2) and

objective function (2.6), the OCP reads

$$\underset{a_i(t)}{\text{minimize}} \quad J_i = \int_{t_{i,0}}^{t_{i,0}+T_{i,f}} m(a_i(t)+h)v_i(t) + b(a_i(t)+h)^2 \, dt,$$

state dynamics

$$\begin{aligned} \dot{x_i} &= v_i(t), \\ \dot{v_i} &= a_i(t), \end{aligned} \tag{5.3}$$

boundary conditions $\mathcal{BC}$:

$$\{x_i(t_{i,0}) = 0, v_i(t_{i,0}) = v_0, x_i(t_{i,0}+T_{i,f}) = D_{i,f}, v_i(t_{i,0}+T_{i,f}) = V_{i,f}\}.$$

where $D_{i,f}$ is the path length from the entry lane's start to the exit lane's end. Since each CCAV solves its OCP, we rewrite the formulation from a global to a local time reference frame as follows

$$\underset{a_i(t)}{\text{minimize}} \quad J_i = \int_{0}^{T_{i,f}} m(a_i(t_i)+h)v_i(t_i) + b(a_i(t_i)+h)^2 \, dt,$$

state dynamics

$$\begin{aligned} \dot{x_i} &= v_i(t_i), \\ \dot{v_i} &= a_i(t_i), \end{aligned} \tag{5.4}$$

boundary conditions $\mathcal{BC}$:

$$\{x_i(0) = 0, v_i(0) = v_0, x_i(T_{i,f}) = D_{i,f}, v_i(T_{i,f}) = V_{i,f}\}.$$

For notation brevity, we will drop the subscript i from t_i in the rest of the chapter. Therefore, $t \in [0, T_{i,f}]$ in the rest of this chapter denotes the time of an individual CCAV $i \in \mathcal{N}(t)$ entering and leaving the CZ at 0 and $T_{i,f}$, respectively.

5.3.1.2 . Constrained-EDOC

As CCAV i enters the intersection, the presence of other higher prioritized CCAVs in the intersection (i.e. $\mathcal{H}^i(t)$ is not empty) can cause a potential conflict. The conflicts between CCAV $i \in \mathcal{N}(t)$ and the vehicles in the conflicting sequences are identified and added as a constraint to the ED-OCP in (5.4). The conflict can be either one of the four fundamental conflicts detailed in Sect. 5.2.2 or a combination of these four. The following section details the mathematical transformation of the fundamental conflicts into constraints to be added to (5.4).

Car-Following/Sequential Constraint: Car-following conflict occurs when CCAV $i \in \mathcal{N}(t)$ and an immediately preceding CCAV $p \in \mathcal{CF}^i(t)$, have the same path. Such a conflict leads to a potential rear-end collision without adjusting CCAV i's speed. A collision of such type is formulated as a position-inequality constraint. CCAV p's motion is predicted for the entire horizon $T_{i,f}$, under the constant acceleration assumption a_p, as

$$x_i(t) \leq x_{p,0} + v_{p,0}t + \frac{1}{2}a_p t^2 - s_{min} - l_p \ , \quad t \in [0, T_{i,f}] \tag{5.5}$$

where $x_{p,0}$, $v_{p,0}$ and a_p are the initial position, velocity and acceleration of CCAV p. s_{min} and l_p denotes the constant safe minimum gap and length of CCAV p. In the rest of the chapter, the term s_{min} and l_p are lumped into the initial position for convenience.

Crossing Constraint: A crossing conflict occurs when the path of two or more CCAVs intersects in the IZ, leading to a potential lateral collision between them. A collision of such type is formulated as an interior-point constraint [18], where equality constraints on the states are imposed point-wise along the horizon. Consider two CCAVs $i \in \mathcal{N}(t)$ and CCAV $c \in \mathcal{CC}^i(t)$ with $\mathcal{CO}(t) = \{c, i\}$. The lateral collision avoidance constraint is formulated as

$$x_i(t + \tau_c^{\mathcal{C}_i}) = \mathcal{C}_{ic} \quad \text{with} \quad \tau_c^{\mathcal{C}_i} = t_c^{\mathcal{C}_i} + dT \,. \tag{5.6}$$

where $\mathcal{C}_{ic}$ represents the distance to the crossing point, see Fig. 5.4. The term dT represents the safety margin between the arrival of the CCAVs at their respective crossing points. CCAV c's required time $t_c^{\mathcal{C}_i}$, to arrive at its crossing point $\mathcal{C}_{ci}$ is computed by solving

$$\mathcal{C}_{ic} = x_{c,0} + v_{c,0} t_c^{\mathcal{C}_i} + \frac{1}{2} a_c {t_c^{\mathcal{C}_i}}^2, \tag{5.7}$$

where $x_{c,0}$, $v_{c,0}$ and a_c are the initial position, velocity and acceleration of CCAV c. Figure 5.4 shows a qualitative example of the interior-point-constraint. CCAV i is constrained to arrive at or after $\tau_c^{\mathcal{C}_i}$ at $\mathcal{C}_{ic}$.

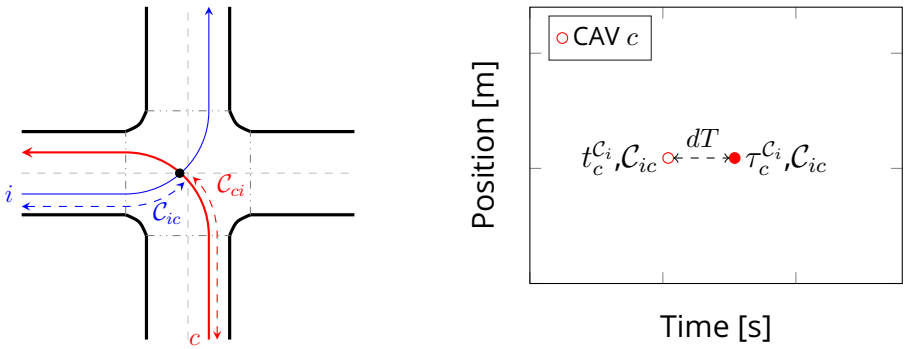

(a) (b)

Figure 5.4: Distance to the crossing conflict (a) for CCAV i is denoted by $\mathcal{C}_{ic}$ and for CCAV c is denoted by $\mathcal{C}_{ci}$. CCAV i is constrained to arrive after or at the interior-point constraint ($\tau_c^{\mathcal{C}_i}, \mathcal{C}_{ic}$), shown on $x - t$ plane (b).

Diverging Constraint: A diverging conflict occurs in the entry lane, when CCAV $i \in \mathcal{N}$ and its immediately preceding vehicle $d \in \mathcal{DC}^i(t)$ have the same entry lane and different heading direction. Once CCAV d changes direction at $\mathcal{D}$, CCAV i is no longer in conflict. Like the car-following, the diverging conflict poses

a potential rear-end collision. It is formulated as a position-inequality constraint except that CCAV i is constrained only until $\mathcal{D}$. More formally

$$x_i(t) \leq \begin{cases} x_{d,0} + v_{d,0}t + \frac{1}{2}a_d t^2 & t \in [0, \tau_d^{\mathcal{D}}] \\ \infty & t \in (\tau_d^{\mathcal{D}}, T_{i,f}] \end{cases} \tag{5.8}$$

As in the car-following constraint, CCAV d's motion is predicted under the constant acceleration assumption until $\mathcal{D}$. The term $\tau_d^{\mathcal{D}}$, see Fig.5.5, denotes the arrival time at $\mathcal{D}$ and is computed as follows,

$$\mathcal{D} = x_{d,0} + v_{d,0}\tau_d^{\mathcal{D}} + \frac{1}{2}a_d {\tau_d^{\mathcal{D}}}^2, \tag{5.9}$$

$x_{d,0}$, $v_{d,0}$ and a_d represent the initial position, velocity and acceleration of CCAV d, respectively.

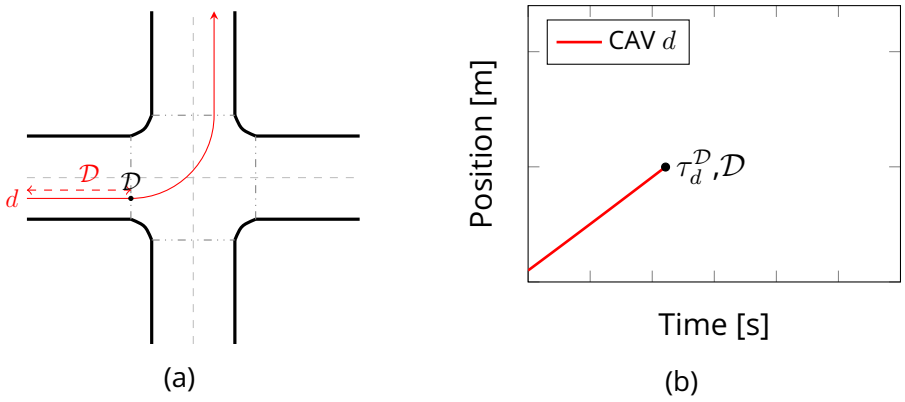

Figure 5.5: The path of CCAV d is shown in (a) and a qualitative example of its constraint on the $x-t$ plane of CCAV i in (b). The term $\tau_d^{\mathcal{D}}$ indicates the arrival time of CCAV d at $\mathcal{D}$.

Merging Constraint: A merging conflict occurs when the path of CCAV $i \in \mathcal{N}(t)$ and CCAV $e \in \mathcal{MC}^i(t)$, merge at $\mathcal{M}_i$. CCAV i remains conflict-free from CCAV e until $\mathcal{M}_i$ but upon entering the exit lane, CCAV e poses a potential rear-end collision. As in (5.8), merging conflict is formulated as a position-inequality constraint but starting from $\mathcal{M}_i$ until the end of the horizon. Explicitly it reads

$$x_i(t) \leq \begin{cases} \infty & t \in [0, \tau_e^{\mathcal{M}_{es}}] \\ (x_{e,m} + \mathcal{M}_i) + v_{e,m}t + \frac{1}{2}a_e t^2 & t \in (\tau_e^{\mathcal{M}_{es}}, T_{i,f}] \end{cases} \tag{5.10}$$

As earlier, the motion of CCAV e in the exit lane is predicted under the constant acceleration assumption. The arrival time $\tau_e^{\mathcal{M}_{es}}$ of CCAV e at $\mathcal{M}_{es} = \mathcal{M}_e + ds$ s.t. $ds > s_{min}$, is computed using

$$\mathcal{M}_{es} = x_{e,0} + v_{e,0}\tau_e^{\mathcal{M}_{es}} + \frac{1}{2}a_e {\tau_e^{\mathcal{M}_{es}}}^2. \tag{5.11}$$

where $x_{e,0}$, $v_{e,0}$ and a_e represent the initial position, velocity and acceleration of CCAV e, respectively.

The term $x_{e,m}$ represents the distance of CCAV e from its merging point $\mathcal{M}_e$ at $\tau_e^{\mathcal{M}_{es}}$, which as per this formulation is equal to ds, see Fig. 5.6b. The velocity and acceleration measured at $x_{e,m}$ are represented by $v_{e,m}$ and a_e, respectively. The term $(x_{e,m} + \mathcal{M}_i)$ ensures that the position of CCAV e is mapped onto the position frame of CCAV i. The choice of ds as a distance margin guarantees[2] that CCAV i arrives at $\mathcal{M}_i$ after CCAV e with a gap of $ds > s_{min}$. This ensures that the position constraint at the first time step $\tau_e^{\mathcal{M}_{es}}$ is not violated.

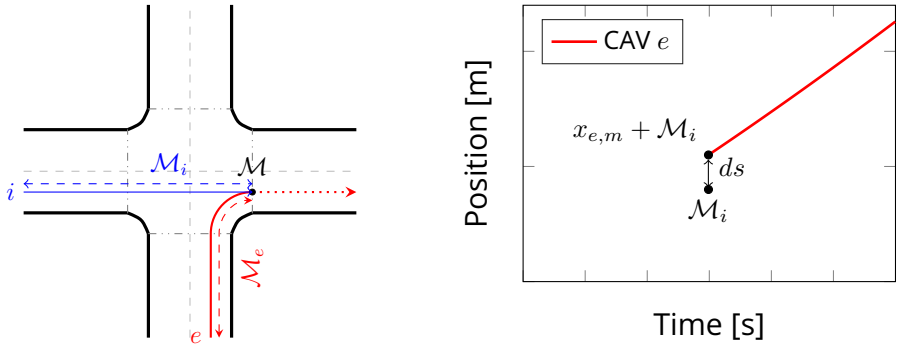

(a) (b)

Figure 5.6: The path of CCAV e is shown in (a) and a qualitative example of its constraint on the $x - t$ of CCAV i plane in (b).

Turning Speed Constraint: The turning speed constraint restricts a CCAV's speed in the IZ to a maximum defined by (5.1). The constraint is enforced by letting the speed of CCAV i equal to $v_{tr} < v_{safe}$ at the midpoint of its path in the IZ, see Fig. 6.12a. The choice of v_{tr}, a lower value than v_{safe}, is a conservative approach that keeps the CCAV's speed below the threshold. More formally,

$$\begin{aligned} v_i(t + \tau_t) &= v_{tr}, \\ x_i(t + \tau_t) &= D_{i,f}/2. \end{aligned} \tag{5.12}$$

Let a_{max} be the maximum acceleration of CCAV i and δ denote the length of CCAV's turning path inside the IZ. The term v_{tr} is obtained by solving the two equations

$$v_{safe} = v_{tr} + a_{max}t \tag{5.13a}$$

$$\frac{\delta}{2} = v_{tr}t + \frac{1}{2}a_{max}t^2 \tag{5.13b}$$

[2] A time based margin does not always guarantee constraint satisfaction at $\mathcal{M}_i$. A small dT might cause $x_{e,m} < \mathcal{M}_i + s_{min}$, while a large dT might be too restrictive

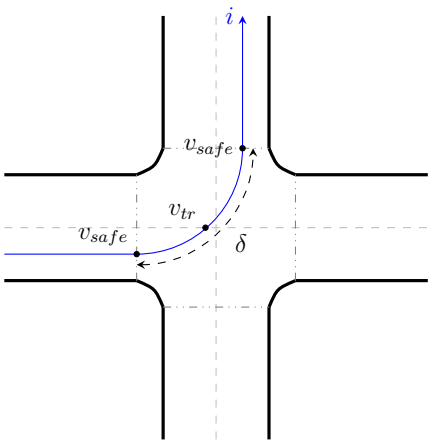

Figure 5.7: CCAV i is constrained to have its speed equal to v_{tr} at the midpoint of its path.

5.3.2 . Solution

The solution to unconstrained and constrained ED-OCP formulated for the NC strategy is presented in this section.

5.3.2.1 . Unconstrained

The solution of the unconstrained ED-OCP formulated in (5.4) follows the same solution method detailed in Sect. (2.2.2) and the obtained solution is a parabolic speed profile as a function of time given by

$$v_i(t) = v_{i,0} + \left(-\frac{4v_{i,0}}{T_{i,f}} - \frac{2V_{i,f}}{T_{i,f}} + \frac{6D_{i,f}}{T_{i,f}^2} \right) t + \left(\frac{3v_{i,0}}{T_{i,f}^2} - \frac{6D_{i,f}}{T_{i,f}^3} + \frac{3V_{i,f}}{T_{i,f}^2} \right) t^2. \qquad t \in [0, T_{i,f}] \quad (5.14)$$

The associated energy consumption of the trip E_b, a function of vehicle parameters m, b, h and boundary conditions, is given by

$$\begin{aligned} E_b = {} & mhD_{i,f} + m\frac{V_{i,f}^2 - v_{i,0}^2}{2} + bh^2 T_{i,f} + 2bh\left(V_{i,f} - v_{i,0}\right) + \\ & + 4b\left(\frac{3D_{i,f}^2}{T_{i,f}^3} - \frac{3D_{i,f}\left(v_{i,0} + V_{i,f}\right)}{T_{i,f}^2} + \frac{v_{i,0}^2 + v_{i,0}V_{i,f} + V_{i,f}^2}{T_{i,f}} \right). \end{aligned} \quad (5.15)$$

5.3.2.2 . Constrained

Car-Following/Sequential Constraint: The car-following constraint is similar to the ED-OCP already solved in Sect. 2.3, where

$$\xi_i(t) = x_i(t) - (x_{p,0} + v_{p,0}t + \frac{1}{2}a_p t^2). \quad (5.16)$$

Following the same method, the optimal speed profile yields,

$$v_i(t) = \begin{cases} v_{i,0} + \left(a_p + \dfrac{4\dot{\xi}_{i,0}}{\theta_i} + \dfrac{6\xi_{i,0}}{\theta_i^2}\right) t - \\ \quad - \left(\dfrac{6\xi_{i,0}}{\theta_i^3} + \dfrac{3\dot{\xi}_{i,0}}{\theta_i^2}\right) t^2, \quad t \in [0, \theta_i) \\ v_{p,0} + a_p\theta_i + \left(a_p - \dfrac{6\xi_{i,0}}{\theta_i^2} - \dfrac{2\dot{\xi}_{i,0}}{\theta_i}\right)(t-\theta_i) + \\ \quad + \left(V_{i,f} - 3v_{p,0} + 2v_{i,0} - 6\dfrac{\xi_{i,0}}{\theta_i} - a_pT_{i,f} + 6\xi_{i,0}\dfrac{T_{i,f}}{\theta_i^2} + \right. \\ \quad \left. + 2\dot{\xi}_{i,0}\dfrac{T_{i,f}}{\theta_i}\right)\dfrac{(t-\theta_i)^2}{(T_{i,f}-\theta_i)^2}. \quad t \in [\theta_i, T_{i,f}]\,. \end{cases} \tag{5.17}$$

The contact time θ_i, that is, where the constraint is met ($\xi_i = 0$), is given by

$$\begin{aligned} &(v_{i,0} - V_{i,f} + a_pT_{i,f})\,\theta_i^3 + \left(4v_{p,0}T_{i,f} + V_{i,f}T_{i,f} - 2v_{i,0}T_{i,f} + a_pT_{i,f}^2/2\right. \\ &\left. -3D_{i,f}\right)\theta_i^2 + \left(6\xi_{i,0}T_{i,f} + v_{i,0}T_{i,f}^2 - v_{p,0}T_{i,f}^2\right)\theta_i - \left(3\xi_{i,0}T_{i,f}^2\right) = 0. \end{aligned} \tag{5.18}$$

Crossing Constraint: The solution to the ED-OCP (5.4) with constraint (5.6) is obtained as follows. The optimal speed profile of CCAV i is composed of two almost-independent unconstrained segments (5.14), defined by $\mathcal{BC} : \{0, v_{i,0}, \mathcal{C}_{ic}, v_i(t+\tau_c^{\mathcal{C}_i})\}$ for the first segment and $\mathcal{BC} : \{\mathcal{C}_{ic}, v_i(t+\tau_c^{\mathcal{C}_i}), D_{i,f}, V_{i,f}\}$ for the second segment. With the position and time at the junction of the two segments imposed by the constraint (5.6), the optimal speed profile is completely defined by the free parameter $v_i(t+\tau_c^{\mathcal{C}_i})$, obtained as follows.

The energy consumption of the whole trip E_{bf} is given as the sum of each segment's energy consumption, and the optimal value for $v_{it} = v_i(t+\tau_c^{\mathcal{C}_i})$ is obtained by minimizing $E_{bf} = E_b^{(1)} + E_b^{(2)}$. The equations for $E_b^{(1)}$ and $E_b^{(2)}$ are obtained from (5.15), and E_{bf} is explicitly given as

$$\begin{aligned} E_{bf} = &\left(\frac{3\mathcal{C}_{ic}^2}{(\tau_c^{\mathcal{C}_i})^3} - \frac{3\mathcal{C}_{ic}\,(v_{i,0}+v_{it})}{(\tau_c^{\mathcal{C}_i})^2} + \frac{v_{i,0}^2 + v_{i,0}v_{it} + v_{it}^2}{\tau_c^{\mathcal{C}_i}}\right) + \\ &\left(\frac{3(D_{i,f}-\mathcal{C}_{ic})^2}{(T_{i,f}-\tau_c^{\mathcal{C}_i})^3} - \frac{3(D_{i,f}-\mathcal{C}_{ic})\,(v_{it}+V_{i,f})}{(T_{i,f}-\tau_c^{\mathcal{C}_i})^2} + \frac{v_{it}^2 + v_{it}V_{i,f} + V_{i,f}^2}{(T_{i,f}-\tau_c^{\mathcal{C}_i})}\right). \end{aligned} \tag{5.19}$$

The free parameter v_{it} is explicitly obtained by setting

$$\frac{\partial E_{bf}}{\partial v_{it}} = 0 \tag{5.20}$$

and is given by

$$v_{it} = \frac{\left(\left(\frac{(3\mathcal{C}_{ic}-3D_{i,f})}{(\tau_c^{\mathcal{C}_i}-T_{i,f})^2} - \frac{V_{i,f}}{(\tau_c^{\mathcal{C}_i}-T_{i,f})}\right) - \left(\frac{3\mathcal{C}_{ic}}{(\tau_c^{\mathcal{C}_i})^2} - \frac{v_{i,0}}{\tau_c^{\mathcal{C}_i}}\right)\right)\left(\tau_c^{\mathcal{C}_i}(\tau_c^{\mathcal{C}_i} - T_{i,f})\right)}{2\tau_c^{\mathcal{C}_i} - 2(\tau_c^{\mathcal{C}_i} - T_{i,f})}. \tag{5.21}$$

Thus, v_{it} is a function completely defined by the two segments' boundary conditions. The optimality of the approach has been shown in [16, 19]. Figure 5.8 shows an example of the optimal speed and position profile satisfying the crossing constraint.

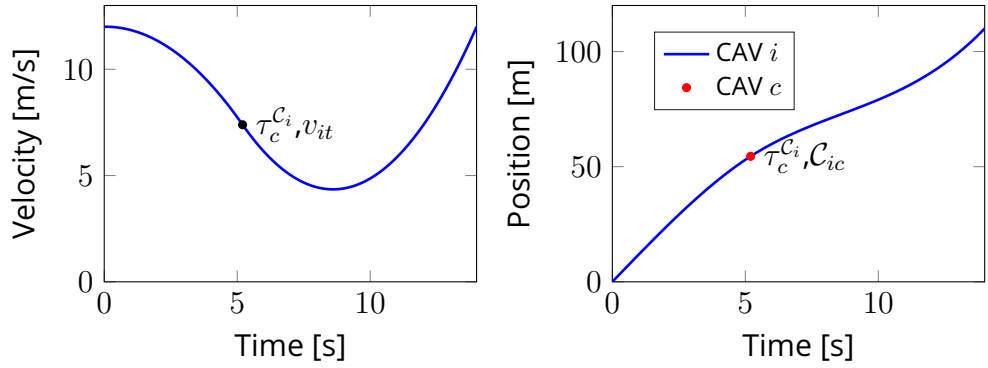

Figure 5.8: The position profile (b) passes through the interior-point $\mathcal{C}_i$ = 54.50 m and $\tau_c^{\mathcal{C}_i}$= 5.2 s. The free parameter v_{it} = 7.39 m/s^2 is shown in the velocity profile (a), with $v_{i,0} = V_{i,f}$ = 12 m/s^2, $D_{i,f}$= 110 m and $T_{i,f}$=14 s.

Diverging Constraint: The optimal solution to the ED-OCP (5.4) with the diverging constraint (5.8) contains two segments. The first segment where (5.17) applies[3], satisfying the inequality constraint $\xi_i(t) \leq 0$ posed by CCAV d. The second segment where (5.14) applies has the constraint jumping to infinity. The $\mathcal{BC}$ for the first and second segments are given as $\{0, v_{i,0}, x_i(t+\tau_d^{\mathcal{D}}), v_i(t+\tau_d^{\mathcal{D}})\}$ and $\{x_i(t+\tau_d^{\mathcal{D}}), v_i(t+\tau_d^{\mathcal{D}}), D_{i,f}, V_{i,f}\}$, respectively. With the time at the junction of the segments imposed by $\tau_d^{\mathcal{D}}$ (arrival time of CCAV d at $\mathcal{D}$), the optimal solution is now defined by two unknown free parameters, $x_{id} = x_i(t+\tau_d^{\mathcal{D}}), v_{id} = v_i(t+\tau_d^{\mathcal{D}})$.

The optimal value for these two parameters is found by minimizing the sum of energies of the two segments (i.e., the total energy consumption of the trip E_{bf}).

$$E_{bf} = E_b^{(1)} + E_b^{(2)}. \tag{5.22}$$

$E_b^{(1)}$ is energy consumption obtained by substituting the solution (5.17) and its corresponding control input $a_i(t)$ in J_i of (5.4). An alternate way of obtaining $E_b^{(1)}$ using (5.15) is by rewriting

$$E_b^{(1)} = E_b^{(1.1)} + E_b^{(1.2)}, \tag{5.23}$$

where $E_b^{(1.1)}$ is the energy consumption of the first parabola of (5.17) for $t \in [0, \theta_i)$ whose $\mathcal{BC} = \{0, v_{i,0}, (x_{d,0} + v_{p,0}\theta_i + 0.5a_d\theta_i^2), (v_{d,0} + a_d\theta_i)\}$ and $E_b^{(1.2)}$ is

[3]Note that the parameters $x_{p,0}, v_{p,0}$ and a_p in (5.17) are replaced with $x_{d,0}, v_{d,0}$ and a_d, respectively and $\xi_i(t)$ is given by $\xi_i(t) = x_i(t) - (x_{d,0} + v_{d,0}t + \frac{1}{2}a_d t^2)$.

the energy consumption of the second parabola of (5.14) for $t \in [\theta_i, \tau_d^{\mathcal{D}}]$ whose $\mathcal{BC} = \{(x_{d,0} + v_{p,0}\theta_i + 0.5a_d\theta_i^2), (v_{d,0} + a_d\theta_i), x_{id}, v_{id}\}$. The equations explicitly read

$$\begin{aligned} E_b^{(1.1)} =& \frac{3(x_{d,0} + v_{d,0}\theta_i + 0.5a_d\theta_i^2)^2}{\theta_i^3} - \\ & \frac{3(x_{d,0} + v_{p,0}\theta_i + 0.5a_d\theta_i^2)\left(v_{i,0} + (v_{d,0} + a_d\theta_i)\right)}{\theta_i^2} + \\ & \frac{v_{i,0}^2 + v_{i,0}(v_{d,0} + a_d\theta_i) + (v_{d,0} + a_d\theta_i)^2}{\theta_i}, \end{aligned} \tag{5.24a}$$

$$\begin{aligned} E_b^{(1.2)} =& \frac{3(x_{id} - (x_{d,0} + v_{d,0}\theta_i + 0.5a_d\theta_i^2))^2}{{\tau_d^{\mathcal{D}}}^3} - \\ & \frac{3(x_{id} - (x_{d,0} + v_{p,0}\theta_i + 0.5a_d\theta_i^2))\left((v_{d,0} + a_d\theta_i) + v_{id}\right)}{{\tau_d^{\mathcal{D}}}^2} + \\ & \frac{(v_{d,0} + a_d\theta_i)^2 + (v_{d,0} + a_d\theta_i)v_{id} + v_{id}^2}{\tau_d^{\mathcal{D}}}. \end{aligned} \tag{5.24b}$$

The term $E_b^{(2)}$ is the energy consumption of the segment where the constraint goes to infinity. With $\mathcal{BC} = \{x_{id}, v_{id}, D_{i,f}, V_{i,f}\}$, $E_b^{(2)}$ using (5.15) is obtained as

$$E_b^{(2)} = \frac{3(D_{i,f} - x_{id})^2}{\theta_i^3} - \frac{3(D_{i,f} - x_{id})\left(v_{id} + v_{i,f}\right)}{\theta_i^2} + \frac{v_{id}^2 + v_{id}V_{i,f} + V_{i,f}^2}{\theta_i}. \tag{5.25}$$

Note that, only the terms in the bracket multiplied with $4b$ in (5.15) is used, as the other terms cancel out when calculating E_{bf}. The total energy consumption of the trip is thereby given as

$$E_{bf} = E_b^{(1.1)} + E_b^{(1.2)} + E_b^{(2)}. \tag{5.26}$$

The E_{bf} now involves three unknown parameters, i.e., the two free parameters x_{id}, v_{id}, and the contact time θ_i. The three parameters are constrained to satisfy the contact time function

$$\begin{aligned} f_{d\theta} \triangleq & \left(v_{i,0} - v_{id} + a_d\tau_d^{\mathcal{D}}\right)\theta_i^3 + \Big(4v_{d,0}\tau_d^{\mathcal{D}} + v_{id}\tau_d^{\mathcal{D}} - 2v_{i,0}\tau_d^{\mathcal{D}} + a_d{\tau_d^{\mathcal{D}}}^2/2 \\ & -3x_{id}\Big)\theta_i^2 + \left(6x_{id}\tau_d^{\mathcal{D}} + v_{i,0}{\tau_d^{\mathcal{D}}}^2 - v_{d,0}{\tau_d^{\mathcal{D}}}^2\right)\theta_i - \left(3x_{d,0}{\tau_d^{\mathcal{D}}}^2\right) = 0. \end{aligned} \tag{5.27}$$

The three unknowns $(v_{id}, x_{id}, \theta_i)$ are obtained by solving the following constrained minimization problem,

$$\begin{aligned} \underset{v_{id}, x_{id}, \theta_i}{\text{minimize}} \quad & E_{bf}, \\ \text{subject to} \quad & f_{d\theta}. \end{aligned} \tag{5.28}$$

The optimization problem (5.28) is solved using the method of Lagrange multipliers (λ) and the solution involves solving four equations in four unknowns $(v_{id}, x_{id}, \theta_i, \lambda)$, see Appendix A.9. An example involving a diverging conflict and its solution is shown in Fig. 5.9.

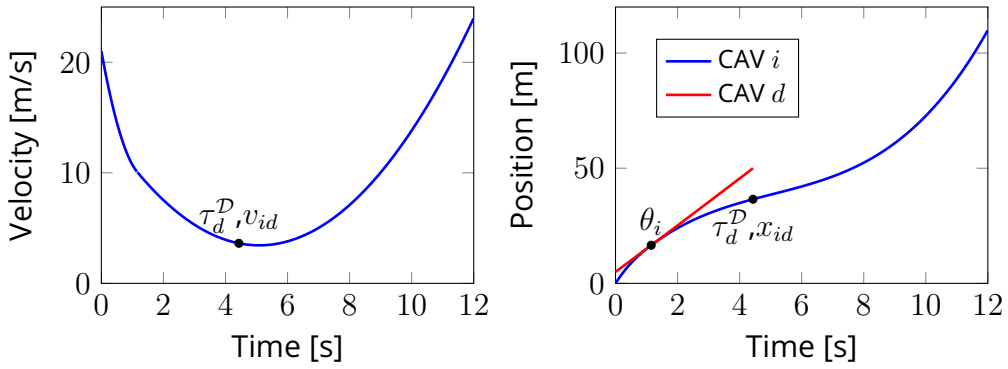

Figure 5.9: Velocity (a) and position (b) of CCAV i in diverging conflict. The $\mathcal{BC}$ for CCAV i is given as $x_{i,0}$= 0 m, $v_{i,0}$ = 21 m/s, $D_{i,f}$=110 m, $V_{i,f}$ = 24 m/s. T_i = 12 s. CCAV d's states are measured as $x_{d,0}$ = 5 m,$v_{d,0}$ = 10 m/s and a_d = 0.07 m/s^2. With $\mathcal{D}$ = 50 m, the arrival time is calculated as $\tau_d^{\mathcal{D}}$ = 4.43 s. The free parameters are calculated as v_{id} = 3.624 m/s and x_{id} = 36.525 m.

Merging Constraint: The merging constraint is similar to the diverging but with the inequality constraint $\xi_i \leq 0$ by CCAV e in the exit lane. Following the same procedure, the optimal solution to the ED-OCP (5.4) with constraint (5.10) is made up of two segments, i.e., the first segment where (5.14) applies and the second segment where (5.17) applies[4]. The $\mathcal{BC}$ for the first and second segments are given as $\{0, v_{i,0}, \mathcal{M}_i, v_i(t+\tau_e^{\mathcal{M}_{es}})\}$ and $\{\mathcal{M}_i, v_i(t+\tau_e^{\mathcal{M}_{es}}), D_{i,f}, V_{i,f}\}$, respectively. CCAV i's position at the end of the first segment is constrained to arrive at $x_i(t+\tau_e^{\mathcal{M}_{es}}) = \mathcal{M}_i$. With both position and time at the junction imposed, the optimal solution is now defined by the one unknown free parameter, $v_{im} = v_i(t+\tau_e^{\mathcal{M}_{es}})$. The optimal value for this parameter is found by minimizing the trip's total energy consumption.

$$E_{bf} = E_b^{(1)} + E_b^{(2)}, \tag{5.29}$$

where $E_b^{(1)}$ is the energy consumption using the unconstrained solution (5.17) for $t \in [0, \tau_e^{\mathcal{M}_{es}}]$, with $\mathcal{BC} = \{0, v_{i,0}, \mathcal{M}_i, v_{im}\}$, is given as

$$E_b^{(1)} = \frac{3{\mathcal{M}_i}^2}{{\tau_e^{\mathcal{M}_{es}}}^3} - \frac{3\mathcal{M}_i\left(v_{i,0}+v_{im}\right)}{{\tau_e^{\mathcal{M}_{es}}}^2} + \frac{v_{i,0}^2 + v_{i,0}v_{im} + v_{im}^2}{\tau_e^{\mathcal{M}_{es}}}. \tag{5.30}$$

and $E_b^{(2)}$ is computed as

$$E_b^{(2)} = E_b^{(2.1)} + E_b^{(2.2)}. \tag{5.31}$$

[4]Note that the parameters $x_{p,0}, v_{p,0}$ and a_p in (5.17) are replaced with $(x_{e,m} - \mathcal{M}_i), v_{e,m}$ and a_e, respectively and $\xi_i(t)$ is given by $\xi_i(t) = x_i(t) - ((x_{e,m} - \mathcal{M}_i) + v_{e,m}t + \frac{1}{2}a_e t^2)$.

For sake of brevity, we will use $\bar{\theta}_i = (\theta_i - \tau_e^{\mathcal{M}_{es}})$ and $\bar{T}_{i,f} = (T_{i,f} - \theta_i)$. The term $E_b^{(2.1)}$ is the energy consumption of (5.14)'s first parabola for $t \in [\tau_e^{\mathcal{M}_{es}}, \theta_i)$ whose $\mathcal{BC} = \{\mathcal{M}_i, v_{im}, (x_{e,m} + v_{e,m}\bar{\theta}_i + 0.5a_e\bar{\theta}_i^2), (v_{e,m} + a_e\bar{\theta}_i)\}$ and $E_b^{(2.2)}$ is the energy consumption of (5.14)'s second parabola for $t \in [\theta_i, T_{i,f}]$ whose $\mathcal{BC} = \{(x_{e,m} + v_{e,m}\bar{\theta}_i + 0.5a_e\bar{\theta}_i^2), (v_{e,m} + a_e\bar{\theta}_i), D_{i,f}, V_{i,f}\}$. The energies $E_b^{(2.1)}$ and $E_b^{(2.2)}$ are given as

$$\begin{aligned} E_b^{(2.1)} =& \frac{3(x_{e,m} + v_{e,m}\bar{\theta}_i + 0.5a_e\bar{\theta}_i^2 - \mathcal{M}_i)^2}{\bar{\theta}_i^3} - \\ & \frac{3(x_{e,m} + v_{e,m}\bar{\theta}_i + 0.5a_e\bar{\theta}_i^2 - \mathcal{M}_i)\left(v_{im} + (v_{e,m} + a_e\bar{\theta}_i)\right)}{\bar{\theta}_i^2} + \\ & \frac{v_{im}^2 + v_{im}(v_{e,m} + a_e\bar{\theta}_i) + (v_{e,m} + a_e\bar{\theta}_i)^2}{\bar{\theta}_i}, \end{aligned} \tag{5.32a}$$

$$\begin{aligned} E_b^{(2.2)} =& \frac{3(D_{i,f} - (x_{e,m} + v_{e,m}\bar{\theta}_i + 0.5a_e\bar{\theta}_i^2))^2}{\bar{T}_{i,f}^3} - \\ & \frac{3(D_{i,f} - (x_{e,m} + v_{e,m}\bar{\theta}_i + 0.5a_e\bar{\theta}_i^2))\left((v_{e,m} + a_e\bar{\theta}_i) + V_{i,f}\right)}{\bar{T}_{i,f}^2} + \\ & \frac{(v_{e,m} + a_e\bar{\theta}_i)^2 + (v_{e,m} + a_e\bar{\theta}_i)V_{i,f} + V_{i,f}^2}{\bar{T}_{i,f}}. \end{aligned} \tag{5.32b}$$

The total energy consumption of the trip is thereby given as

$$E_{bf} = E_b^{(1)} + E_b^{(2.1)} + E_b^{(1.2)}. \tag{5.33}$$

The E_{bf} now involves 2 unknown parameters, i.e. the free parameter v_{im} and the contact time θ_i. The two parameters are constrained to satisfy the contact time function

$$\begin{aligned} f_{m\theta} \triangleq & \left(v_{im} - V_{i,f} + a_e\bar{T}_{i,f}\right)\bar{\theta}_i^3 + \left(4v_{e,m}\bar{T}_{i,f} + v_{im}\bar{T}_{i,f} - 2v_{im}\bar{T}_{i,f} + a_e\bar{T}_{i,f}^2/2\right. \\ & \left. -3\bar{D}_{i,f}\right)\bar{\theta}_i^2 + \left(6\bar{D}_{i,f}\bar{T}_{i,f} + v_{im}\bar{T}_{i,f}^2 - v_{e,m}\bar{T}_{i,f}^2\right)\bar{\theta}_i - \left(3x_{e,m}\bar{T}_{i,f}^2\right) = 0. \end{aligned} \tag{5.34}$$

where $\bar{D}_{i,f} = (D_{i,f} - \mathcal{M}_i)$. The two unknowns (v_{im}, θ_i) are obtained by solving the following constrained minimization problem,

$$\begin{aligned} \underset{v_{im},\theta_i}{\text{minimize}} \quad & E_{bf}, \\ \text{subject to} \quad & f_{m\theta}. \end{aligned} \tag{5.35}$$

The optimization problem (5.35) is solved using the method of Lagrange multipliers (λ) and the solution involves solving three equations in three unknowns $(v_{im}, \theta_i, \lambda)$, see Appendix A.8. An example involving a merging conflict and its solution is shown in Fig. 5.10.

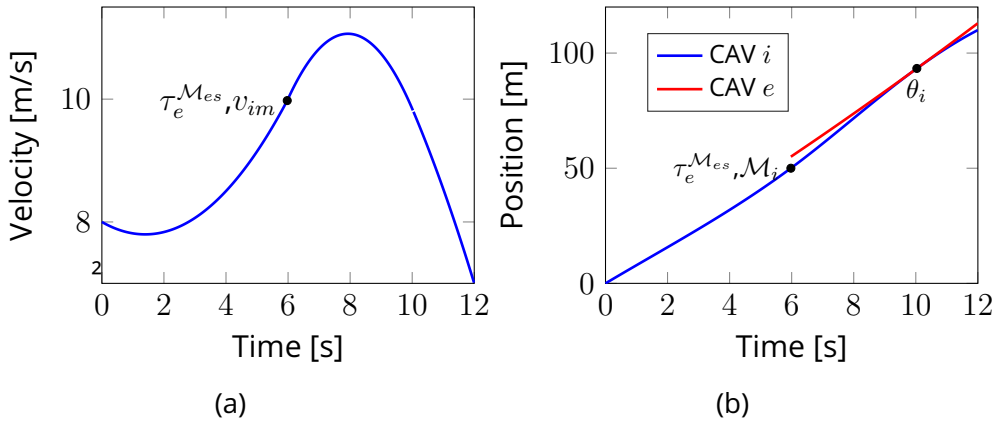

Figure 5.10: Velocity (a) and position (b) of CCAV i under a merging conflict. The $\mathcal{BC}$ for CCAV i is given as $x_{i,0}$= 0 m, $v_{i,0}$ = 8 m/s, $D_{i,f}$=110 m, $V_{i,f}$ = 7 m/s. T_i = 12 s. CCAV e's states are measured as $x_{e,m}$ = 5 m, $v_{e,m}$ = 9.07 m/s and a_e = 0.18 m/s^2. With $\mathcal{M}_i$ = 50 m, the arrival time is calculated as $\tau_e^{\mathcal{M}_{es}}$ = 5.97 s. The free parameter, v_{im} = 9.97 m/s.

Remark 2. *When there is only one CCAV in $\mathcal{H}_i(t)$, then CCAV $i \in \mathcal{N}(t)$ can face either one of the four conflicts or no conflict. However, in the presence of several CCAVs in $\mathcal{H}_i(t)$, CCAV $i \in \mathcal{N}(t)$ could face none, any one, or a combination of the four basic conflicts. All possible combinations of conflicts are identified a priori (see Appendix A.10). Each combination is translated into a constraint (either a piecewise combination, or two or more constraints on the position state) and is appended to the OCP (5.4) and its general solutions are computed a priori. The optimal solution consists of two or more segments depending on the constraint. The free parameters at the junctions of the optimal solution are identified, and the optimal value for these parameters is obtained by minimizing the energy of the entire trip, as demonstrated previously.*

Turning Speed Constraint: As mentioned earlier, turning speed constraint restricts a CCAV's speed in the IZ to a maximum defined by (5.1). The formulated constraint (5.12), is an interior-point constraint like (5.6). However, position and velocity are fixed with τ_t as the free parameter. The optimal solution has two almost-unconstrained segments with $\mathcal{BC}$ for the first and second segment given by $\{0, v_{i,0}, D_{i,f}/2, v_{tr}\}$ and $\{D_{i,f}/2, v_{tr}, D_{i,f}, V_{i,f}\}$, respectively. The term τ_t is found by minimizing the energy of the entire trip. The procedure is similar to that of crossing conflict. An example of the optimal solution satisfying the turning safe speed is shown in Fig. 5.11.

5.3.3 . Implementation

This section describes the algorithm of how the ED driving solutions are implemented in CCAVs crossing an intersection. A pseudo algorithm of the ED intersection scenario is presented in Algorithm. 1.

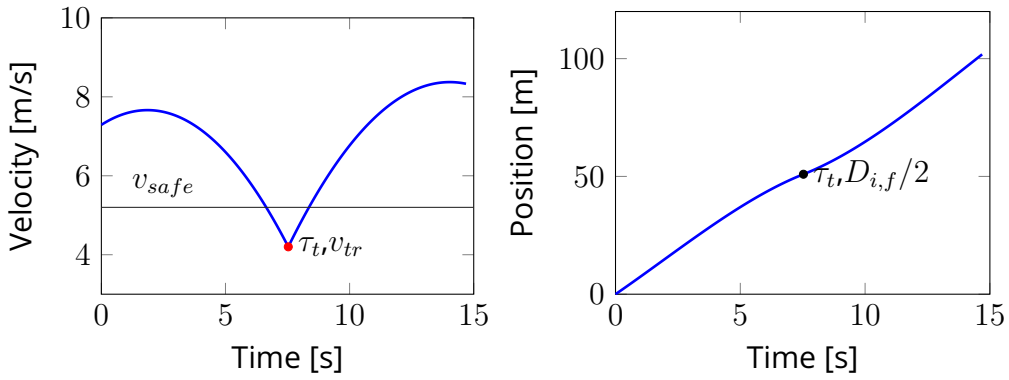

Figure 5.11: The velocity (a) and position (b) of CCAV i having its speed below v_safe when taking a right turn of radius 5 m is shown here. The $\mathcal{BC}$ for CCAV i is given as $x_{i,0}$= 0 m, $v_{i,0}$ = 7.29 m/s, $D_{i,f}$=101.85 m, $V_{i,f}$ = 8.33 m/s. T_i = 14.69 s. The free parameter, k_t = 7.53 s.v_{safe} = 5.2 m/s and v_{tr} is computed as 4.2 m/s.

At each time t, CCAVs in the intersection, i.e., $\mathcal{N}(t)$, solve their OCP sequentially in the order dictated by $\mathcal{CO}(t)$. A CCAV $i \in \mathcal{N}(t)$, entering the intersection at a time $t_{i,0}$, performs the following tasks to obtain its optimal control input: (i) obtains its set of $\mathcal{BC}$ (see line (7) in Algo. 1); (ii) identifies the conflicts posed by the other CCAVs already in the intersection; (iii) computes the optimal solution and; (iv) implements the computed solution.

Conflict Identification: In the NC-ED scenario, CCAV i decelerates to a fixed distance before $\mathcal{D}$ called the visibility distance D_{vis}, at which it determines whether a higher prioritized CCAV poses a crossing or merging conflict. The desired speed at D_{vis} is equal to a_{max} multiplied by one second. However, CCAV i can detect a diverging or car-following conflict from $x_i(0)$. This approach is followed in [20] and illustrated in Fig. 5.12. In the absence of conflicting CCAVs in the intersection or when it has the highest priority, CCAV $i \in \mathcal{N}(t)$ is considered unconstrained. However, in the presence of one or more conflicting vehicles in $\mathcal{H}^i(t)$, CCAV $i \in \mathcal{N}(t)$ could face one of the four fundamental conflicts or a combination of them. If only one CCAV belongs to any of the conflicting sets, CCAV i has one of the four conflicts. On the other hand, if there is one CCAV from more than one of the conflicting sets, then CCAV i has a combination of the four conflicts. The portion of the algorithm detailing conflict identification is presented in Appendix.A.10.

Optimal Solution: With the conflicts and conflicting CCAVs in $\mathcal{H}^i(t)$ identified for CCAV i, all possible solutions satisfying the constraints posed by these conflicts are evaluated. With the OCP of the CCAVs solved sequentially, all CCAVs in $\mathcal{H}^i(t)$ have already computed their optimal solution. This allows for a CCAV i

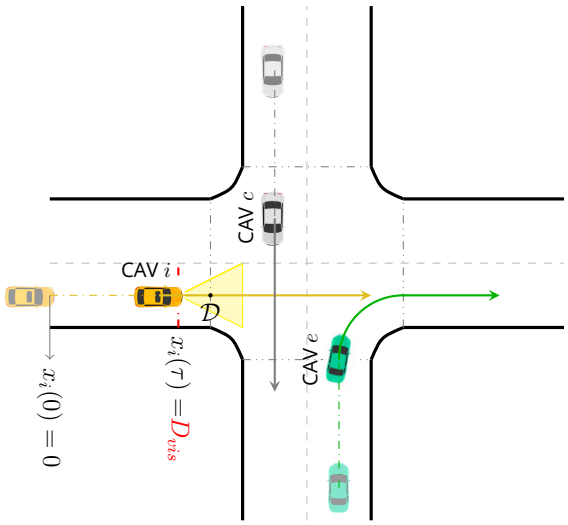

Figure 5.12: An illustration of conflicting CCAV's detection by CCAV i at D_{vis}. CCAV i at $x_i(0)$ cannot detect the CCAVs c and e arriving from the top and bottom lane. Only on reaching D_{vis} at a velocity $a_{max} \times 1$ m/s at $t = \tau$, CCAV i can identify the crossing and merging conflict posed by CCAV c and e, respectively. The conflicting sets at $x(0) = 0$ are given as $\mathcal{CO}(0) = (c, e, i)$, $\mathcal{DC}^i(0) = (\varnothing)$, $\mathcal{MC}^i(0) = (\varnothing)$, $\mathcal{CC}^i(0) = (\varnothing)$, $\mathcal{CF}^i(0) = (\varnothing)$, and at $x(\tau) = D_{vis}$ as $\mathcal{CO}(\tau) = (c, e, i)$, $\mathcal{DC}^i(\tau) = (\varnothing)$, $\mathcal{MC}^i(\tau) = (e)$, $\mathcal{CC}^i(\tau) = (c)$, $\mathcal{CF}^i(\tau) = (\varnothing)$.

to sense the instantaneous states and control input of the conflicting CCAVs to compute its optimal control input. In an unconstrained case, CCAV i can follow the solution in (5.14). In the presence of conflicts, all possible solutions for the given constraint are evaluated and CCAV i applies the solution with no constraint violation and the least energy consumption. The optimal solution computation part of the algorithm is detailed in Appendix.A.10.

Implementation: As new CCAVs enter and exit the intersection, the $\mathcal{CO}(t)$ changes based on the defined priority criterion and subsequently, the CCAVs in the conflicting sets also change. Furthermore, the acceleration of the CCAVs posing a conflict varies in time, needing to update its constant acceleration motion prediction. To capture the changing environment and predict conflicting CCAVs better, the solutions are implemented in a shrinking horizon MPC fashion as detailed in Sect. 2.3.3. The final boundary conditions and the optimal control input are computed as shown in lines (6) and (15) of algorithm. 1, respectively.

5.4 . Cooperative EDOC

This section describes the formulation, solution, and implementation of CCAVs entering an intersection under the Cooperative eco-driving scenario. In the C-ED,

Algorithm 1 Calculate $a_i^*(t)$

Require: $\{x_0, v_0, D_f, V_f\}$ for all CCAVs simulated
for $t \leftarrow 0$ to T_{sim} **do**
  Obtain $\mathcal{N}(t)$, $\mathcal{CO}(t)$ from coordinator
  for $j \leftarrow 1$ to $N(t)$ **do**
    CCAV i = $\mathcal{CO}_j(t)$
    Measure $x_i(t)$, $v_i(t)$
    Compute $T_i = T_{i,f} - t$, $D_i = D_{i,f} - x_i(t)$, $V_i = V_{i,f}$
    $\mathcal{BC} = \{0, v_i(t), D_i, V_i\}$
    if $j = 1$ **then**
      No conflicting CCAVs
      Optimal solution $\rightarrow$ Unconstrained $a_i(k)$ ▷ Using Eqn. (5.17)
    else
      Identify conflicts and conflicting CCAVs ▷ Refer to App. A.10
      Compute optimal solution $\rightarrow a_i(k)$ ▷ Refer to App. A.10
    end if
    Apply only the first control input $\rightarrow a_i^*(t) = a_i(0)$
  end for
end for

each CCAV still optimizes for itself like the NC-ED. However, it shares future intentions with the other CCAVs in the intersection.

5.4.1 . OCP Formulation

Consider a CCAV $i \in \mathcal{N}(t)$ with the same $\mathcal{BC}$ as in the NC-EDOC (5.4).

5.4.1.1 . Unconstrained EDOC

In the event of CCAV $i \in \mathcal{N}(t)$ being the only one in the intersection, an unconstrained OCP is formulated precisely as in (5.4).

5.4.1.2 . Constrained EDOC

As in Sect. 5.3.1.2, the conflicts posed by higher prioritized CCAVs are mathematically transformed into constraints to be added to the OCP.

Car-Following/Sequential Constraint: The potential rear-end collision avoidance is formulated as a state-inequality constraint, as in (5.5) with the exception that the preceding CCAV's motion is predicted using its shared solution. To be used in the eco-driving control of CCAV $i \in \mathcal{N}(t)$, this information is lumped into one "future mean value" $\tilde{a}_p$, evaluated over a preview window length L, as

$$\tilde{a}_p(t) = \frac{1}{L} \int_t^{t+L} a_p(\tau) d\tau. \tag{5.36}$$

The state-inequality constraint is written as,

$$x_i(t) \leq x_{p,0} + v_{p,0} t + \frac{1}{2} \tilde{a}_p t^2 \ , \tag{5.37}$$

where $x_{p,0}$ and $v_{p,0}$ are the initial position and velocity of CCAV $p \in \mathcal{CF}^i(t)$. The shared intentions $\tilde{a}_p$ in the C-ED scenario replaces the instantaneous measured acceleration a_p of the NC-ED.

Crossing Constraint: The potential lateral collision avoidance in the IZ is formulated as an interior-point constraint as in Sect. 5.3.1.2. Considering two CCAVs $i \in \mathcal{N}(t)$ and CCAV $c \in \mathcal{CC}^i(t)$ with $\mathcal{CO}(t) = \{c, i\}$, the constraint is formulated as,

$$x_i(t + \tilde{\tau}_c^{\mathcal{C}_i}) = \mathcal{C}_{ic} \quad \text{with} \quad \tilde{\tau}_c^{\mathcal{C}_i} = \tilde{t}_c^{\mathcal{C}_i} + dT \,, \tag{5.38}$$

where $\mathcal{C}_{ic}$ is the distance to the crossing point. The term dT is a safety margin between arrival of the CCAVs at their respective crossing points. Differing form the NC-ED, the arrival time $\tilde{k}_c^{\mathcal{C}_i}$ of CCAV c at its own crossing point $\mathcal{C}_{ci}$, is computed using its shared solution. Lets assume, for example, CCAV c follows (5.14). Its arrival time $\tilde{t}_c^{\mathcal{C}_i}$ at $\mathcal{C}_i$ is given by solving

$$\begin{aligned} \mathcal{C}_{ci} = x_{c,0} + v_{c,0}\tilde{t}_c^{\mathcal{C}_i} + \left(-\frac{2v_{c,0}}{T_{c,f}} - \frac{V_{c,f}}{T_{c,f}} + \frac{3D_{c,f}}{T_{c,f}^2} \right) \left(\tilde{t}_c^{\mathcal{C}_i}\right)^2 + \\ \left(\frac{v_{c,0}}{T_{c,f}^2} - \frac{2D_{c,f}}{T_{c,f}^3} + \frac{V_{c,f}}{T_{c,f}^2} \right) \left(\tilde{t}_c^{\mathcal{C}_i}\right)^3 \end{aligned} \tag{5.39}$$

Diverging Constraint: The potential rear-end collision avoidance in the entry lane is formulated as a piece-wise constraint as in Sect. 5.3.1.2, with the exception that the preceding CCAV $d \in \mathcal{DC}^i(t)$'s motion is predicted using its shared solution. More formally

$$x_i(t) \leq \begin{cases} x_{d,0} + v_{d,0}t + \frac{1}{2}\tilde{a}_d t^2 & t \in [0, \tau_d^{\mathcal{D}}] \\ \infty & t \in (\tau_d^{\mathcal{D}}, T_{i,f}] \end{cases} \tag{5.40}$$

where $x_{d,0}$ and $v_{d,0}$ are the CCAV d's initial position and velocity. $\tilde{a}_d$ represents the average acceleration of d computed by replacing p with d in (5.36). $\tau_d^{\mathcal{D}}$ is the arrival time of CCAV d using $\tilde{a}_d$ as the acceleration.

Merging Constraint: Similar to Sect. 5.3.1.2, the piece-wise constraint in the exit lane to avoid a rear-end collision is formulated as

$$x_i(t) \leq \begin{cases} \infty & t < \tau_e^{\mathcal{M}_{es}} \\ (x_{e,m} - \mathcal{M}_i) + v_{e,m}t + \frac{1}{2}\tilde{a}_e t^2 & t \geq \tau_e^{\mathcal{M}_{es}} \end{cases} \tag{5.41}$$

where $\tau_e^{\mathcal{M}_{es}}$ is the arrival time of CCAV e at $\mathcal{M}_{es} = \mathcal{M}_e + ds$ s.t. $ds > s_{min}$, obtained from the shared solution of CCAV e. Its motion in the exit lane is predicted using the average acceleration $\tilde{a}_e$ obtained by replacing p with e in (5.36). The term $v_{e,m}$ represents the velocity measured at $x_{e,m} = \mathcal{M}_{es}$.

Apart from the four fundamental conflicts, a CCAV $i \in \mathcal{N}(t)$ could face a combination of the conflicts, see Appendix A.10.

Turning Speed Constraint: With turning speed constraint independent of other CCAVs, the formulation given in Sect. 5.3.1.2 remains unchanged.

5.4.2 . Solution

The method to obtain the solutions to the OCP (5.3.1.1), with the constraints (5.37), (5.38), (5.40) and (5.41) remains the same as detailed in Sect. 5.3.2. When the optimal solution consists of two or more segments, the free parameters at the junctions are identified and the optimal value for the free parameters are obtained by minimizing the energy of the entire trip. The parameters replaced in NC-ED's solutions to obtain the C-ED's solution are

- Unconstrained: No Change
- Car-Following Constraint: $\tilde{a}_p$ replaces a_p
- Crossing Constraint: $\tilde{\tau}_c^{\mathcal{C}_i}$ and $\tilde{t}_c^{\mathcal{C}_i}$ replaces $\tau_c^{\mathcal{C}_i}$ and $t_c^{\mathcal{C}_i}$ respectively
- Diverging Constraint: $\tilde{a}_d$ replaces a_d
- Merging Constraint: $\tilde{a}_e$ replaces a_e

5.4.3 . Implementation

The scenarios NC-ED and C-ED in an intersection differs in two aspects : (i) the amount of information shared to CCAV i, discussed in Sect. 5.4.2; (ii) the point at which CCAV i identifies its conflicting vehicles. Unlike the NC-ED scenario, where CCAV i can identify the conflicting CCAVs only D_{vis} m before $\mathcal{D}$; in the C-ED CCAV i can identify, with the help of communication, its conflicting CCAVs as soon as it enters the intersection (i.e., $x_i(0)$). An illustration of this is shown in Fig. 5.13.

Besides the conflict identification point, the computation of the solution and its implementation in the shrinking horizon MPC remains the same as in the NC-ED.

5.5 . Simulation Results

In this section, we evaluate the performance of the proposed NC-ED and C-ED algorithms in terms of energy consumption in a MATLAB simulation environment. the energy consumption of each CCAV is computed using the model described in [**?**]. The algorithms are compared against a baseline scenario generated by the traffic simulation software SUMO using the Intelligent Driver Model (IDM). SUMO is an open-source microscopic and continuous multi-modal traffic simulation package designed to handle large networks. An isolated intersection model is first created in SUMO with $l = 47$ m and $w = 4$ m. Three flow rates of 800, 1200 and 1600 veh/hr are simulated thrice for convergence of total energy consumption in each flow rate. A total of $N = 30$ CCAVs are set to enter the intersection

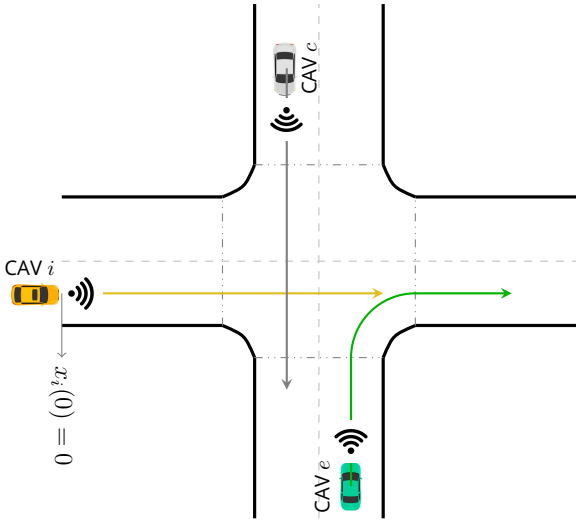

Figure 5.13: An illustration of conflicting CCAV's detection by CCAV i at $x_i(0)$. CCAV i at $x_i(0)$ detects the CCAVs c and e arriving from the top and bottom lane and is able to identify the crossing and merging conflict posed by them, respectively. The conflicting sets at at $t = 0$ as $\mathcal{CO}(0) = (c, e, i)$, $\mathcal{DC}^i(0) = (\varnothing)$, $\mathcal{MC}^i(0) = (e)$, $\mathcal{CC}^i(0) = (c)$, $\mathcal{CF}^i(0) = (\varnothing)$.

with randomized boundary conditions using uniform distribution on initial velocity, entry lane and direction. The arrival time of each CCAV is obtained using negative exponential distribution given by

$$t_{i,0} = -\lambda \log(X) \tag{5.42}$$

where λ is the mean headway between vehicles (flowrate/3600) and X is a random variable between 0 and 1. The CCAVs is SUMO are modelled using the built-in reactive IDM car-following strategy given by

$$\begin{aligned} \dot{v}_i &= a\left(1 - \left(\frac{v_i}{v_0}\right)^{\delta} - \left(\frac{s^*\left(v_i, \Delta v_i\right)}{s_i}\right)^2\right) \\ \text{with } s^*\left(v_i, \Delta v_i\right) &= s_0 + v_i T + \frac{v_i \Delta v_i}{2\sqrt{ab}} \end{aligned} \tag{5.43}$$

where v_0, s_0, T, a, and b are model parameters which represent desired velocity, minimum spacing, desired time headway, the maximum vehicle acceleration and comfortable braking deceleration, respectively. The dealing of conflicts amongst CCAVs in an intersection in SUMO is detailed in [20].

The parameters for the ED algorithm in MATLAB are such that, the minimum safety distance s_{min} = 7 m and the safety dT to avoid a lateral collision is set to 2.5 s. The distance margin ds for merging constraint is chosen as 9 m. The initial speed is uniformly distributed in the interval 8.3 m/s $\pm$ 2 m/s. The maximum acceleration and deceleration of the CCAVs are set to 4 m/s^2.

The IDM cannot enforce a prescribed final time or speed unlike the ED solutions. The final time and speed of the CCAVs obtained at the end of the simulation in SUMO are used as inputs in the EDOC. This ensures the same average speed for a CCAV $i \in \mathcal{N}(t)$ across the algorithms. The right-before-left criterion is given as the crossing order in SUMO and is also maintained across the NC-ED and C-ED.

The velocity trajectories of the CCAVs, arriving at a flow rate of 800 veh/h, equipped with IDM, NC-EDOC and C-EDOC algorithms are shown in Fig. 5.14. The CCAVs using IDM and NC-ED decelerate to 4 m/s^2 at D_{vis}, which is 4.5 m before $\mathcal{D}$. At D_{vis}, CCAV i checks for merging or crossing conflicts with higher prioritized CCAVs and obtains only the instantaneous control input from the conflicting CCAVs. In the event of a conflict, the CCAV i adjust its speed profile, with some of them coming to an almost complete stop, e.g., the purple CCAV at 130 s. On the other hand, CCAVs with C-EDOC do not decelerate to check for conflicts. They can identify the conflicts CCAVs as soon as they enter and plan their trajectory accordingly. CCAVs taking a left or right turn also decelerate to satisfy turning speed constraints, e.g. CCAV 5, green speed profile at around 40 s, is taking a right turn and has a safe speed of 5.24 m/s inside the IZ.

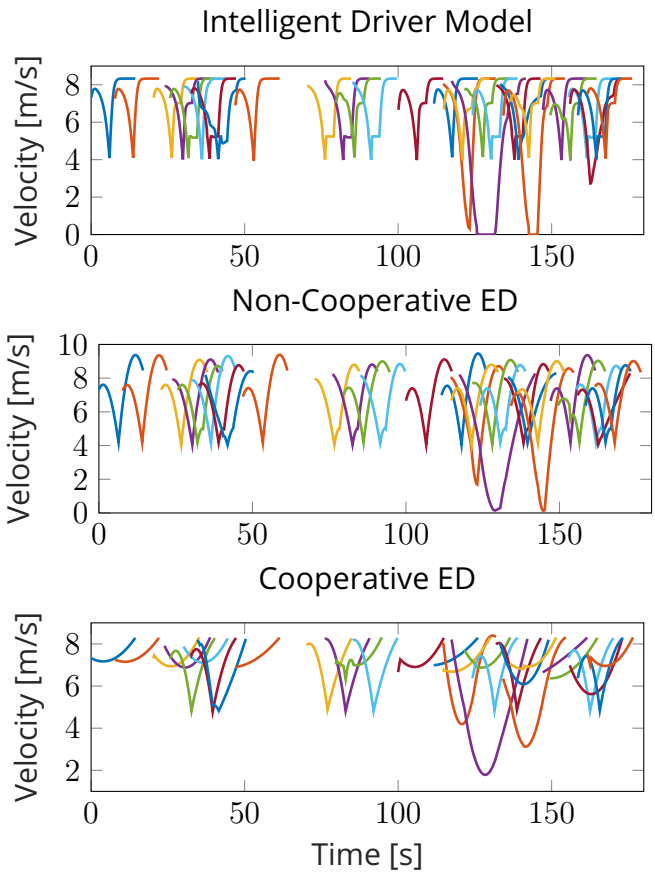

Figure 5.14: Velocity trajectories of CCAVs at 800 veh/h

The velocity trajectories of flow rates 1200 veh/h and 1600 veh/h are shown in Fig. 5.16 and Fig. 5.17, respectively. With higher flow rates, shorter is the interval between arrival times of CCAVs. For clarity only odd numbered CCAVs are displayed in figures 5.16 and 5.17. It can be noticed that the number of slow downs or stops increase from 800 veh/h to 1600 veh/h. This can be attributed to the increase in number of vehicles in the intersection simultaneously and consequently increased conflicts. This causes the CCAVs to slow down avoid collision. Another reason that causes the vehicles to come to a complete stop is the assigned crossing order from SUMO. The right-before-left criterion often causes vehicles to come to a complete stop, especially at high flow rates. For example, CCAV 9 (orange line) in Fig. 5.17 has to come to a come stop to give way to three CCAVs coming from its right side. Similar behavior can be observed towards the end from 60 s to 80 s where a CCAV (green) comes to stop to give way to higher prioritized CCAVs and creates an almost deadlock situation with the light and dark blue CCAVs. Such behavior indicates the need to well define criterion for priority. The velocity trajectories also indicate a high jerk at the point where the CCAV starts to accelerate again after slowing down, especially in the NC-ED and IDM. Such a behavior could cause discomfort to the passengers. This could be overcome by decreasing the average velocity of the CCAVs (i.e., increasing $T_{i,f}$). However, for the sake of fair comparison between the three algorithms the average speed is maintained uniformly.

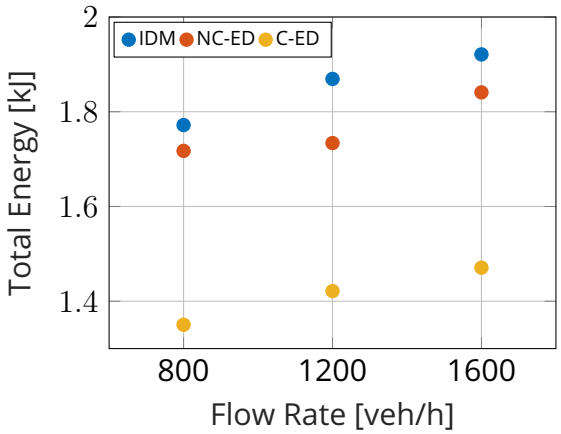

Figure 5.15: Total energy consumption of 30 CCAVs at flow rates of 800, 1200, 1600 veh/h.

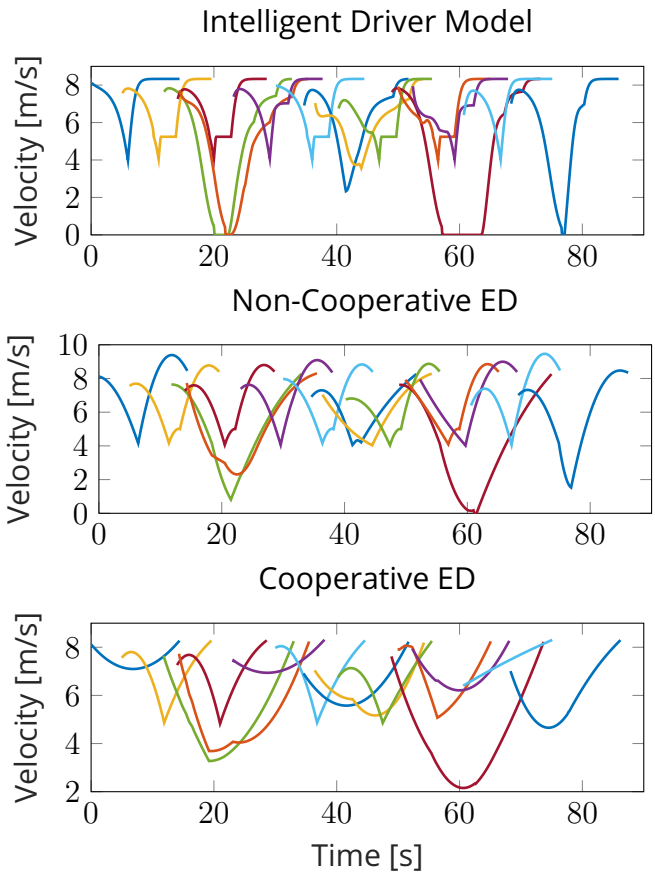

Figure 5.16: Velocity trajectories of CCAVs at 1200 veh/h

The total mean energy consumption of 30 CCAVs in the three runs are given in Fig. 5.15. It can been seen that the total energy consumption increases with an increase in flow rate. This is due to the increased conflicts amongst the CCAVs causing a CCAV $i \in \mathcal{N}(t)$ to adjust its speed profile. The CCAVs in NC-ED consumes 3 $\%$ less energy than IDM. With IDM and NC-ED having same information on conflicting vehicles, the energy reduction is caused by the optimal ED speed profiles employed by the CCAVs. The C-ED performs best amongst the three, with a reduction of 23.7 $\%$ over IDM and 21.3 $\%$ over the NC-ED. The CCAVs with cooperation have more accurate information about the conflicting vehicles and get this information much earlier (i.e. at $x_i(0)$) than the other two algorithms. This enables better anticipation and hence the CCAVs can adjust their speed profiles accordingly.

5.6 . Conclusion

This chapter addressed the problem of finding the optimal ED speed trajectory for the entire horizon (i.e., entry lane, IZ and exit lane) of an urban isolated

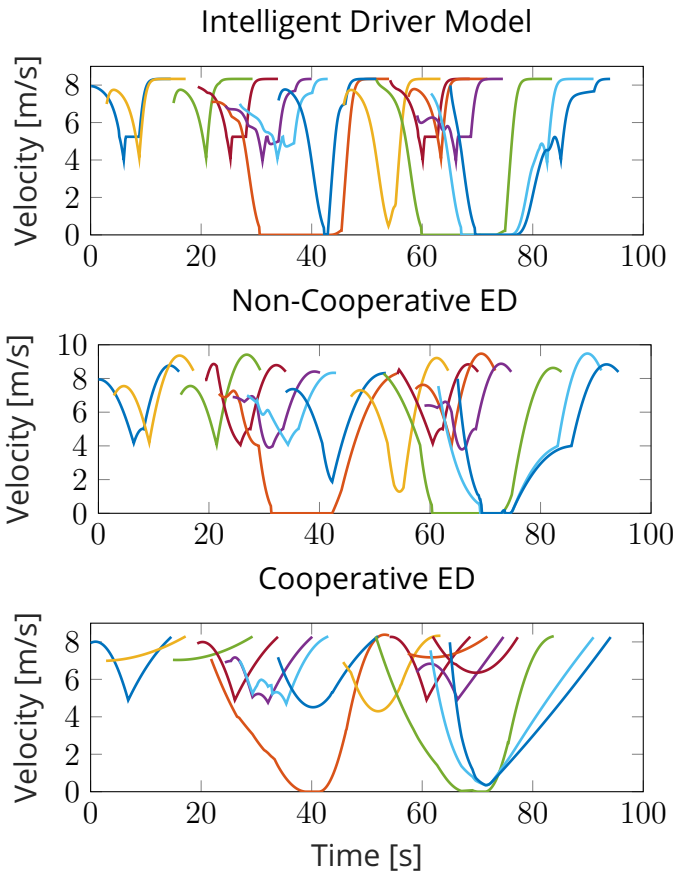

Figure 5.17: Velocity trajectories of CCAVs at 1600 veh/h

intersection. Various conflicts in the intersection were formulated has as constraints to the CCAV and its solutions were presented. Two levels of cooperation, namely, the Non-Cooperative and Cooperative, were studied and evaluated for energy consumption in comparison to the baseline, IDM. The Cooperative algorithm performed best, with a reduction of 23.7 % over IDM and 21.3 % over the NC-ED. The C-ED indicates that, earlier determination of conflicts with higher prioritized CCAVs and better prediction of their arrival time and motion, leads to better energy efficiency.

Bibliography

[1] Kurt M. Dresner and Peter Stone. A multiagent approach to autonomous intersection management. J. Artif. Intell. Res., 31:591–656, 2008.

[2] Qiu Jin, Guoyuan Wu, Kanok Boriboonsomsin, and Matthew Barth. Multi-agent intersection management for connected vehicles using an optimal scheduling approach. In Proceedings of the 2012 International Conference on Connected Vehicles and Expo, ICCVE '12, page 185–190, 2012.

[3] Mohamad Hafizulazwan Bin Mohamad Nor and Toru Namerikawa. Optimal control of connected and automated vehicles at intersections with state and control constraints. In 2019 IEEE/ASME International Conference on Advanced Intelligent Mechatronics (AIM), pages 1397–1402, 2019.

[4] Brian Paden, Michal Čáp, Sze Zheng Yong, Dmitry Yershov, and Emilio Frazzoli. A survey of motion planning and control techniques for self-driving urban vehicles. IEEE Transactions on Intelligent Vehicles, 1, 04 2016.

[5] Jackeline Rios-Torres and Andreas A. Malikopoulos. A survey on the coordination of connected and automated vehicles at intersections and merging at highway on-ramps. IEEE Transactions on Intelligent Transportation Systems, 18(5):1066–1077, 2017.

[6] Lei Chen and Cristofer Englund. Cooperative intersection management: A survey. IEEE Transactions on Intelligent Transportation Systems, 17(2):570–586, 2016.

[7] Youssef Bichiou and Hesham A. Rakha. Real-time optimal intersection control system for automated/cooperative vehicles. International Journal of Transportation Science and Technology, 8(1):1–12, 2019.

[8] Robert Hult, Mario Zanon, Sébastien Gros, and Paolo Falcone. Energy-optimal coordination of autonomous vehicles at intersections. In 2018 European Control Conference (ECC), pages 602–607, 2018.

[9] Laleh Makarem and Denis Gillet. Model predictive coordination of autonomous vehicles crossing intersections. In 16th International IEEE Conference on Intelligent Transportation Systems (ITSC 2013), pages 1799–1804, 2013.

[10] Gabriel R. Campos, Paolo Falcone, Henk Wymeersch, Robert Hult, and Jonas Sjöberg. Cooperative receding horizon conflict resolution at traffic intersections. In 53rd IEEE Conference on Decision and Control, pages 2932–2937, 2014.

[11] Maximilian Kloock, Patrick Scheffe, Sascha Marquardt, Janis Maczijewski, Bassam Alrifaee, and Stefan Kowalewski. Distributed model predictive intersection control of multiple vehicles. In 2019 IEEE Intelligent Transportation Systems Conference (ITSC), pages 1735–1740, 2019.

[12] Andreas A. Malikopoulos, Christos G. Cassandras, and Yue J. Zhang. A decentralized energy-optimal control framework for connected automated vehicles at signal-free intersections. Automatica, 93:244–256, 2018.

[13] Yue Zhang and Christos G. Cassandras. Decentralized optimal control of connected automated vehicles at signal-free intersections including comfort-constrained turns and safety guarantees. Automatica, 109:108563, 2019.

[14] Vinith Kumar Lakshmanan, Antonio Sciarretta, and Ouafae El-Ganaoui Mourlan. Cooperative levels in eco-driving of electric vehicle platoons. In 2021 IEEE International Intelligent Transportation Systems Conference (ITSC), pages 1163–1170, 2021.

[15] Vinith Kumar Lakshmanan, Antonio Sciarretta, and Ouafae El Ganaoui-Mourlan. Cooperative eco-driving of electric vehicle platoons for energy efficiency and string stability. IFAC-PapersOnLine, 54(2):133–139, 2021. 16th IFAC Symposium on Control in Transportation Systems CTS 2021.

[16] Jihun Han, Ardalan Vahidi, and Antonio Sciarretta. Fundamentals of energy efficient driving for combustion engine and electric vehicles: An optimal control perspective. Automatica, 103:558–572, 2019.

[17] Mary Thompson, Oh Kwon, and Min Park. The application of axiomatic design theory and conflict techniques for the design of intersections: Part 1. pages Paper ICAD–2009, 01 2009.

[18] A. E. Bryson and Y. C. Ho. Applied Optimal Control. Blaisdell, 1969.

[19] Antonio Sciarretta and Ardalan Vahidi. Energy-Efficient Driving of Road Vehicles. Springer, 2020.

[20] Daniel Krajzewicz and Jakob Erdmann. Road intersection model in sumo. pages 212–220, 05 2013.

6 - Experimental Implementation of Eco-Driving Concepts

6.1 . Introduction

This chapter discusses the experiments on implementing ED solutions in an electric vehicle. The work focused on using mostly existing vehicle hardware, with the additional benefit from cloud-based servers.

6.2 . System Overview

The ED solutions obtained in Chapter 2 for en electric vehicle is implemented in a Renault Zoe, the specifications of which are detailed in Table 6.1. The effective implementation of the ED solutions would ideally be in a SAE level-3 electric CAV or a current off-the-shelf electric vehicle retrofitted with an autonomous stack (systems including localization, perception and planning/control). However, with the main focus on using pre-existing hardware, we resort to the use of Visual Assistance Systems (VAS). The VAS is a dedicated personal device tablet physically located on the dashboard of the car, which presents the computed recommended optimal speed v^* for the driver to follow, see Fig. 6.1.

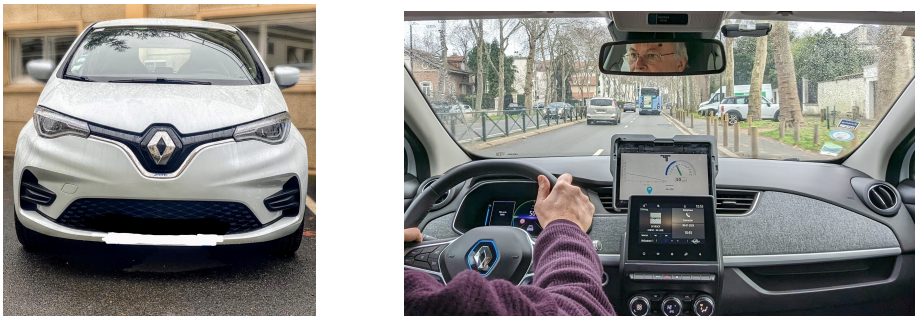

(a) Renault Zoe ZE-50 (b) IFPEN Tablet on the dashboard

Figure 6.1: A picture of Renualt Zoe and the VAS on the dashboard

A conceptual schematic of the ED algorithm implementation is shown in Fig. 6.2. The EDOC communicates with the human driver using a Human-Machine-Interface *HMI*. Before the start of a trip, the driver enters their origin and destination in the *HMI Eco-Charging*, using a HERE maps interface. The origin and destination inputs are then communicated to the IFPEN's *MOBI-Cloud*[1] server via the *Web Socket Server (WSS)* technology. The *MOBI-Cloud* server

[1] https://mobicloud.ifpen.com/

hosts an algorithm named Eco-Charging *EC*, which computes the route for the given origin destination pair as one of its outputs. The EC algorithm then breaks the trip into sub-trips called links, based on certain *break-point detection criteria* [2]. Each link is assigned an id and contains attributes such as, latitude and longitude coordinates, speed limit, link length, predicted travel time and predicted final speed. The *WSS* acts only as a central coordinator, with minimal computational capability, hosting three sub-functions, namely, *Links Aggregation*, *Map Matching*, and $\mathcal{BC}$ *and Constraints*. Its responsibility is to receive and dispatch the information between the various sub-functions.

The link length D_f is given by the length of the path between the start and end of each link. The average speed in a link, which is a function of the free-flow speed and average traffic speed and computed as a result of a graph based optimization problem in EC, gives the predicted final time T_f. In the presence of a traffic light or a stop-sign the final speed V_f is considered zero and in the absence of any, the final speed is predicted to be the average speed of the next link. Note that, the signal phase of all traffic lights are assumed red and its timing is not taken into consideration.

The links along with its attributes are passed back to the *Links Aggregation* via *WSS*, which further performs, based on certain heuristic rules, an aggregation process on the links that are too small or where the driver will not perceive any major changes.

During the trip (i.e., real-time), the function *Position Service* measures the states (i.e., current speed and coordinates) of the vehicle along the trip and is displayed on the *HMI Eco-Charging*. These measurements are carried out either using a GPS module connected via an USB or a smartphone connected via blue-tooth. Using the measured coordinates, the *Map Matching* module in the *WSS* identifies the current link i the vehicle is in and passes its attributes, mainly $\{D_f, T_f, x(t)\}$, to the $\mathcal{BC}$ *and Constraints* module. This in turn computes the $\mathcal{BC} = \{0, v(t), D, V\}$ and the constraints and passes it to the *Eco-Driving Optimal Controller (EDOC)*. The $\mathcal{BC}$ computed using the shrinking horizon MPC are detailed in Sect. 2.2.3. The *EDOC* computes the ED speed profile for the given $\mathcal{BC}$ and displays the optimal speed $v(t)^*$ to be followed for the next instance on the *HMI Eco-Driving*, see Fig. 6.3.

The lack of V2V, V2I and perception module, limits us from knowing the traffic light SPaT and lead vehicle behavior. As stated earlier, all traffic lights are considered to be in a red phase thus imposing its link's final speed to zero. The absence of a camera or a lidar/radar module, at the time of writing this thesis, limits the EDOC to account for the lead vehicle constraint and compute $v(t)^*$ only using unconstrained ED solutions in (2.2.3). In the presence of a maximum speed constraint $v(t)^*$ is computed using the solutions detailed in [1].

[2] A few of the criteria include change of speed limit, a new lane and, presence of an intersection, traffic light or a stop-sign.

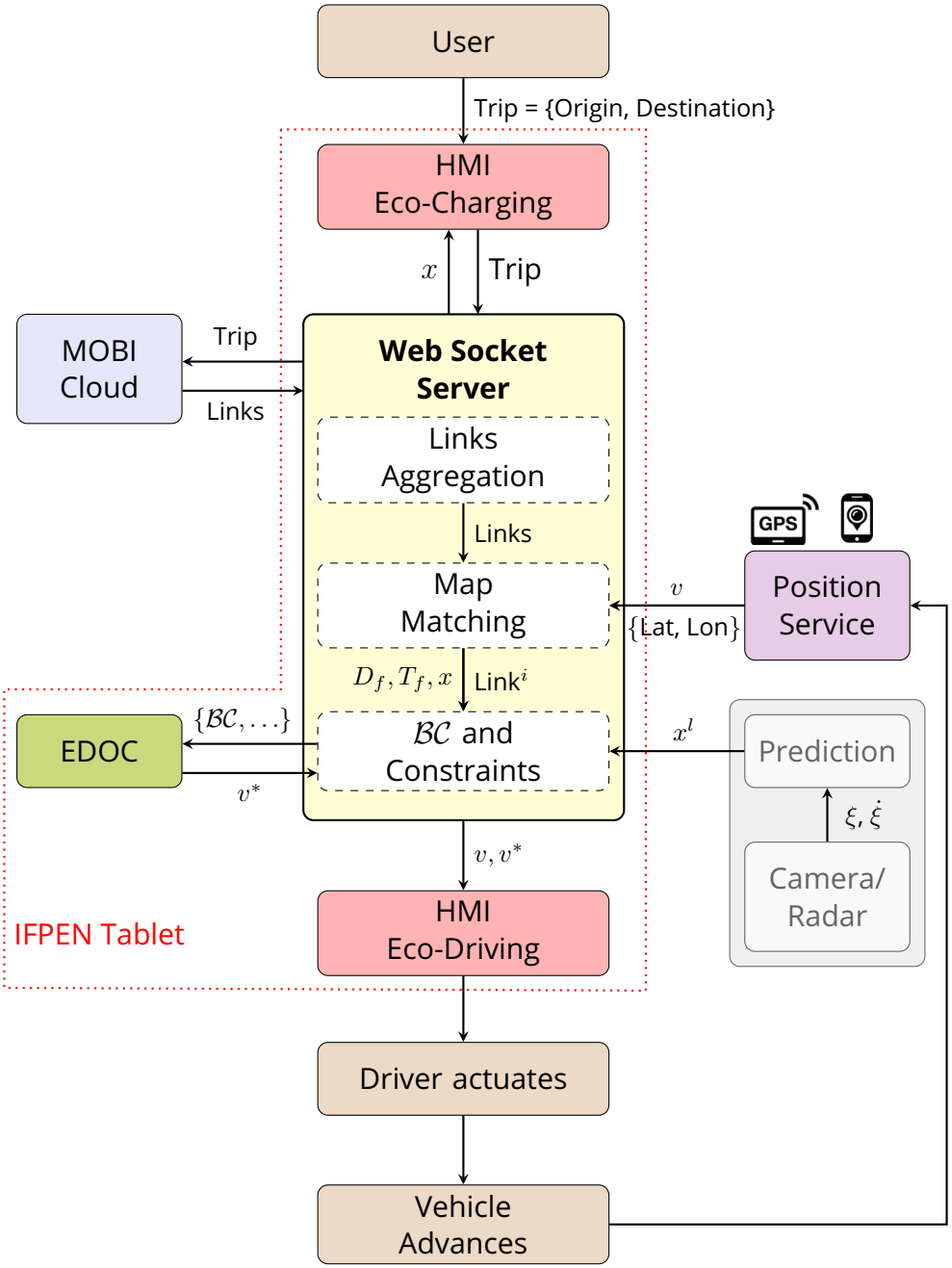

Figure 6.2: Schematic of the various functions in the VAS

6.3 . Experimental Procedure

Testing was performed by driving the vehicle on an urban route between Rueil-Malmaison and Chatou in France's Île-de-France region. Figure 6.4 shows the route and the various links created for the route. The experiments were conducted

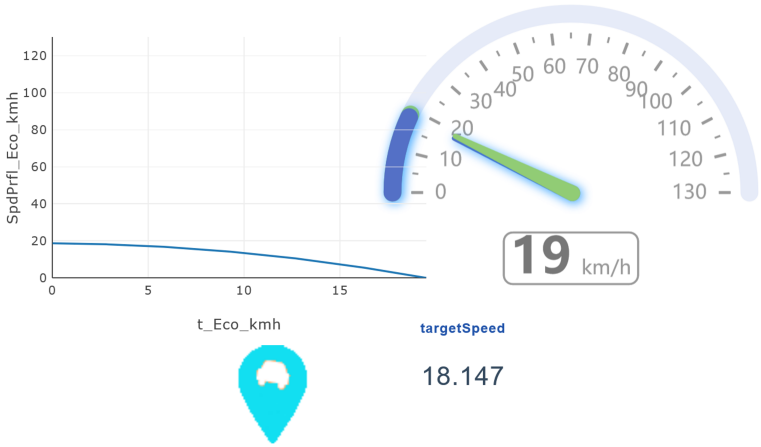

Figure 6.3: The figure shows the HMI-Eco-Driving. The blue arrow on the odometer indicates the speed to be followed at the next instance, v^* and the green arrow indicates the current speed

Table 6.1: Technical Specification of Renault Zoe ZE-50

Performance		Battery	
0 - 100 km/h	11.4 sec	Nominal Capacity	54.7 kWh
Top Speed	135 km/h	Battery Type	Lithium-ion
Electric Range	315 km	Nominal Voltage	350 V
Total Power	80 kW	Number of Cells	192
Total Torque	225 Nm	Useable Capacity	52.0 kWh
Drive	Front	Architecture	400 V

on the same route and time of the day for repeatability and to reduce variability in traffic conditions.

6.4 . Results

This section discusses the results of five trips, numbered from 1 to 5, conducted on the earlier shown route. As stated in Sect. 6.2, the lack of V2V, V2I and perception module, limits us from knowing the traffic light SPaT and lead vehicle behavior. Therefore, the following assumptions were made:

- No traffic Queue
- Red signal phase for all traffic lights
- No traffic.

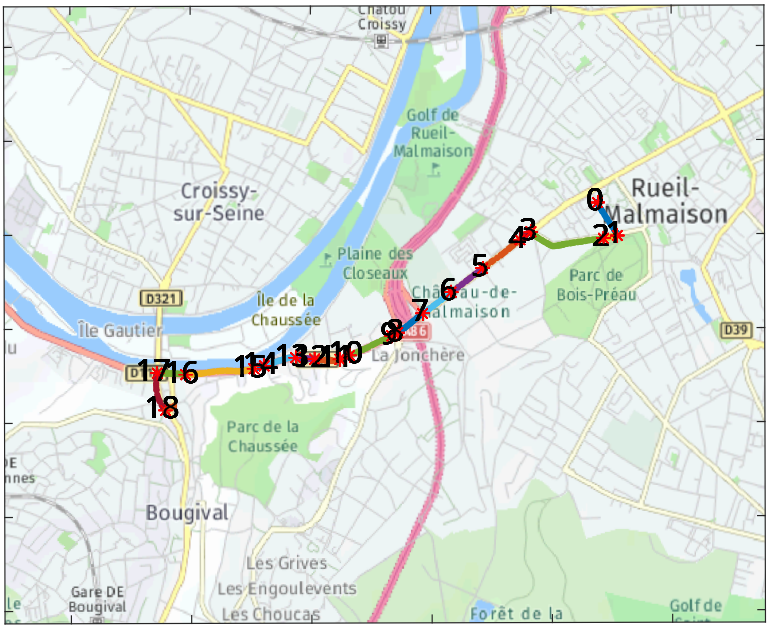

Figure 6.4: The experiment route

Note that the impact of signal timing is excluded as we do not consider eco-approach and departure in the current implementation. The results discussed below includes a posteriori analysis on the impact of these assumptions on the $\mathcal{BC}$ identification. The impact is quantified in terms of energy consumption for the five trips while a single trip named Trip 1, among the five, is used as a working example to describe the methodology of the analysis. Note that, this section doesn't discuss or compare the energy gains of the system with or without eco-driving.

Fig 6.5 and Fig 6.6 show the speed traces of Trip 1 as a function of time and distance respectively. The predicted speed profile (referred to as ex-ante thereafter) is shown in Fig. 6.5a and Fig. 6.6a. The ex-ante is computed at the start of the trip, an output of EC, under the assumptions of no traffic and traffic queue, red signal phase and no signal timing for traffic lights. The driven speed profile along with its target/advised speed is shown in Fig. 6.5b and Fig. 6.6b. The target/advised (blue) speed is computed in real-time under the shrinking horizon MPC and similar assumptions, using measured the measured speed and position as its new initial conditions at each time, t. The vertical lines in the figures indicate the start of the different links, given by *Links Aggregation*, along the trip.

The influence of the no traffic queue assumption can be seen in link 4 in Fig. 6.6b. While the vehicle, at a red traffic light, has stopped a few meters earlier

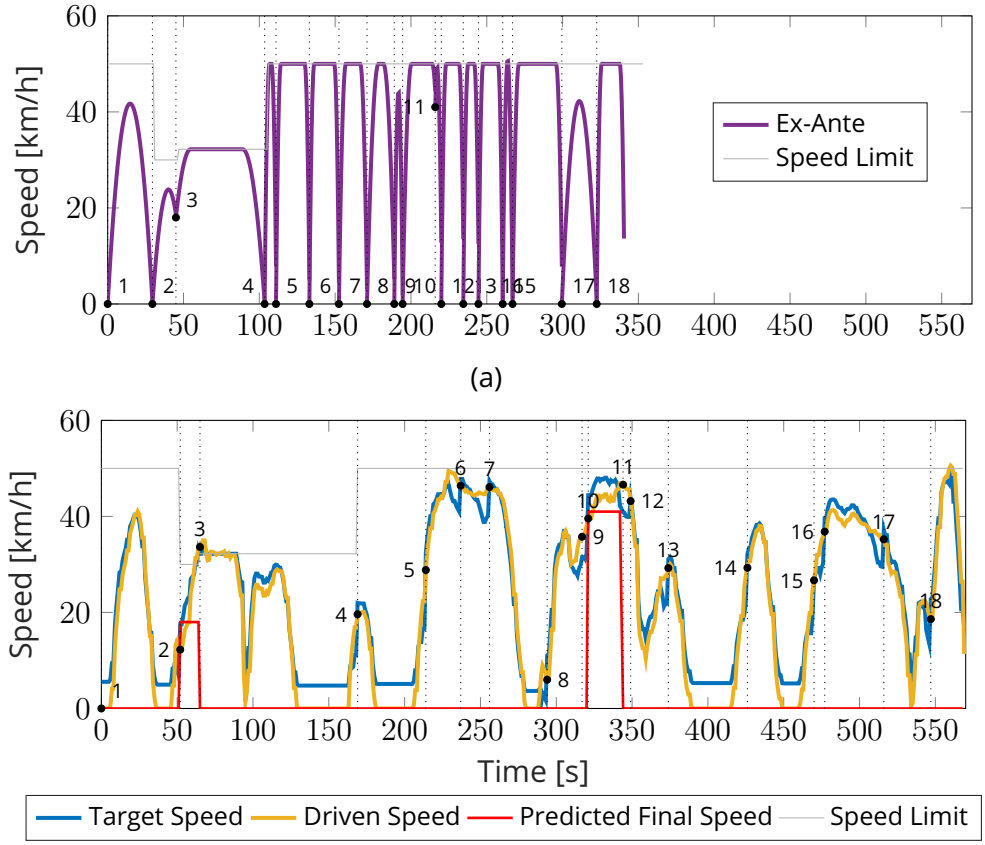

Figure 6.5: The ex-ante and driven speed profile as a function of time for Trip 1.

than the stop line, possibly due to the presence of leading vehicles, the link is deemed complete only when the vehicle crosses the stop line when the signal turns green.

The advised speed is effective in anticipating stops or maintaining a certain average speed. For instance, the first link has a zero predicted final speed due to the presence of a traffic light and the target speed advises the driver to decelerate to a stop. The same can be noticed in links three and four. However, in links five and six, while advised to decelerate to predicted zero final speed, the driver maintains the current speed. The advise to decelerate is due to the red signal phase assumption at a traffic light, when it was green in reality.

Finally, the driven speed profile without considering stops takes much longer ($\sim$ 442 s) to complete the trip while the ex-ante predicts a shorter travel time, owing to the no traffic assumption.

6.4.1 . Impact of the Assumptions

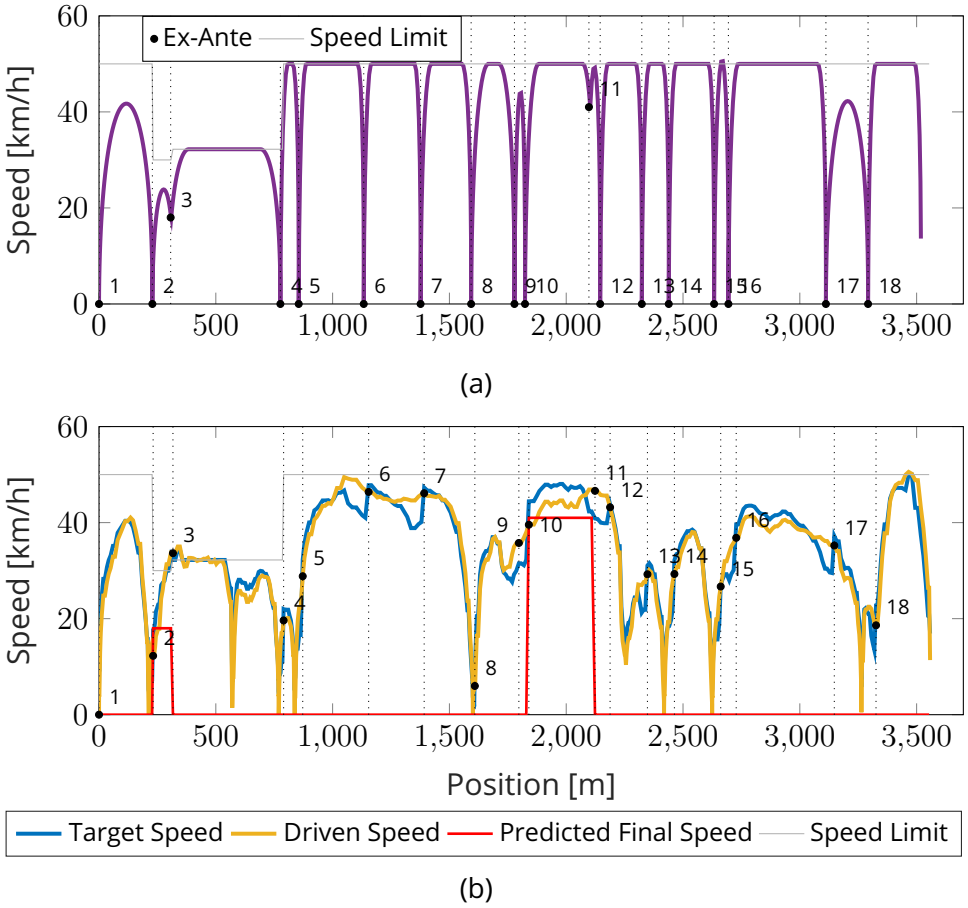

Figure 6.6: The ex-ante and driven speed profile as a function of position for Trip 1.

The impact of red signal phase, no traffic queue and no traffic, on the ex-ante speed profile is determined by conducting a posteriori analysis using the driven speed profile. The impact of the assumptions are quantified in terms of energy consumption. This subsection answers the question, *what should have been the ex-ante speed profile computed at the start of the trip, if we had access to traffic, traffic queue length and signal phase?* To do so, traffic queue, the actual signal phase and traffic are identified from the driven speed profile and the theoretical speed profiles are recomputed.

6.4.1.1 . Identification of Traffic Queue Length and Signal Phase

Fig. 6.7 shows a trip where the vertical black lines indicate the predicted start/end of each link. A link is considered complete when the remaining distance D in the link is zero. The total length of the link D_f is computed assuming that the car will stop precisely at the stop line. However, it is not always the case due to the presence of a queue at the traffic light or a stop sign. A closer

look at the end of link 13 indicates that the car stops earlier (brown dashed line with number 14) than its predicted end (black dashed line with number 14). This queue is identified from the driven profile using a heuristic rule stating that if the car stops within a certain distance from the predicted end of a link, it is identified as complete. The new identified start of links (brown) are shown in Fig 6.7. Note that no additional links are created, and only existing ones are re-positioned. The boundary conditions for each of the links, $\mathcal{BC}^i = \{0, v_0, D_f, V_f\}$, with the adjusted break points are extracted to compute the theoretical speed profiles, discussed in Sect. 6.4.2. The actual signal phase at the time of driving is identified by choosing the speed at the end of each link as V_f. A zero V_f indicates the signal phase was red and a non-zero V_f indicated a green signal phase.

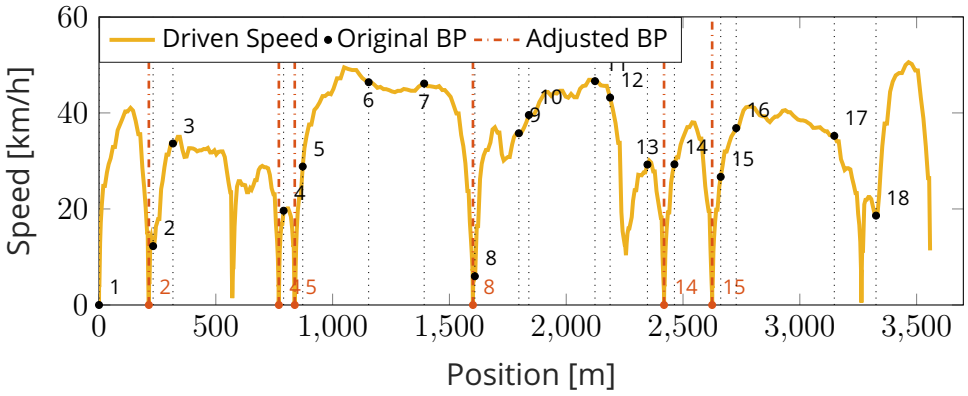

Figure 6.7: Break Points (BP) Adjusted to consider Traffic Queue for Trip 1

6.4.1.2 . Identification of Traffic, Traffic Queue Length and Signal Phase

The influence of traffic (i.e. presence of preceding vehicle), is identified by looking at significant speed decrease in the driven profile, for example in link 13 at around 2300 m in Fig. 6.8. Such reduction in speeds are identified using the concept of prominence and the reference level from which the prominence is computed is identified as new break points (blue dots in Fig. 6.8) for links. Note that this step leads to new links in addition to the ones initially given by *Links Aggregation*. Similarly, the boundary conditions for each of the links, $\mathcal{BC}^i = \{0, v_0, D_f, V_f\}$, are extracted to compute the theoretical speed profiles, discussed in Sect. 6.4.2.

6.4.2 . Energy Analysis

With traffic, queue and signal phase identified from the driven profile, their impact is evaluated systematically in terms of energy consumption. The $\mathcal{BC}^i$ extracted from each link are used to compute the theoretical speed profiles using either (2.14) or speed constrained solutions detailed in [1]. The theoretical speed profiles computed using $\mathcal{BC}^i$ identified a posteriori, will thereafter be referred to as

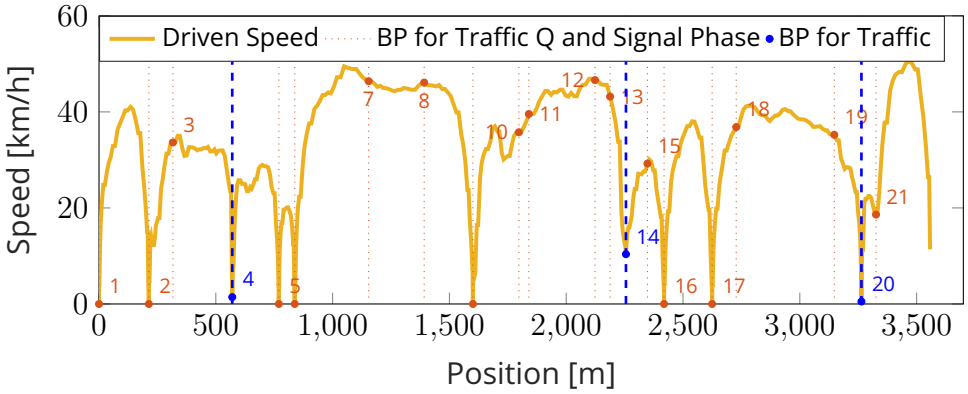

Figure 6.8: Break Points (BP) Identified for Traffic in Trip 1

ex-post speed profiles.

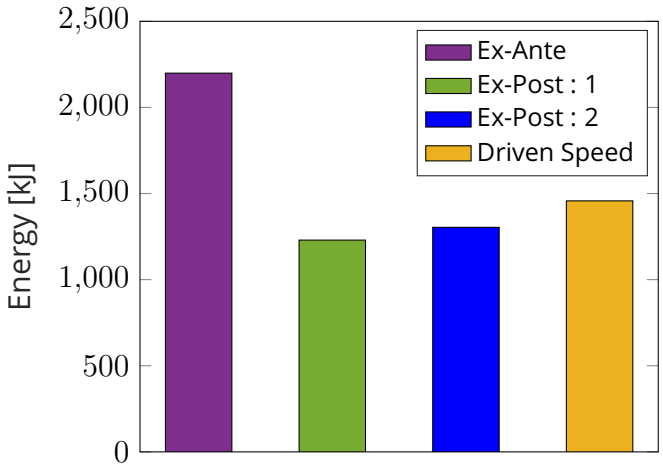

Figure 6.9: This figure shows the energy consumption of the ex-ante, ex-post with traffic queue and signal phase (ex-post:1), ex-post with traffic, traffic queue and signal phase (ex-post:2), and the driven speed profile of Trip 1.

Fig. 6.10a repeats the ex-ante speed profile computed at the start of Trip 1 assuming no traffic, traffic queue and signal phase. Fig. 6.10b shows the ex-post speed profile computed knowing the traffic queue and signal phase but no traffic and Fig. 6.10c shows the ex-post speed profile computed knowing the traffic, traffic queue and signal phase. The four-speed profiles of the other trips are shown in Appendix A.11.

Fig. 6.9 shows the energy consumption of the four speed profile, namely, ex-ante, ex-post with traffic queue and signal phase (ex-post:1), ex-post with traffic, traffic queue and signal phase (ex-post:2), and the driven speed profile. The higher energy consumption of the ex-ante can be attributed to the combination of red

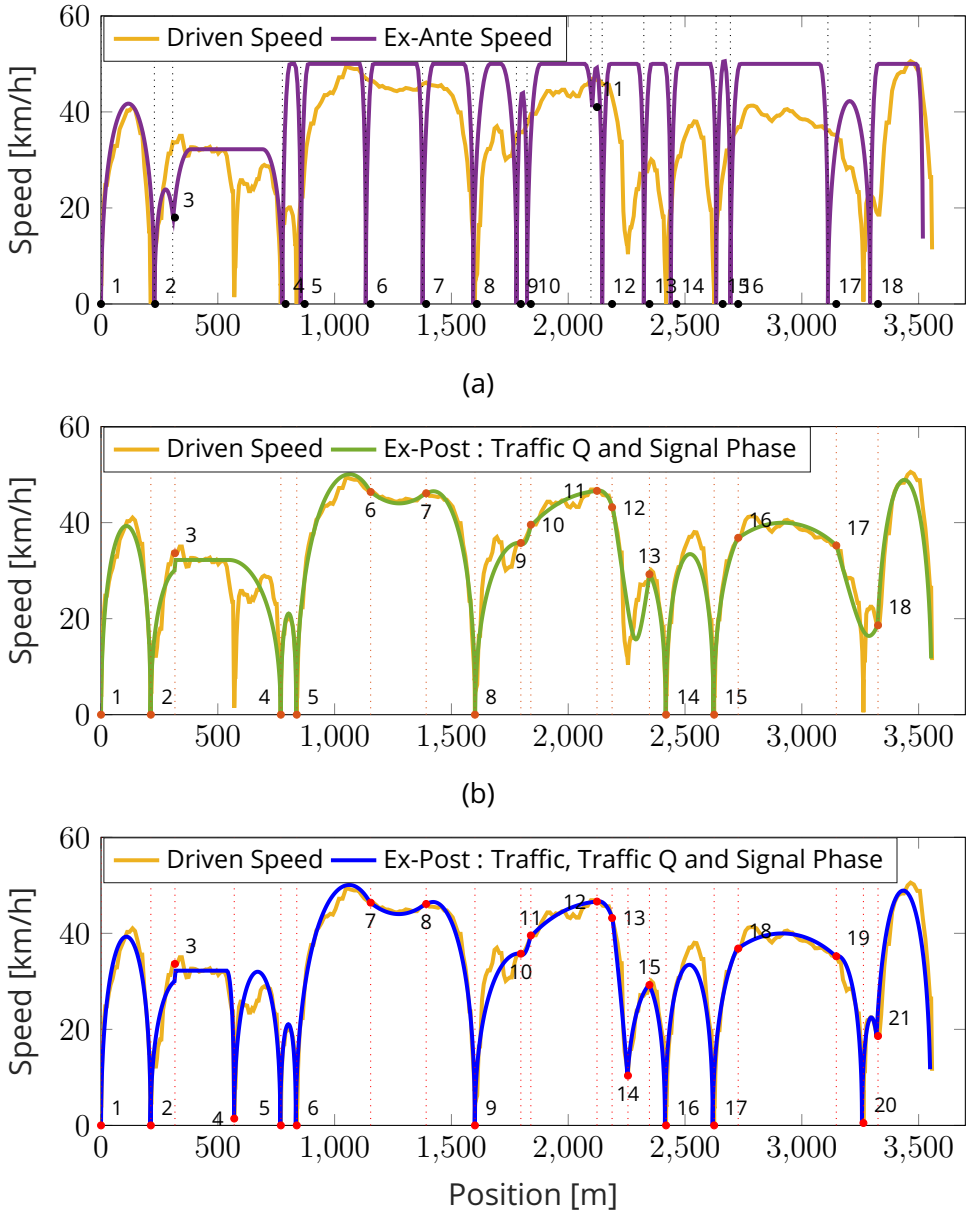

Figure 6.10: Figure showing the ex-ante, ex-post:1, ex-post:2 and the driven speed of Trip 1

signal phase and no traffic assumption. These assumptions cause the vehicle to travel at a higher average speed while stopping and starting at every link. The heavy accelerations and decelerations lead to an increased energy consumption. The increase in energy between the ex-post:1 and 2 indicates the additional accelerations/decelerations due to preceding traffic. If we had access to traffic, traffic

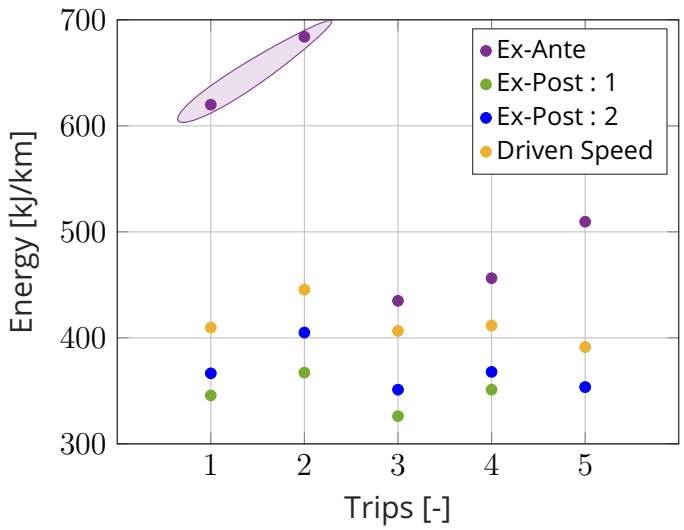

Figure 6.11: Energy Consumption Analysis of the five trips

queue and signal phase information, the ex-post:2 speed profile would have been the optimal ex-ante computed at the start of the trip. The driven profile's increase in consumption with respect to the ex-post:2 can then be attributed to the driver's ability to follow the advised speed.

The energy consumption of all five trips for the four-speed profiles is shown in Fig. 6.11. The energy consumption is computed using the model described in Sect. 2.4 with driven speed logged during the trip. While the model in Sect. 2.4 is for a Nissan Leaf, it still serves as a base for analysing the trends and behavior in energy consumption. It can be observed that each trip has the same trend indicating the effect of pessimistic/worst-case assumption of stopping at every traffic light and the over-optimistic assumption of no traffic. The higher energy consumption in Trips 1 and 2 is due to shorter travel times (or higher average traffic speed) predicted from the *MOBI-Cloud* at the start of the trip. In combination with coming to a stop at every traffic light, satisfying this high average speed requires high accelerations/decelerations, sometimes even beyond the car's physical limit. This, however, is corrected in real-time by the EDOC, when computing the target speed to respect the maximum acceleration limits of the vehicle leading to a lower average speed. It can be noticed from Fig. 6.12, that Trip 1 generally has a higher predicted average speed for many links than Trip 5. Let us consider Trip 1's link 14 which has a predicted average speed slightly above 40 km/h, see Fig. 6.12. The same link has a traffic light at its beginning and at the end, see the predicted final speed in Fig. 6.5b. The ex-ante predicts a speed profile that requires very high acceleration/deceleration, shown in Link 14 of Fig 6.10a, satisfying the average speed slightly above 40 km/h and stopping at the lights. However, the driven and target profile can only satisfy an average speed of 20 km/h (see Fig. 6.12a)

considering the car's maximum acceleration limits.

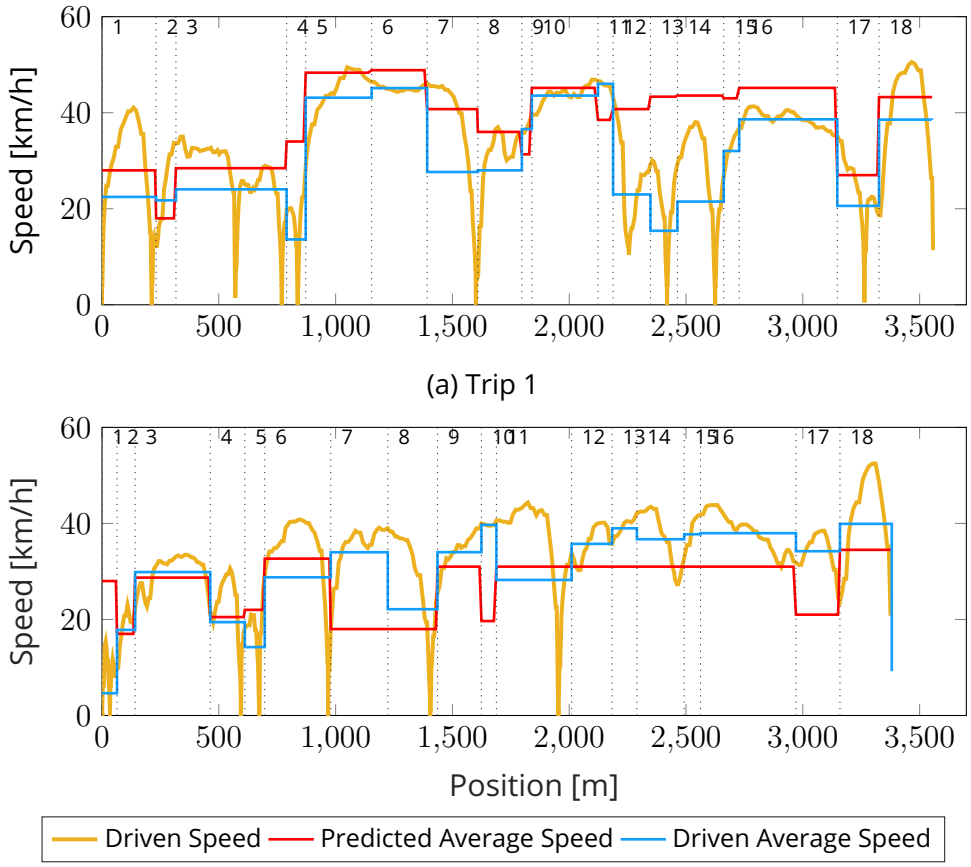

(a) Trip 1

(b) Trip 5

Figure 6.12: Figure showing the predicted and driven average speed of the links for Trip 1 and Trip 5.

6.5 . Conclusion

This chapter discussed the implementation of the ED solutions via a Virtual Assistance System (VAS) in a Renault Zoe. The VAS takes as user input the trip's origin and destination and breaks them into smaller segments called links. The boundary conditions of each of these links are predicted, a priori, under the assumptions of no traffic, no traffic queue and red signal phase at every traffic light. In real-time, the driver is advised a target speed, computed by the EDOC under a shrinking horizon MPC paradigm, to follow on the next time step. The driven profile is analysed a posteriori, to study the impact of the made assumptions and are quantified in terms of energy consumption using ex-post theoretical speed profiles. The ex-ante speed profile for trips 1 and 2 and trips 3, 4 and 5 consume

on average 52.3 % and 15.9 % more than the driven profile, respectively. The worst case assumption of all red signal phases and the over-optimistic assumption of no traffic predicts a speed profile with high accelerations/decelerations and in turn, increased energy consumption for the reference speed (ex-ante). While this is corrected under the MPC framework in real-time, having accurate surrounding information, especially on traffic and signal phase, will reduced the energy gap between predicted and driven speed profile. At the time of writing this thesis, the experimental setup has no perception system. Future works includes the installation of a roof-mount stereoscopic camera perception system. This allows to obtain information on leading vehicle's relative speed and position and the signal phase status of the traffic light within the system's vision.

Bibliography

[1] Antonio Sciarretta and Ardalan Vahidi. Energy-Efficient Driving of Road Vehicles. Springer, 2020.

7 - Conclusion and Perspectives

In this final chapter, the research objectives presented in Chap. 1 are answered by conclusions linked to different chapters of this thesis. Additionally recommendations for future directions in each chapter will be given.

7.1 . Conclusion

The adoption of electric CCAVs designed to maximize energy efficiency can be regarded as an integrated approach to meet the changing trends in the automotive sector. This motivated the development of eco-driving algorithms for CCAVs in different driving scenarios in this thesis. The choice to obtain analytical solutions was driven by real-time implementation and to have insight into ED behavior. For the sake of readability, the research objectives presented in Chap. 1 will be repeated in the following paragraphs. Below each objective, the conclusions of this thesis that address the respective objective are detailed.

Research Objective 1

- To experimentally assess a known baseline Non-Cooperative ED strategy for a single CAV

This objective has been addressed in Chap. 6 of this thesis. The NC-ED baseline algorithm presented in Chap. 2 has been implemented in a Renault Zoe via a Visual Assistance System (VAS). The experimental setup at the time of writing is only equipped with a localization system and does not include a perception system to detect traffic (lead vehicle and signal phase). Experiments were conducted on a route connecting Rueil-Malmaison and Chatou in France. The implementation of the algorithm consists of two major parts. In the first part, the EC algorithm breaks the route into smaller links for a given origin and destination, and computes a reference speed profile for each link. This step is carried out on IFPEN's cloud-based server *MOBI-Cloud* at the trip's start. The reference speed profile is computed under the assumptions of no traffic, no traffic queue and only red signal phase and its $\mathcal{BC}$ are extracted. The second part of the algorithm occurs in real-time under a a shrinking horizon MPC framework. Optimal speed profiles are computed for the vehicle's current link with initial $\mathcal{BC}$ from the measured states (i.e., $x(t)$, $v(t)$) and final $\mathcal{BC}$ from the reference speed (i.e., $D = D_f$, $V = V_f$). The driver is then advised via the VAS to follow the optimal speed for the next second, after which the states are measure again and the optimal speed is re-computed with the new $\mathcal{BC}$. This process is repeated every second until the end of trip.

The driven profile was analysed a posteriori, to study the impact of the made assumptions and they were quantified in terms of energy consumption. The worst

case assumption of all red signal phases and the over-optimistic assumption of no traffic predicts a speed profile with high accelerations/decelerations and in turn, increased energy consumption for the reference speed. While this is corrected under the MPC framework in real-time, having accurate surrounding information, especially on traffic and signal phase, will reduced the energy gap between predicted and driven speed profile.

Research Objectives 2 & 3

- To obtain analytical eco-driving solutions for a fleet of electric CCAVs, with varying levels of cooperation, for platooning and un-signalized intersection scenarios
- To evaluate the influence of the varying levels of cooperation, namely, NC-ED, C-ED, and CC-ED, on fleet energy consumption

The above research objectives have been addressed in chapters 4 and 5. Chapter 4 extended the NC-ED car-following scenario presented in Chap. 2 to a platooning ED scenario. The platoon was modeled as homogeneous with predecessor following topology and eco-driving was cast as an OCP for the NC-ED, C-ED and CC-ED strategy. With electric vehicles as the choice of powertrain, the running cost was chosen as the instantaneous battery power of a single CCAV for the NC-ED and C-ED, and as the sum of all the CCAV's battery power in the platoon for the CC-ED. The boundary conditions required the platoon starting with a certain initial speed and position to cover a fixed distance over within a certain time. Collision avoidance in the platoon was formulated as a state-inequality constraint. The preceding vehicle's motion was predicted using constant acceleration to facilitate analytical solutions. The NC-ED using the instantaneous acceleration and the C-ED using the average of the future accelerations. The OCP problem was solved using PMP and closed form analytical solutions were presented for the three strategies. This chapter also addressed the issue of string stability in a platoon. Theoretical linear stability condition was employed to see if the optimal control inputs of the three cooperative strategies were string stable. This analysis showed us that the NC-ED is only marginally string stable, while C-ED and CC-ED are string stable under certain conditions. Platoons equipped with NC-ED, C-ED and CC-ED strategies were tested in a simulation environment against ACC as a baseline. The performance were evaluated in terms of energy consumption and string length and the results indicated that increasing levels of cooperation improved energy efficiency and compactness of the platoon.

Prediction of preceding vehicle's behaviour plays an important role when following a car as in the car-following and platooning scenarios. The certainty of the prediction affects safety and energy efficiency. To this end in Chap. 3, we proposed two model-based predictors, namely CA-AB and EDM-LOSP, for preceding vehicle's behavior. The proposed predictors were modifications of the already existing

CA and EDM-LOS models. The predictors were implemented in a DP based ED algorithm for a mild hybrid electric vehicle. We performed simulations over 6 real-world routes representing urban and mixed driving scenarios with the developed predictors and the results showed energy savings, especially in urban scenarios with high traffic light or stop sign density.

Chapter 5 addresses ED in an un-signalized urban intersection. With the same objective function as in the platooning scenario, ED was formulated as an OCP for the NC-ED and C-ED strategies. The intersection considered was a four-road, right-angled intersection. The various conflicts that arise in an intersection were transformed into mathematical constraints to be appended to the OCP. The OCP along with the various constraints were solved using PMP to facilitate analytical solutions. The C-ED algorithm has access to more accurate information and much earlier compared to the NC-ED. The two algorithms were tested for energy efficiency against IDM as a baseline. Simulations were performed for various traffic flow rates and the results indicated the best performance for the Cooperative ED.

7.2 . Future Perspectives

This section describes some possible recommendations for future works in chapters 3 to 6.

Chapter 3 This chapter has been devoted to predicting the behavior of the preceding vehicle to incorporate into an OCP. The two proposed models, CA-B and EDM-LOS, were only validated through numerical simulations. An experimental validation through on a real car (mHEV) would provide better insight on the performance of the predictors. Another direction for future works would be the online parameter estimation, in particular δ and θ, of the EDM-LOSP using tools like extended Kalman filter. Incorporating the timing information from the traffic lights could also improve prediction accuracy.

Chapter 4 This chapter assumes platoons to be homogeneous and without any communication delays. The model could be extended to consider heterogeneous CCAVs and study the effect of delays on string stability. A future direction, that is already under way at IFPEN, is the experimental validation via a robotic testbed. Before CCAVs are deployed en masse on the road, a thorough performance evaluation from numerical to real-world testing is required. Scaled-down robotic testbeds offer flexibility on quick and repeatable tests that go one step beyond simulations.

Chapter 5 The intersection scenario in Chap. 5 opens up several directions for future works. The first one includes generalization of the algorithm to suit all types of intersection. Secondly, the scheduling and path planning problem, which is currently assumed given, can be addressed. The CC-ED remains an open problem

that has not been dealt with, in this thesis. Finally, an experimental validation on a robotic test bed is planned for the future.

Chapter 6 Future works in Chap. 6, include the implementation of a stereoscopic camera perception system to obtain information on leading vehicle's relative speed and position and the signal phase status of the traffic light within the system's vision. The installation of the camera system is currently ongoing and the testing of the NC-ED car-following algorithm will follow.

A - Appendix

A.1 . Pontryagin's Minimium Principle

Let bold face $\mathbf{x}$ and $\mathbf{u}$ represent a vector of n-state and q-control variables, respectively. PMP is based on the definition of the Hamiltonian function that is formed as

$$H(\mathbf{x}, \mathbf{u}, t) = L(\mathbf{x}, \mathbf{u}, t) + \lambda f(\mathbf{x}, \mathbf{u}, t) \tag{A.1}$$

where $\lambda \subset \mathbb{R}^n$ is a vector of costates, having the same dimension n as the state vector. If state constraints are not present, the necessary conditions for the optimality of a control trajectory $\mathbf{u}(t), t \in [0, t_f]$ include: the state dynamics

$$\dot{\mathbf{x}}(t) = \frac{\partial H}{\partial \lambda}(\mathbf{x}(t), \mathbf{u}(t), t) \tag{A.2}$$

with the boundary conditions

$$\mathbf{x}(0) = \mathbf{x}_i, \quad x_j\left(t_f\right) = x_{j,f}, \quad j = 1, \ldots, q \tag{A.3}$$

the costate dynamics (Euler-Lagrange equations)

$$\dot{\lambda}(t) = -\frac{\partial H}{\partial \mathbf{x}} \tag{A.4}$$

with the transversality conditions and the Hamiltonian minimization condition of the minimum principle

$$\mathbf{u}(t) = \arg \min_{u \in U(\mathbf{x}, t)} H(\mathbf{x}(t), u, t). \tag{A.5}$$

This $2n$-dimensional system of coupled differential equations forms a two-point boundary value problem (TPBVP), since n boundary conditions are given at the initial time and the other n values at the final time. Of these latter values, q concern state variables and the remaining $n - q$ concern costate variables.

A.2 . Indirect Adjoining Method

When the problem presents pure state inequality constraints of the form $g(\mathbf{x}(t), t) \leq 0$, the indirect adjoining method can be used. Consider the case with $\ell = 1$ (just one such constraint). If $g(\mathbf{x}(t), t)$ is of the p th order, that is, it is differentiated p times with respect to time until the control variable $\mathbf{u}$ explicitly appears, then the term $g^{(p)}(\mathbf{x}, \mathbf{u}, t)$ is adjoined to the Hamiltonian with a multiplier η, to form the Lagrangian

$$\mathcal{L}(\mathbf{x}(t), \mathbf{u}(t), t) \triangleq H(\mathbf{x}(t), \mathbf{u}(t), t) + \eta g^{(p)}(\mathbf{x}(t), \mathbf{u}(t), t). \tag{A.6}$$

In this case the necessary conditions for a control trajectory to be optimal are still eqs. (A.2) to (A.5), with the Lagrangian replacing the Hamiltonian, together with the jump conditions at times at which state constraints become active (entry or contact times). The jump conditions derive from imposing that $\left[g^{(0)}(\theta), \ldots, g^{(p-1)}(\theta)\right] = 0$ and treating these tangency conditions as interior point constraints that are adjoined to the Lagrangian through the additional multipliers π 's.

$$\begin{aligned} \lambda\left(\theta^{-}\right) &= \lambda\left(\theta^{+}\right) + \sum_{j=0}^{p-1} \pi_j \frac{\partial g^{(j)}}{\partial \mathbf{x}}(\mathbf{x}(\theta), \theta), \\ H\left(\theta^{-}\right) &= H\left(\theta^{+}\right) - \sum_{j=0}^{p-1} \pi_j \frac{\partial g^{(j)}}{\partial t}(\mathbf{x}(\theta), \theta), \end{aligned} \tag{A.7}$$

well as the complementary slackness conditions

$$\eta(t) g(\mathbf{x}(t), t) = 0, \quad (-1)^j \eta^{(j)}(t) \geq 0, \quad j = 0, \ldots, p, \tag{A.8}$$

and

$$\pi_j \geq 0, \quad \pi_j g(\mathbf{x}(\theta), \theta) = 0, \quad j = 0, \ldots, p-1. \tag{A.9}$$

For the special yet common case of first-order constraints ($p = 1$), (A.8) reduces o $\eta(t) g(\mathbf{x}(t), t) = 0, \eta(t) \geq 0, \dot{\eta}(t) \leq 0$ with $\eta(t)$ as an additional unknown to be determined. These conditions mean that when the constraint is not active $(g(\mathbf{x}(t), t) < 0)$, then $\eta(t)$ is set to zero. When the constraint is active $(g(\mathbf{x}(t), t) = 0), \eta(t)$ must be positive but unknown. The condition $g(\cdot) = 0$ provides the additional equation necessary in this case to determine the newly added unknown η. Equation A.9 holds for the single unknown multiplier π_0. In summary, inequality constraints introduce additional unknowns that have to be determined as well, and additional conditions.

A.3 . Proof of CF ($a_0^l < 0$) in EDM-LOSP is equivalent to CA

Following, a proof is given that the CF ($a_0^l < 0$) in EDM-LOSP is equivalent to a constant acceleration prediction. The proof is given for the predictor equations in continuous time, but the same result holds for the discrete system. Given the current instantaneous speed v_0^l and acceleration a_0^l, let $\hat{x}^l(t)$, $\hat{v}^l(t)$, be the lead vehicle position and speed, respectively, where:

$$\frac{d\hat{x}^l}{dt} = \hat{v}^l(t), \qquad \hat{x}^l(0) = 0. \tag{A.10}$$

The stop mode in EDM-LOSP is then given by:

$$\begin{aligned} \hat{a}^l(t) = \frac{d\hat{v}^l}{dt} &= -\frac{1}{|a_0^l|} \left(\frac{\hat{v}^l(t)^2}{2\Delta x(t)} \right)^2 = -\frac{a_{kin}(t)^2}{|a_0^l|} \\ &= -a_{kin}(t) \left(\frac{a_{kin}(t)}{|a_0^l|} \right), \quad \hat{v}^l(0) = v_0^l, \end{aligned} \tag{A.11}$$

where $\Delta x(t)$ is the distance of the lead vehicle from the next predicted stop.

Theorem 1. *If* $\Delta x(t) := \frac{{v_0^l}^2}{2|a_0^l|} - \hat{x}^l(t)$, *then* $\hat{a}^l(t) = -|a_0^l|$

Proof: The proof proceeds by showing that:

1. $a_{kin}(t) = |a_0^l|$, is an equilibrium point for the acceleration.
2. By the definition of $\Delta x(t)$, the equilibrium is attained at $t = 0$ and $\hat{a}^l(t) = -|a_0^l|$

Let $a_{kin}(t) = \frac{\hat{v}^l(t)^2}{2\Delta x(t)}$, then:

$$\begin{aligned} \frac{da_{kin}}{dt} &= \frac{4\hat{v}^l(t)\frac{d\hat{v}^l}{dt}\Delta x(t) - 2\hat{v}^l(t)^2\frac{d\Delta x}{dt}}{4\Delta x(t)^2} \\ &= \frac{\hat{v}^l(t)}{\Delta x(t)}\left(\frac{a_{kin}(t)}{|a_0|}\right)(|a_0| - a_{kin}(t))\,. \end{aligned} \tag{A.12}$$

Hence $a_{kin}(0) = |a_0^l|$ entails that a_{kin} remains constant. Now, from the definition of Δx it follows $\Delta x(0) = \frac{{v_0^l}^2}{2|a_0^l|}$. By substitution in the expression for a_{kin} and recalling the initial condition on $\hat{v}^l$ it can be shown:

$$a_{kin}(0) = \frac{\hat{v}^l(0)^2}{2\Delta x(0)} = \frac{{v_0^l}^2}{2\left(\frac{{v_0^l}^2}{2|a_0^l|}\right)} = \left|a_0^l\right| \quad \rightarrow \quad \hat{a}(t) = \frac{d\hat{v}^l}{dt} = -\frac{a_{kin}(t)^2}{|a_0^l|} = -\left|a_0^l\right|. \tag{A.13}$$

A.4 . Six lead vehicle profiles considered for simulation

The six real-world lead vehicle's speed profiles considered for simulation are shown in Fig. A.1.

A.5 . String Stability Transfer Function of C-EDOC

The derivation of the transfer function $\mathcal{G}_{c,i}$ is detailed here.
Laplace transform of a average operator is given by,

$$\begin{aligned} \tilde{a}_{i-1} &= \frac{1}{L}\int_0^{t+L} a_{i-1}\, d\tau \\ \tilde{a}_{i-1} &= \frac{1}{L}\left(\int_0^{t+L} a_{i-1}\, d\tau - \int_0^{t} a_{i-1}\, d\tau\right) \\ \tilde{a}_{i-1}(s) &= \frac{1}{L}\left(\frac{e^{sL}\mathcal{L}(a_{i-1}(\tau))}{s} - \frac{\mathcal{L}(a_{i-1}(\tau))}{s}\right), \\ \tilde{a}_{i-1}(s) &= \frac{e^{sL}-1}{sL}\mathcal{L}(a_{i-1}(\tau)) \end{aligned} \tag{A.14}$$

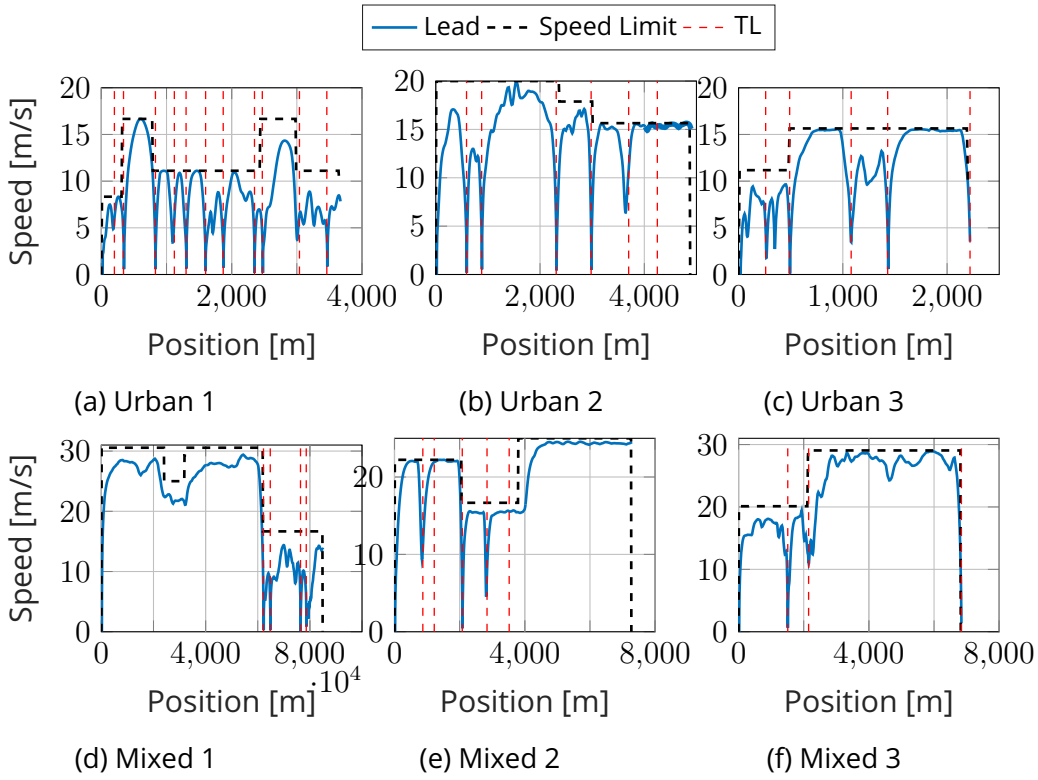

Figure A.1: The six drive cycles considered for the lead vehicle

The error dynamics of $\ddot{\tilde{\xi}}_{i-1}$ is given by

$$\dddot{\tilde{\xi}}_{i-1} = \tilde{a}_{i-2} - \tilde{a}_{i-1} \tag{A.15}$$

Taking Laplace transform and substituting $\tilde{a}_{i-1}(s)$ gives

$$\begin{aligned} \ddot{\tilde{\xi}}_{i-1}(s) &= \frac{e^{sL}-1}{sL}\left(\mathcal{L}(a_{i-2}(\tau)) - \mathcal{L}(a_{i-1}(\tau))\right), \\ \dddot{\tilde{\xi}}_{i-1}(s) &= \frac{e^{sL}-1}{sL}\left(\mathcal{L}(\dddot{\tilde{\xi}}_{i-1}(\tau))\right). \end{aligned} \tag{A.16}$$

Taking Laplace transform and employing $\dddot{\tilde{\xi}}_{i-1}(s)$ in

$$\ddot{\xi}_i + (f_{\dot{\xi}} - f_v)\dot{\xi}_i + f_\xi \xi_i = f_a \ddot{\tilde{\xi}}_{i-1} + f_{\dot{\xi}}\dot{\xi}_{i-1} + f_\xi \xi_{i-1} \tag{A.17}$$

we obtain the string stability transfer function,

$$\mathcal{G}_{i,c}(s) = \frac{\xi_i}{\xi_{i-1}} = \frac{(f_a/L(e^{(sL)}-1) + f_{\dot{\xi}})s + f_\xi}{s^2 + (f_{\dot{\xi}} - f_v)s + f_\xi} \tag{A.18}$$

A.6 . Distribution of the Boundary Conditions considered

The distributions of the states z_i and boundary condition V_i used for the numerical evaluation of string stability conditions in Sect. 4.6.2.4 is shown in Fig. A.2. The distribution has a sample number of forty following a normal distribution around equilibrium.

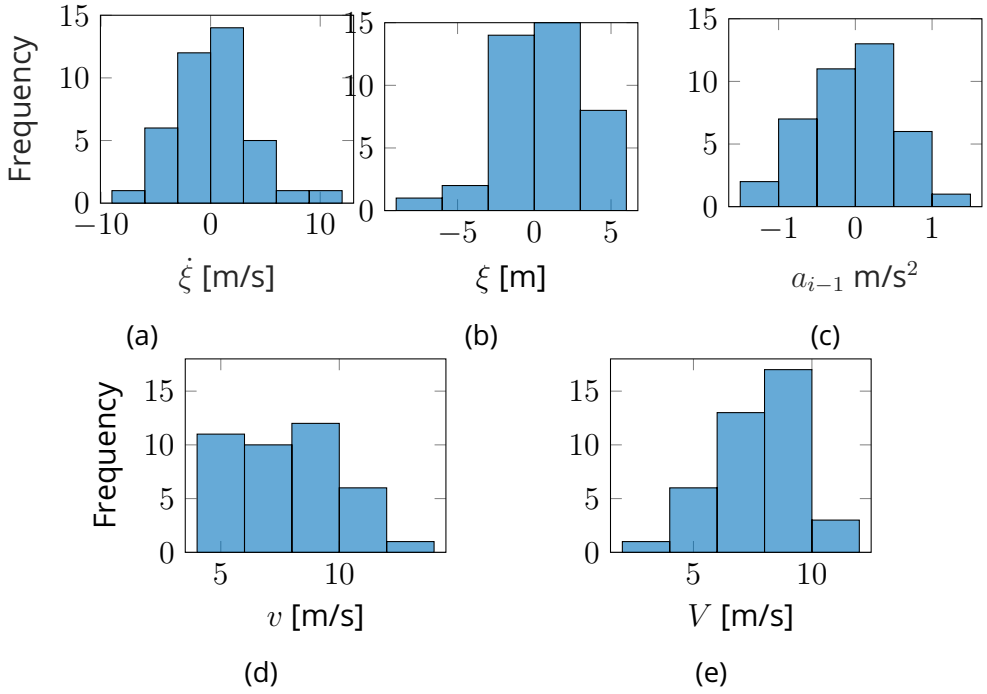

Figure A.2: The distribution of the state z_i and final speed V_i

A.7 . The terms ξ_{min} and k_1

The local minimum, ξ_{min}, when $w_i(t) \leq 0$ and $\Delta\xi_i \leq 0$ and the proof that local minimum occurs with the interval $[0, T_i]$ is given in this section.

Local minimum ξ_{min} The local minimum for the case $w_i(t) \leq 0$ and $\Delta\xi_i \leq 0$ is given by

$$\xi_{min} = \frac{A(\xi_i(t), w_i(t), \Delta\xi_i, \xi_{i,f})}{B(\Delta\xi_i, w_i(t))} , \tag{A.19}$$

where

$$\begin{aligned} A &= 216\xi_i(t)|\Delta\xi_i|^3 - 4T_i^4|w_i(t)|^4 + 20T_i^3\xi_i(t)|w_i(t)|^3 \\ &\quad + 7T_i^3\xi_{i,f}|w_i(t)|^3 + 324T_i\xi_i(t)|\Delta\xi_i|^2|w_i(t)| \\ &\quad - 36T_i^2|\Delta\xi_i|^2|w_i(t)|^2 - 24T_i^3|\Delta\xi_i||w_i(t)|^3 \\ &\quad + 144T_i^2\xi_i(t)|\Delta\xi_i||w_i(t)|^2 + 18T_i^2\xi_{i,f}|\Delta\xi_i||w_i(t)|^2 , \\ B &= 27\left(2|\Delta\xi_i| + T_i|w_i(t)|\right)^3 \end{aligned} \tag{A.20}$$

The condition $\xi_{min} \geq 0$ ensures $\xi_i(k) \geq 0, \forall\ k \in [0, T_i]$, when $w_i(t) \leq 0$ and $\Delta\xi_i \leq 0$

Proof that k_1 lies in the interval $[0, T_i]$ Imposing $k_1 \leq T_i$ one obtains

$$\begin{aligned}
&\frac{T_i\,|w_i(t)|}{3\,|w_i(t)| + \frac{6|\Delta\xi_i|}{T_i}} \leq T_i,\\
&T_i\,|w_i(t)| \leq 3T_i\,|w_i(t)| + 6|\Delta\xi_i|,\\
&2T_i\,|w_i(t)| + 6|\Delta\xi_i| \geq 0.
\end{aligned}$$

The latter inequality is always satisfied for non-negative values for T_i, proving that k_1 lies in the interval $[0, T_i]$

A.8 . Merging Constraint

This section describes the solution to the minimization problem formulated in (5.35) to obtain the free parameter v_{im} and the unknown contact time θ_i. Using Lagrange multipliers method, the Lagrangian is formulated as,

$$L = E_{bf} + \lambda f_{m\theta} \tag{A.21}$$

where λ is the Lagrange multiplier. At the constrained optimum the necessary conditions for optimum are given as,

$$\frac{\partial E_{bf}}{\partial v_{im}} + \lambda \frac{\partial f_{m\theta}}{\partial v_{im}} = 0 \tag{A.22a}$$

$$\frac{\partial E_{bf}}{\partial \theta_i} + \lambda \frac{\partial f_{m\theta}}{\partial \theta_i} = 0 \tag{A.22b}$$

In addition to the above equations, $f_{m\theta}$ (5.34), must hold. The three equations, (A.22a),(A.22b), and (5.34) are solved using *fsolve* in MATLAB.

A.9 . Diverging Constraint

This section describes the solution to the minimization problem formulated in (5.28) to obtain the two free parameters v_{id} and x_{id} and the third unknown contact time θ_i. Using the Lagrange multipliers method, the Lagrangian is formulated as,

$$L = E_{bf} + \lambda f_{d\theta} \tag{A.23}$$

where λ is the Lagrange multiplier. At the constrained optimum, the necessary conditions for optimum are given as,

$$\frac{\partial E_{bf}}{\partial v_{id}} + \lambda \frac{\partial f_{d\theta}}{\partial v_{id}} = 0 \tag{A.24a}$$

$$\frac{\partial E_{bf}}{\partial x_{id}} + \lambda \frac{\partial f_{d\theta}}{\partial x_{id}} = 0 \tag{A.24b}$$

$$\frac{\partial E_{bf}}{\partial \theta_i} + \lambda \frac{\partial f_{d\theta}}{\partial \theta_i} = 0 \tag{A.24c}$$

In addition to the above equations, $f_{d\theta}$ (5.27), must hold. The four equations, (A.24a),(A.24b), (A.24c) and (5.27) are solved using *fsolve* in MATLAB.

A.10 . Possible Conflicts, its identification and optimal solution computation in an Intersection

This section describes the possible conflicts a CCAV can face inside an intersection, how to identify them and how its an optimal solution is chosen for that conflict type.

A.10.1 . Combination of possible conflicts

Section 5.2.2 described the four fundamental conflicts in a traffic conflict analysis. When a CCAV $i \in \mathcal{N}(t)$, with only one CCAV in $\mathcal{H}_i(t)$, it can face either one of the four conflicts or none of them. However, in reality, there are often more CCAVs in $\mathcal{H}_i(t)$ and hence a CCAV $i \in \mathcal{N}(t)$ can face none, one or a combination of the four conflicts. This section identifies all the possible combinations of the four conflicts that a CCAV $i \in \mathcal{N}(t)$ could face. To this end, we analyze the conflicts in the entry, IZ, and exit lanes.

Let's consider where CCAV $i \in \mathcal{N}(t)$ enters the intersection through the left lane[1] and goes straight. Under the assumptions of $\mathcal{CF}^i(t) = \varnothing$ and only one CCAV in $\mathcal{CC}^i(t)$, its maximum constraining case (i.e., the maximum possible combination of conflicts) is the presence of a conflict in the entry (diverging), IZ (crossing), and exit lanes (merging). Such a scenario is shown in Fig. A.3a, labeled S^0_{max}. CCAV i's higher prioritized CCAVs are given as $\mathcal{H}^i(t) = (d, e, c)$, and its conflicting sets are given as $\mathcal{DC}^i(t) = (d)$, $\mathcal{CC}^i(t) = (c)$, $\mathcal{CF}^i(t) = \varnothing$ and $\mathcal{MC}^i(t) = (e)$. A qualitative example of scenario S^0_{max}'s translation into constraints on the position-time plane is shown in Fig A.3b. While S^0_{max} represents the maximum conflicting combination under the above-stated assumptions, the other possible conflicts are detailed in Table A.1. Logical 1 and 0 indicate the presence or absence of diverging, crossing, or merging conflict. All conflicts under the assumptions of $\mathcal{CF}^i(t) = \varnothing$ and only one CCAV in $\mathcal{CC}^i(t)$ are categorically labeled S^0.

We now relax one of the above assumptions to consider the presence of a CCAV $p \in \mathcal{CF}^i(t)$. Suppose both the sequences $\mathcal{DC}^i(t)$ and $\mathcal{CF}^i(t)$ have higher conflicting CCAVs. In that case, CAV i conflicts only with its immediately preceding vehicle in the entry lane (i.e., CCAV with the lowest priority in $|\mathcal{DC}^i(t) \cup \mathcal{CF}^i(t)|$). It should be noted that CAV i can face a diverging conflict or a car-following conflict, not both simultaneously. Let k and q represent the crossing order such

[1] The same procedure applies to any other entry lane.

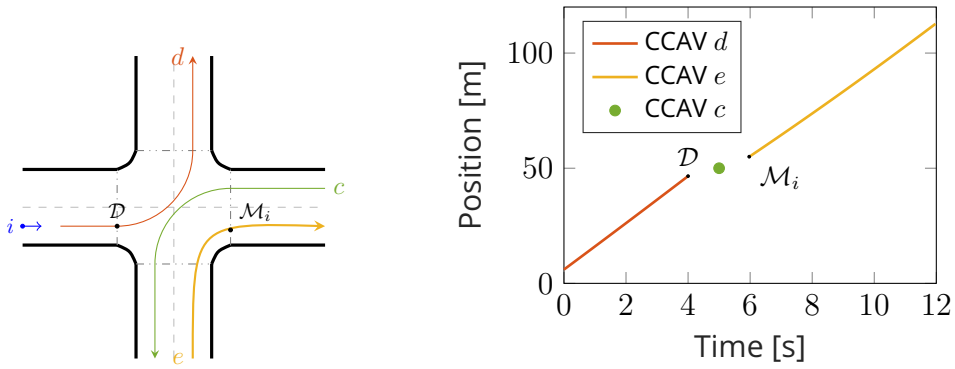

(a) (b)

Figure A.3: The paths of the CCAVs (a) for scenario S^0_{max} and constraint on the CCAV i's $x-t$ plane (b).

Table A.1: Conflicts in S^0

S^0		
Diverging	Crossing	Merging
0	0	0
1	0	0
0	1	0
0	0	1
1	1	0
1	0	1
0	1	1
1	1	1

that $\mathcal{CO}_k(t) = e$ and $\mathcal{CO}_q(t) = p$. Assuming CCAV $e \in \mathcal{MC}^i(t)$ has higher priority than CCAV p (i.e., $k < e$), then the maximum constraining case (S^1_{max}) for CCAV i is a car-following conflict and a crossing conflict, as shown in Fig. A.4a. A qualitative example of scenario S^1_{max}'s translation into constraints on the position-time plane is shown in Fig A.4b. While S^1_{max} represents the maximum conflicting combination under the above-stated assumptions, the other possible conflicts are detailed in Table A.2. Logical 1 and 0 indicate the presence or absence of a car-following or crossing conflict. All conflicts under the assumptions of $k < e$ and only one CCAV in $\mathcal{CC}^i(t)$ are categorically labeled S^1.

Assuming CCAV $e \in \mathcal{MC}^i(t)$ has lower priority than CCAV p (i.e., $k > e$), then the maximum constraining case (S^2_{max}) for CCAV i is a car-following, crossing and a merging conflict, as shown in Fig. A.5a. A qualitative example of scenario S^2_{max}'s translation into constraints on the position-time plane is shown in Fig A.5b. While S^2_{max} represents the maximum conflicting combination, the other possible conflicts are detailed in Table A.3. Logical 1 and 0 indicate the presence or absence of a

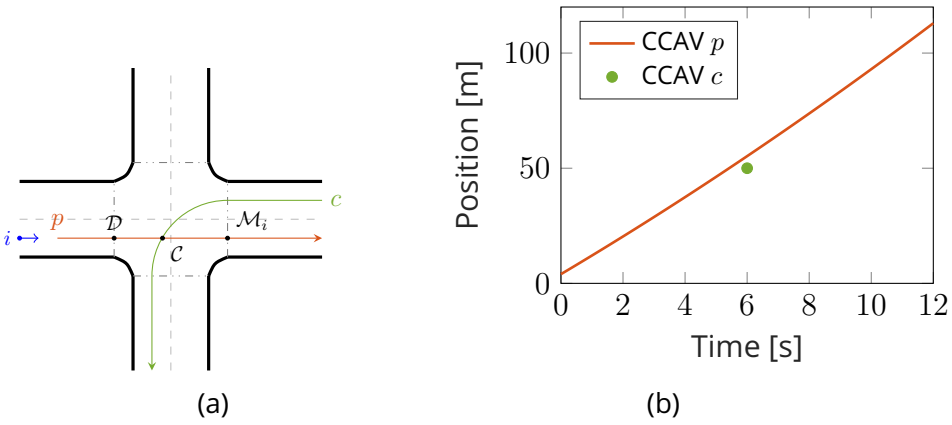

(a) (b)

Figure A.4: The paths of the CCAVs (a) for scenario S^1_{max} and constraint on the CCAV i's $x-t$ plane (b).

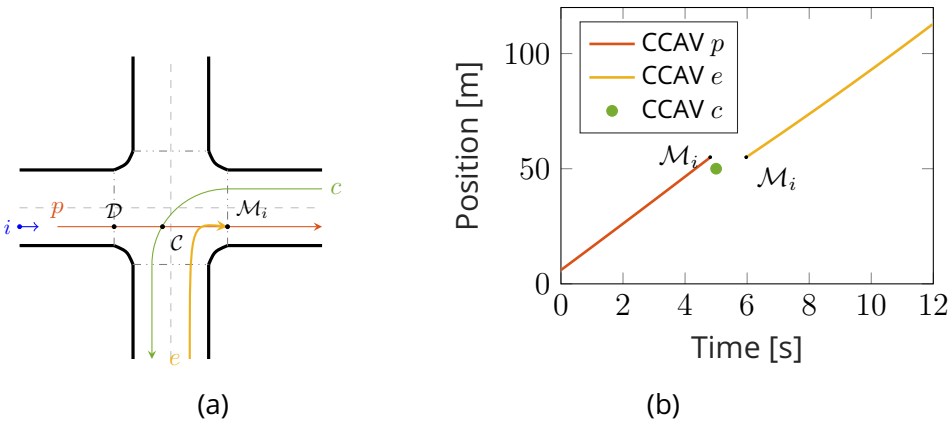

(a) (b)

Figure A.5: The paths of the CCAVs (a) for scenario S^2_{max} and constraint on the CCAV i's $x-t$ plane (b).

car-following, crossing, or merging conflict. All conflicts under the assumptions of $k > e$ and only one CCAV in $\mathcal{CC}^i(t)$ are categorically labeled S^2.

Remark 3. *In certain instances, the combinations of conflicts identified in S^0, S^1, and S^2 are repeated. For example, the conflict combination 10 in S^1 and 100 in S^2 indicates that a CCAV $i \in \mathcal{N}(t)$ is subject to the car-following conflict in both scenarios.*

Remark 4. *The conflicts combination are independent of NC-ED or C-ED.*

All the above possible conflicts are identified under the assumption that there is only one CCAV in $\mathcal{CC}^i(t)$. If there are several higher prioritized CCAVs in $\mathcal{CC}^i(t)$, the CCAV that causes the maximum violation of the unconstrained solution of CCAV i, a method inspired from [1], is the conflicting CCAV.

Table A.2: Conflicts in S^1

S^1	
Car-Following	Crossing
0	0
1	0
0	1
1	1

Table A.3: Conflicts in S^2

S^2		
Car-Following	Crossing	Merging
0	0	0
1	0	0
0	1	0
0	0	1
1	1	0
1	0	1
0	1	1
1	1	1

A.10.2 . Identification of Conflicts

This section expands a portion of algorithm 1 presented in Sect 5.3.3 on how any CCAV $i \in \mathcal{N}(t)$ computes its conflicting sets and then identifies which conflict, among the conflicts presented in Sect. A.10.1, it faces. Algorithm 2 describes the process for a CCAV $i\ in\mathcal{N}(t)$ in identifying conflicts with $x_i(t) \leq D_{vis}$ for NC-ED and algorithm 3 describes the process when $x_i(t) > D_{vis}$. The C-ED follows the same steps as in algorithm 3 from $x_i(0)$.

Algorithm 2 Conflict identification NC-ED with $x_i < D_{vis}$

Initialize CF = 0, DC = 0
$\mathcal{H}^i = \mathcal{CO}_1 : \mathcal{CO}_{j-1}$
Conflicting sets ▷ Computed using the entry lane and direction of CCAVs in $\mathcal{H}^i$
for $q \leftarrow 1$ to length ($\mathcal{H}^i$) **do**
    if $\mathcal{H}^i_q \in \mathcal{CF}^i$ **then**
        CF$_{ccav}$ = $\mathcal{H}^i_q$
        CF$_{priority}$ = q
    end if
    if $\mathcal{H}^i_q \in \mathcal{DC}^i$ **then**
        DC$_{ccav}$= $\mathcal{H}^i_q$
        DC$_{priority}$ = q
    end if
    if CF$_{ccav} \neq \varnothing$ AND DC$_{ccav} \neq \varnothing$ **then**
        maxP = max(CF$_{priority}$,DC$_{priority}$)
        if $\mathcal{H}^i_{maxP}$ == DC$_{ccav}$ **then**
            DC = 1
            DC$_{ccav}$ = $\mathcal{H}^i_{maxP}$
        else
            CF = 1
            CF$_{ccav}$ = $\mathcal{H}^i_{maxP}$
        end if
    end if
end for
if CF == 1 **then**
    Conflict falls in S^1
    Conflict = CF
else
    Conflict falls in S^0
    Conflict = DC
end if

Algorithm 3 Conflict identification for C-ED and NC-ED with $x_i > D_{vis}$

Initialize CF = 0, DC = 0, MC = 0, CC = 0, MC_M = 0
$\mathcal{H}^i = \mathcal{CO}_1 : \mathcal{CO}_{j-1}$
Conflicting sets ▷ Computed using entry lane and direction of CCAVs in $\mathcal{H}^i$
for $q \leftarrow 1$ to length ($\mathcal{H}^i$) **do**
    if $\mathcal{H}^i_q \in \mathcal{CF}^i$ **then**
        CF_{ccav} = $\mathcal{H}^i_q$
        $\text{CF}_{priority}$ = q
    end if
    if $\mathcal{H}^i_q \in \mathcal{DC}^i$ **then**
        DC_{ccav}= $\mathcal{H}^i_q$
        $\text{DC}_{priority}$ = q
    end if
    if $\mathcal{H}^i_q \in \mathcal{CC}^i$ **then**
        CC_{ccav} = $\mathcal{H}^i_q$
        CC = 1
    end if
    if $\mathcal{H}^i_q \in \mathcal{MC}^i$ **then**
        MC_{ccav} = $\mathcal{H}^i_q$
        $\text{MC}_{priority}$ = q
        MC = 1
    end if
    if $\text{CF}_{ccav} \neq \varnothing$ AND $\text{CF}_{ccav} \neq \varnothing$ **then**
        maxP = max($\text{CF}_{priority}$,$\text{DC}_{priority}$)
        if $\mathcal{H}^i_{maxP}$ == DC_{ccav} **then**
            DC = 1
            DC_{ccav} = $\mathcal{H}^i_{maxP}$
        end if
        if $\mathcal{H}^i_{maxP}$ == CF_{ccav} **then**
            if MC = 1 **then**
                if ($\mathcal{H}^i_{maxP}$ == MC_{ccav}) OR ($\text{MC}_{priority}$ > maxP) **then**
                    CF = 1
                    MC = 0
                    CF_{ccav} = $\mathcal{H}^i_{maxP}$
                else if ($\text{MC}_{priority}$ < maxP) **then**
                    MC_M = 1
                    CF = 1
                else if MC = 0 **then**
                    CF = 1
                    CF_{ccav} = $\mathcal{H}^i_{maxP}$
                end if
            end if
        end if
    end if
end for

45: **if** $\text{MC}_M == 1$ **then**
46: Conflict falls in S^2
47: Conflict = [CF CC MC_M]
48: **else if** CF == 1 **then**
49: Conflict falls in S^1
50: Conflict = [CF CC]
51: **else**
52: Conflict falls in S^0
53: Conflict = [DC CC MC]
54: **end if**

A.10.3 . Optimal Solution Computation

Once the type of conflict is identified, the states are measured or communicated from the conflicting CCAVS, be it, CF_{ccav}, MC_{ccav}, DC_{ccav}, or CC_{ccav}. With this information, CCAV $i \in \mathcal{N}(t)$ evaluates all possible solutions for a conflict type and applies the one with the least energy consumption satisfying all the constraints. General solutions for all types are conflicts are computed a priori as detailed in remark. 2. The optimal solution consists of two or more segments depending on the constraint. For instance, conflict type $S^0 - 110$ has 4 possible solutions, i.e., unconstrained solution has one segment, solution satisfying only diverging conflict ($S^0 - 100$) has three segments, solution satisfying only crossing conflict $S^0 - 010$ has two segments and the solution satisfying both diverging and crossing conflict $S^0 - 110$ has four segments. Figure A.6 shows the four possible solutions. It can be noticed that the solution in Fig. A.6a and Fig. A.6c violates the diverging conflict. The point constraint by CCAV c is violated only if the solution passes before the constraint. Solutions in figures A.6b and A.6d satisfy both the constraints. However, solution in Fig. A.6b consumes the least energy[2]. Hence the optimal solution for CCAV i facing the conflict $S^0 - 110$ is the solution given in Fig. A.6b. A pseudo-algorithm of the process is shown in Algorithm 4.

Remark 5. *Once a solution z with the least energy consumption satisfying all the position- state constraints are obtained, the turning speed constraint is checked. If the safe turning speed is violated, then the z is not the optimal solution. The process of evaluating all possible solutions is repeated. However, the possible solutions are now obtained by splitting the solution presented in Sect. 5.3.2.2 into segments, such that it satisfies the position-constraints.*

[2]The less constrained a solution is, the lesser is the energy consumption

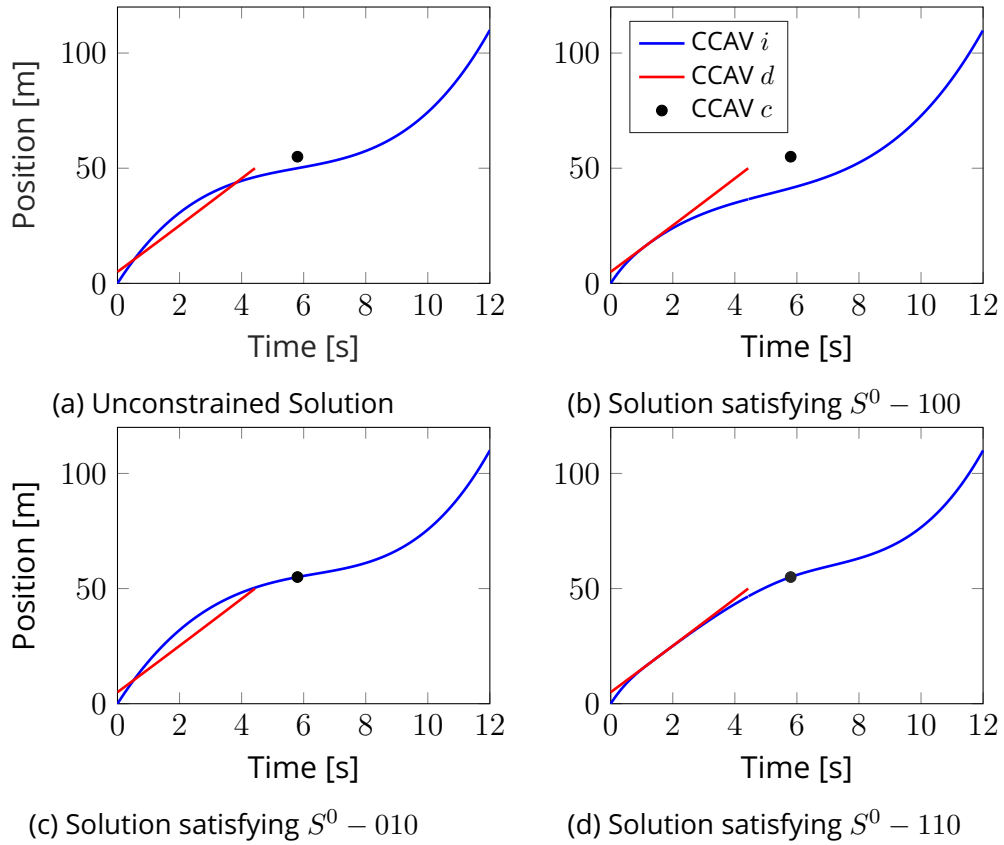

(a) Unconstrained Solution

(b) Solution satisfying $S^0 - 100$

(c) Solution satisfying $S^0 - 010$

(d) Solution satisfying $S^0 - 110$

Figure A.6: Figure showing all the four possible solutions for conflict $S^0 - 110$

Algorithm 4 Optimal Solution Computation

Require: Identified Conflict type
Require: Possible solutions for the conflict type
Energy* $\leftarrow \infty$
Let s be the number of possible solutions
for $z \leftarrow 1$ to s **do**
    if Solution z satisfies all constraints **then**
        Compute E_{bf}
        if $E_{bf} <$ Energy* **then**
            Energy* $\leftarrow \infty$
            Optimal Solution $\leftarrow z$
        end if
    end if
end for

A.11 . Speed Profiles from Experiments

The speed profiles from experiments for trips 2 to 5 are shown here.

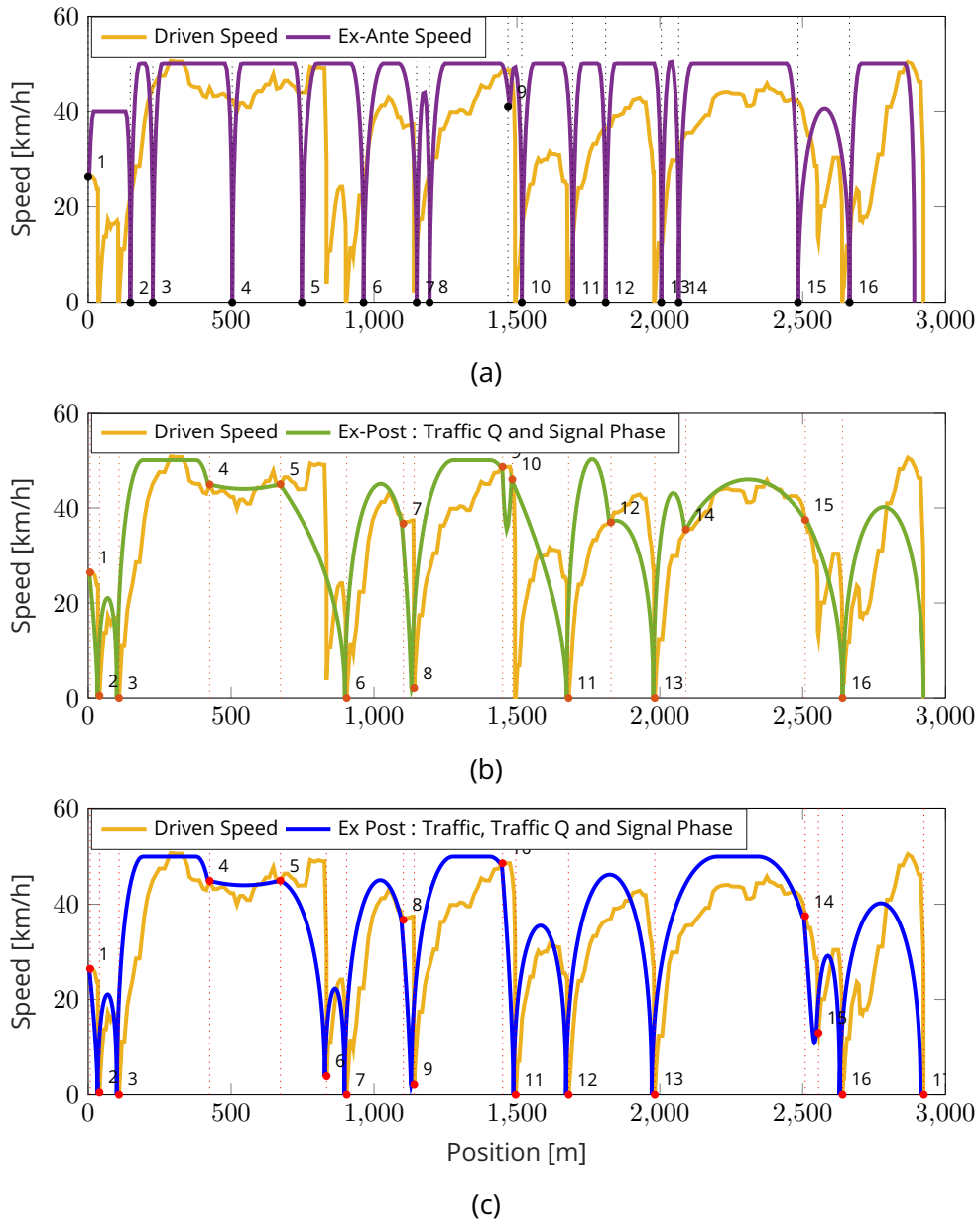

Figure A.7: Figure showing the ex-ante, ex-post:1, ex-post:2 and the driven speed of Trip 2

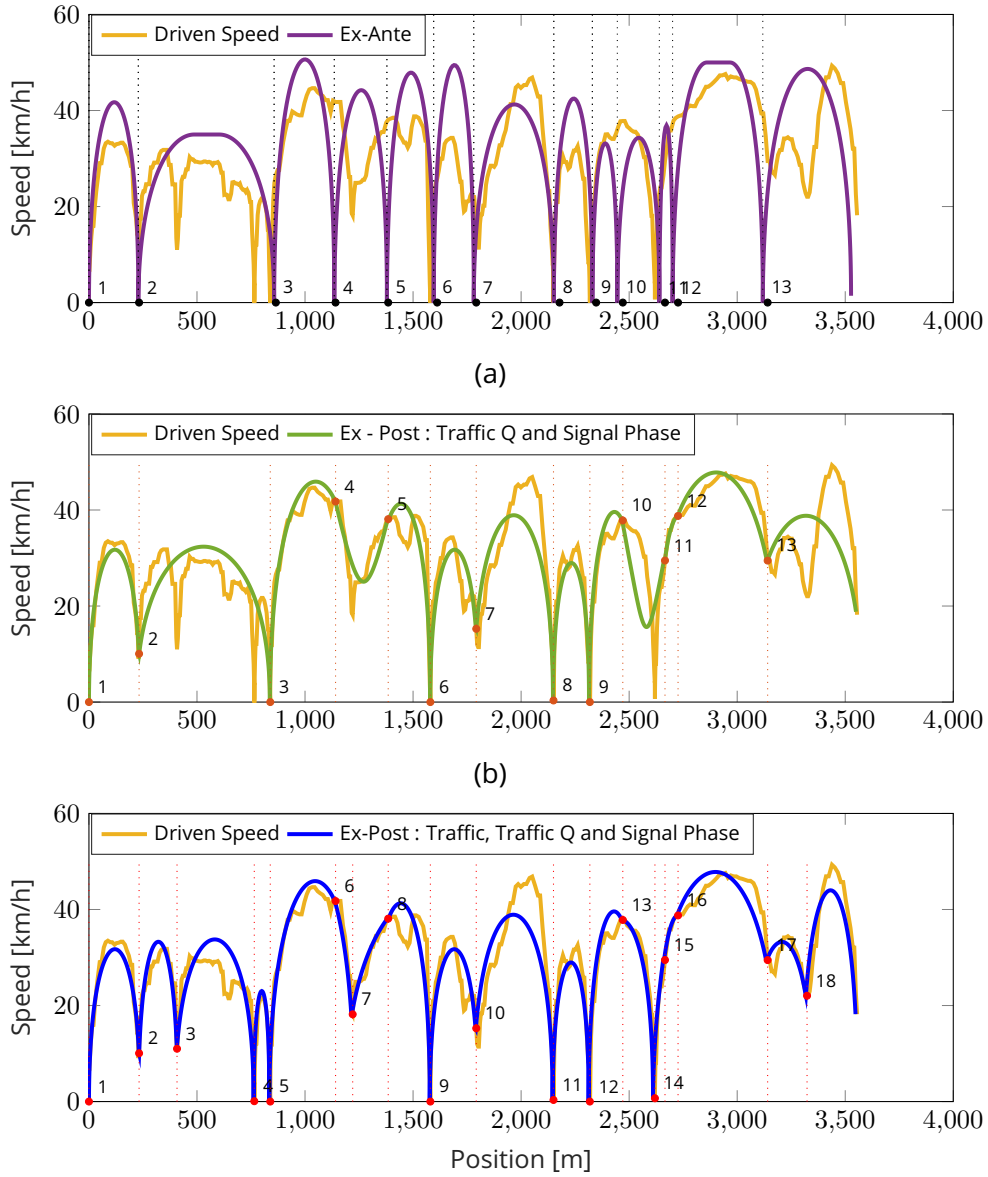

Figure A.8: Figure showing the ex-ante, ex-post:1, ex-post:2 and the driven speed of Trip 3

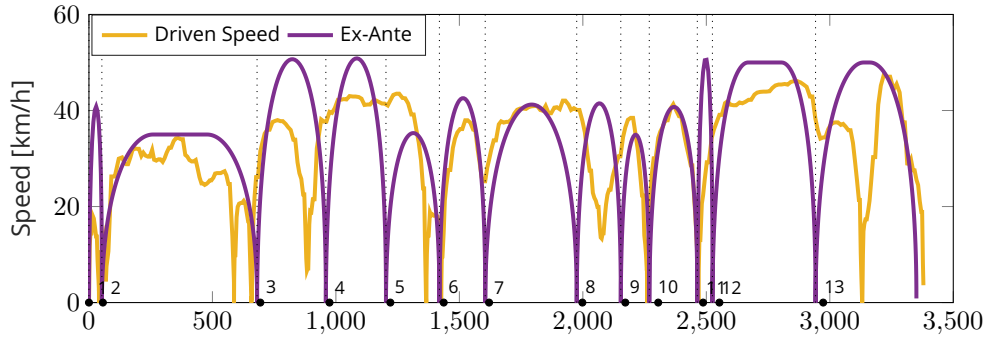

(a)

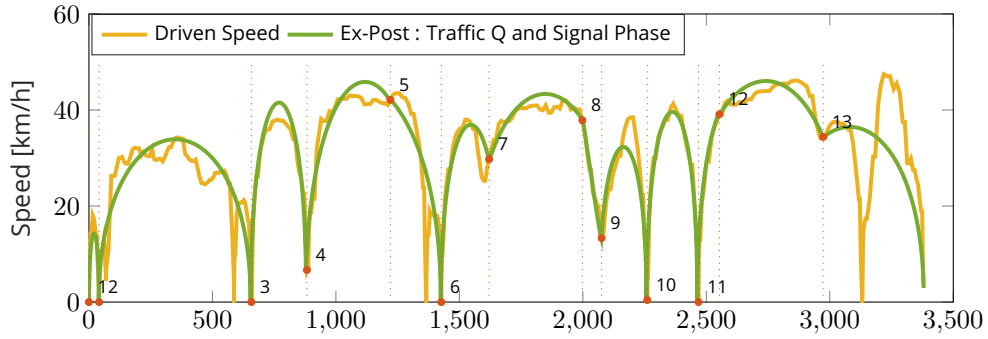

(b)

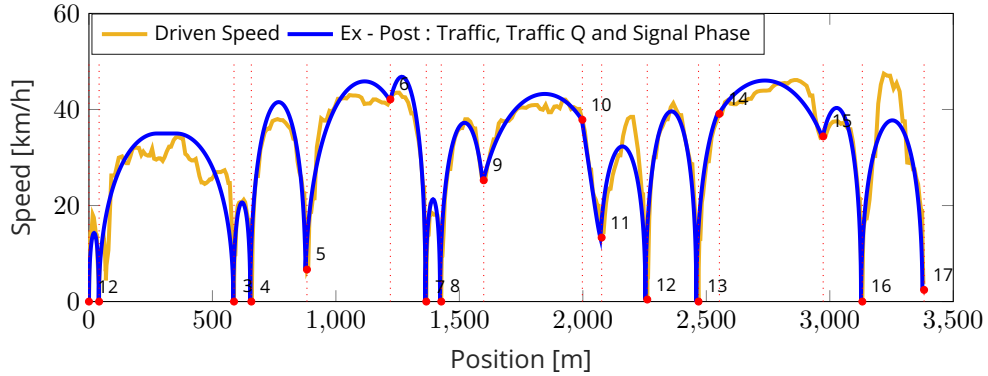

(c)

Figure A.9: Figure showing the ex-ante, ex-post:1, ex-post:2 and the driven speed of Trip 4

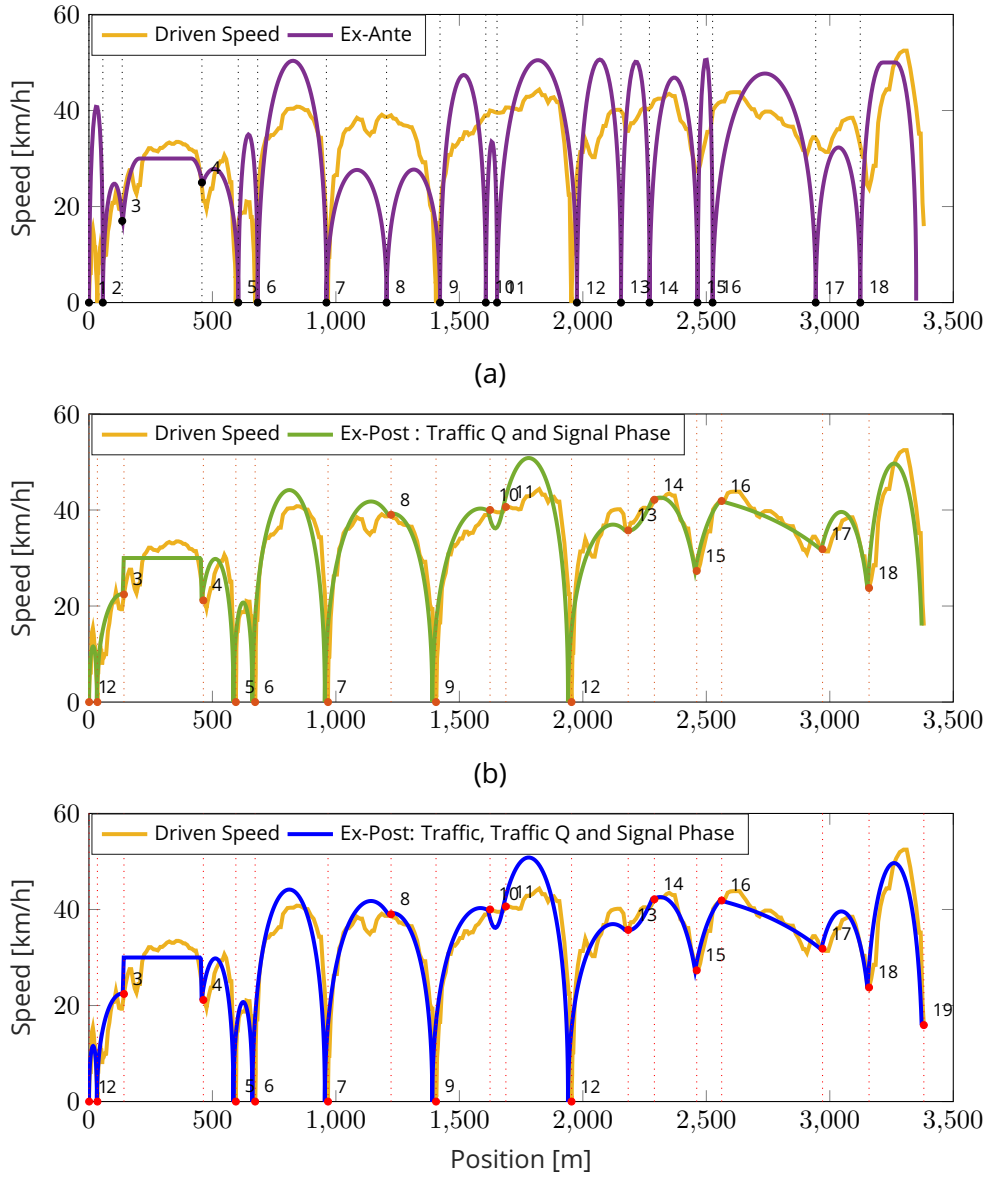

(a)

(b)

(c)

Figure A.10: Figure showing the ex-ante, ex-post:1, ex-post:2 and the driven speed of Trip 5

Bibliography

[1] Thijs van Keulen, Jan Gillot, Bram de Jager, and Maarten Steinbuch. Solution for state constrained optimal control problems applied to power split control for hybrid vehicles. Automatica, 50(1):187–192, 2014.